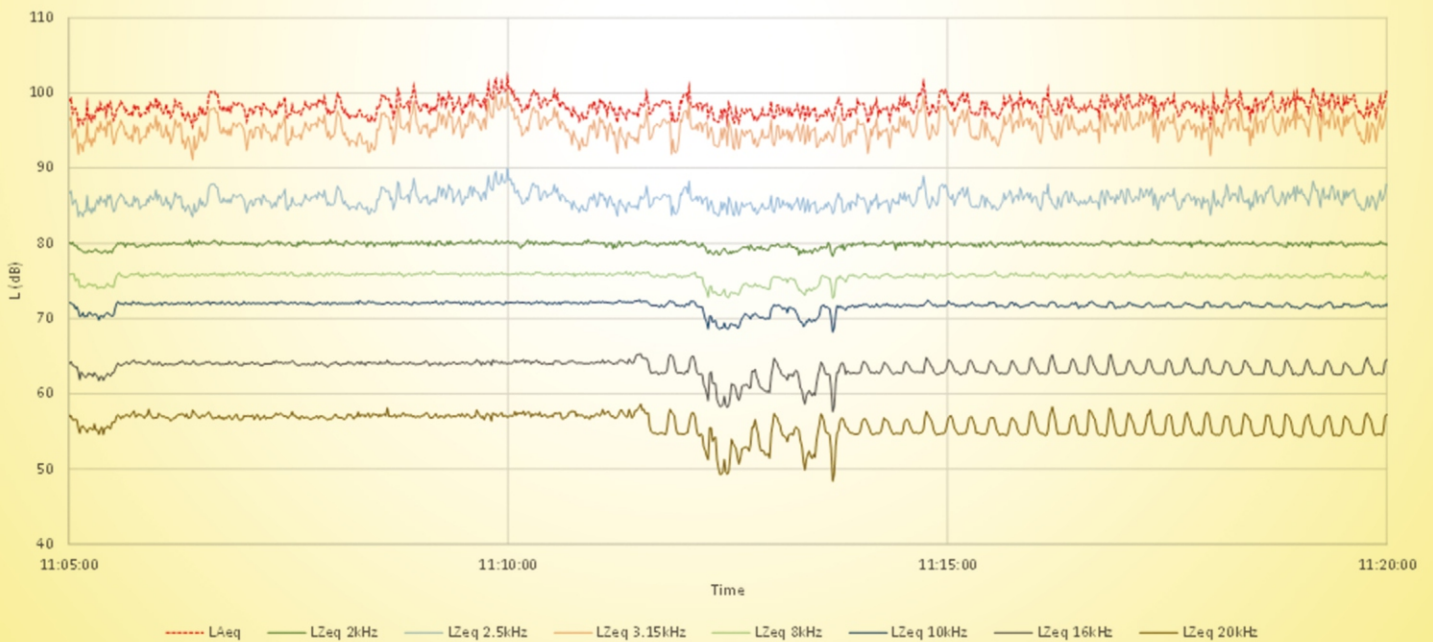


Journal of Modern Physics



ISSN: 2153-1196



Journal Editorial Board

ISSN: 2153-1196 (Print) ISSN: 2153-120X (Online)

<http://www.scirp.org/journal/jmp>

Editor-in-Chief

Prof. Yang-Hui He

City University, UK

Executive Editor-in-Chief

Prof. Marko Markov

Research International, Buffalo Office, USA

Managing Executive Editor

Prof. Chang Liu

Wuhan University, China

Editorial Board

Prof. Nikolai A. Sobolev

Universidade de Aveiro, Portugal

Prof. Yohannes Abate

California State University, USA

Dr. Mohamed Abu-Shady

Menoufia University, Egypt

Dr. Hamid Alemohammad

Advanced Test and Automation Inc., Canada

Prof. Emad K. Al-Shakarchi

Al-Nahrain University, Iraq

Prof. Changle Chen

University of Science and Technology of China, China

Prof. Stephen Robert Cotanch

NC State University, USA

Prof. Ju Gao

The University of Hong Kong, China

Prof. Sachin Goyal

University of California, USA

Dr. Wei Guo

Florida State University, USA

Prof. Alioscia Hamma

Tsinghua University, China

Prof. Cosmin Ilie

Los Alamos National Laboratory, USA

Prof. Haikel Jelassi

National Center for Nuclear Science and Technology, Tunisia

Prof. Preston B. Landon

The University of California, USA

Prof. Chunlei Liu

Carnegie Mellon University, USA

Prof. Christophe J. Muller

University of Provence, France

Prof. Ambarish Nag

National Renewable Energy Laboratory, USA

Dr. Rada Novakovic

National Research Council, Italy

Prof. Valery Obukhov

Tomsk State Pedagogical University, Russia

Prof. Tongfei Qi

University of Kentucky, USA

Prof. Mohammad Mehdi Rashidi

University of Birmingham, UK

Prof. Richard Saurel

University of Aix Marseille I, France

Prof. Alejandro Crespo Sosa

Universidad Nacional Autónoma de México, Mexico

Prof. Bo Sun

Oregon State University, USA

Prof. Mingzhai Sun

Ohio State University, USA

Dr. Sergei K. Suslov

Arizona State University, USA

Dr. A. L. Roy Vellaisamy

City University of Hong Kong, China

Prof. Yuan Wang

University of California, Berkeley, USA

Prof. Fan Yang

Fermi National Accelerator Laboratory, USA

Prof. Peter H. Yoon

University of Maryland, USA

Dr. S. Zerbini

University of Trento, Italy

Prof. Meishan Zhao

University of Chicago, USA

Prof. Pavel Zhuravlev

University of Maryland at College Park, USA

Table of Contents

Volume 8 Number 10

September 2017

**Measuring Sound Pressure Levels during Thermoacoustic
Instabilities in Large Engines: Case Study**

A. E. González, J. C. Ottieri, P. G. Kovar, J. M. Crouccée, M. R. Lisboa.....1685

**Sobolev Spaces, Schwartz Spaces, and a Definition of the
Electromagnetic and Gravitational Coupling**

J.-P. Montillet.....1700

**Curvature Energy and Their Spectrum in the Spinor-Twistor
Framework: Torsion as Indicium of Gravitational Waves**

F. Bulnes, Y. Stropovskiy, I. Rabinovich.....1723

**Resonant Modes of One-Dimensional Metamaterial
Containing Helmholtz Resonators with Point Defect**

D. B. Gao, X. W. Zeng, X. J. Liu, K. F. Han.....1737

Journal of Modern Physics (JMP)

Journal Information

SUBSCRIPTIONS

The *Journal of Modern Physics* (Online at Scientific Research Publishing, www.SciRP.org) is published monthly by Scientific Research Publishing, Inc., USA.

Subscription rates:

Print: \$89 per issue.

To subscribe, please contact Journals Subscriptions Department, E-mail: sub@scirp.org

SERVICES

Advertisements

Advertisement Sales Department, E-mail: service@scirp.org

Reprints (minimum quantity 100 copies)

Reprints Co-ordinator, Scientific Research Publishing, Inc., USA.

E-mail: sub@scirp.org

COPYRIGHT

Copyright and reuse rights for the front matter of the journal:

Copyright © 2017 by Scientific Research Publishing Inc.

This work is licensed under the Creative Commons Attribution International License (CC BY).

<http://creativecommons.org/licenses/by/4.0/>

Copyright for individual papers of the journal:

Copyright © 2017 by author(s) and Scientific Research Publishing Inc.

Reuse rights for individual papers:

Note: At SCIRP authors can choose between CC BY and CC BY-NC. Please consult each paper for its reuse rights.

Disclaimer of liability

Statements and opinions expressed in the articles and communications are those of the individual contributors and not the statements and opinion of Scientific Research Publishing, Inc. We assume no responsibility or liability for any damage or injury to persons or property arising out of the use of any materials, instructions, methods or ideas contained herein. We expressly disclaim any implied warranties of merchantability or fitness for a particular purpose. If expert assistance is required, the services of a competent professional person should be sought.

PRODUCTION INFORMATION

For manuscripts that have been accepted for publication, please contact:

E-mail: jmp@scirp.org

Measuring Sound Pressure Levels during Thermoacoustic Instabilities in Large Engines: Case Study

Alice Elizabeth González, José Cataldo Ottieri, Pablo Gianoli Kovar,
Joaquín Montero Crouccié, Marcos Raúl Lisboa

Department of Environmental Engineering, IMFIA—Faculty of Engineering, Universidad de la República, Montevideo, Uruguay
Email: alicelizabethgonzalez@gmail.com, elizabet@fing.edu.uy

How to cite this paper: González, A.E., Ottieri, J.C., Kovar, P.G., Crouccié, J.M. and Lisboa, M.R. (2017) Measuring Sound Pressure Levels during Thermoacoustic Instabilities in Large Engines: Case Study. *Journal of Modern Physics*, 8, 1685-1699. <https://doi.org/10.4236/jmp.2017.810099>

Received: July 19, 2017

Accepted: August 31, 2017

Published: September 4, 2017

Copyright © 2017 by authors and Scientific Research Publishing Inc. This work is licensed under the Creative Commons Attribution International License (CC BY 4.0).

<http://creativecommons.org/licenses/by/4.0/>



Open Access

Abstract

This paper attempts to present some registers of sound pressure levels during the operation of large diesel engines (10 MW). During these registers we have found the preparation, occurrence and ending of events of thermoacoustic instability. They appear after a loosing of chaos period or a reduction in fluctuations in some frequencies. The most interesting phenomena were registered at low frequencies. However, they were accompanied by variations in sound emissions at medium and high frequencies. As there has been very little published data concerning these phenomena at real scale, it is imperative to point out that every quasi-stationary state we have measured during these episodes has lasted some minutes, significantly much more time than that of lab scale results.

Keywords

Thermoacoustic Instabilities, Large Engines, Real Scale Measurements

1. Introduction

Thermoacoustic instabilities are a growing concern when working with large machines. A lot of work has been developed about gas turbines, but very few experiences are reported measuring this phenomenon in real scales engines.

Noise in diesel engines is highly consistent with the variation of the pressure inside each cylinder along the time. As combustion has random features, the cylinder pressure and the emitted noise are dominated by randomness over a wide range of frequencies where noise is produced [1].

When working for determining the acoustic power of large engines (10 MW),

we detected some unusual patterns in several third octave bands (TOB) recordings. We went through the analysis and we found we have measured some thermoacoustic instabilities episodes during the tests.

Thermoacoustic oscillations cause increased damage on the engines. The high sound pressure levels associated with the oscillations that occur during thermoacoustic instability, impose an additional load on the wall of the combustion chamber. In addition, non-stationary flow increases heat transfer to the coating and local overheating may occur. Even the electronic systems that control combustion could fail due to high levels of vibration or temperature, leading loss of the system control.

According to Schemel *et al.* (2004) when the flow is homogeneous, the noise in a combustion chamber is an overlapping of the solution of three independent wave equations: the waves traveling upflow and downflow at sound speed, the turbulent convective waves and the entropy convective waves. If the flow ceases to be homogeneous, the entropy convective waves will begin to emit (radiate) sound [2].

Combustion instabilities arise due to complex feedback interactions between pressure and heat release oscillations. When these oscillations are sufficiently in phase, a large amplification of the initial perturbation is expected. Thus, the instabilities of the combustion refer to the feedback of a coherent phase oscillation at a fixed frequency.

The pressure oscillations occurring in the combustion chamber appear as fluctuations in the output flow of the injector. As a consequence, fluctuations in the incoming air flow occur in turn. Then, fluctuations in the release of heat would also appear. The frequency of these oscillations depends on the main cause of them. Low frequency oscillations (from 4 Hz to 70 Hz) are mainly due to instabilities in the flame front progressing in a heterogeneous way throughout the combustion chamber. They are related to low frequency emissions. From 70 Hz to 700 Hz stationary waves with different phase angles appear [3]. If those oscillations couple with the operating frequencies of the equipment, high intensity noise emissions will be released.

Polifke *et al.* (2001) point out that the feedback between the combustion chamber acoustics and the entropy waves would be important, especially for lower modes and even at higher frequencies than those normally associated with convection waves [4]. The relative phase between the acoustic signal at the combustion chamber outlet and the pressure pulse generated by the entropy wave determines whether the combustion chamber's susceptibility to thermoacoustic oscillations is improved or reduced by the interaction between the entropy waves and the acoustics of the combustion chamber.

The main issues affecting the occurrence of interferences are fluctuations and heterogeneities in fuel concentration, temperature regions, rate of heat release and also localized phenomena at the inlet and the fuel injection point. Depending on the characteristic times of the convection and acoustic phenomena, the

entropy waves and the acoustic of the combustion chamber could couple in a constructive or destructive way.

It should be noted that the rotational frequencies of the machines in our case of study are within the proper range for flame front fluctuations.

The most important mechanisms responsible for instability in combustion are related to the injection of propellants, the formation of liquid droplets and the combustion process itself. If a high temperature region passes through a supersonic nozzle (*i.e.* where $Ma > 1$), the interaction with the non-uniform flow region developed produces an acoustic wave which propagates upstream. Then, the action of the acoustic wave in the combustion processes can generate new regions of non-uniform temperature, with the usual consequences on the stability of the combustion. Therefore, there is a feedback loop within the chamber which maintains the oscillatory phenomena and which, under certain conditions, may lead to a condition of instability. The evolution of eddies can excite oscillations, either by purely fluid interactions or by influencing combustion processes [5]. The first one leads to relatively weak instabilities because the available mechanical energy is relatively small. In contrast, when combustion is involved, significant oscillations can occur. Eddies can carry reagents and due to delays or chemicals or in the mixing time, the combustion may subsequently occur at times and in spatial locations favorable to destabilize an acoustic mode.

The oscillations in pressure and velocity in the gas phase (acoustic disturbances) can influence the rate of vaporization of the liquid droplets if the period of oscillation corresponds to one of the characteristic times of the vaporization, namely [6]: life time of the drop; period of thermal inertia of the liquid; period of thermal diffusion of the liquid; period of diffusion of the gas phase of the gas mixture contained in the combustion chamber; period of diffusion of the gas phase by forced convection.

According to Schuermans (2003), fluctuations in fuel concentration are the main (but not the only) cause of the interaction between the heat release and the sound field [7]. Litak *et al.* (2005) conclude that the noise level of the internal pressure when calculating the entropy of the variations of the maximum pressures in successive cycles is not monotonous function of the load [3]. The results show that the combustion dynamics is a non-linear, multidimensional process mediated by noise. This method allows distinguishing a particular signal, including chaos with its short-term prediction scale, and random noise.

The “soul” of the problem is that all the ideal processes under which combustion is studied in small machines are no longer valid in large ones. The hypotheses about instantaneous ignition, homogeneity of the mixture and all phenomena occurring inside of each cylinder are no longer applicable.

This paper is organized in four sections. After this introduction, some ways to early detecting thermoacoustic instabilities are presented. Then, our own experimental findings when measuring at several 10 MW engines are detailed. At last, our conclusions are remarked.

2. Early Detection of Thermoacoustic Instabilities

Research about thermoacoustic instabilities has mostly developed around gas turbines and at a laboratory scale. There are not enough published data about real scale cases. There are many proposals for detection of the occurrence of these phenomena. Hereby we present three of them; we think our experimental findings can help to deeper studies on them.

2.1. Loss of Chaos

The phenomenon of loss of chaos was studied by Vinneeth *et al.* (2013) [8]. They present convincing evidence that combustion noise is deterministic. Therefore, the traditional “signal plus noise” paradigm that is usually implicitly assumed in the models and analyzes of experimental data sets needs to be re-examined if capturing instabilities in the combustion chambers is wanted because these irregular fluctuations might contain useful prognostic information. Vinneeth *et al.* generate a way to predict the impending passage to unstable combustion by applying the 0 - 1 test for chaos on sequentially acquired pressure measurements. For low level of combustion noise the measured K value is quite close to 1 in the initial stages, indicating that the combustion noise is chaotic. The value of K has a decreasing tendency as the Reynolds number of the flux increases, reaching values close to 0 at the beginning of the instability. Since the loss of the chaos condition occurs in a gentle manner, the value of K can be used as a measure of the proximity of an imminent instability condition. Choosing a threshold value of K that corresponds to the initial stages of loss of chaos (e.g. 0.9), it is possible to know the condition enough in advance to take actions that modify the operation parameters and thus avoid the occurrence of instability and therefore its subsequent installation as an operating regime [8].

The precursor turns out to be an objective measure of the proximity of the combustion chamber to the unstable operating regimes and is independent of the details of the geometry, the composition of the fuel and the stabilization of the flame.

2.2. Rapid Detection by Analyzing Trends of Variation

During the preparation of a thermoacoustic instability event, some early “symptoms” should be detected, thus allowing taking actions to avoid the instability occurrence. Ibrahim (2007) proposes the use of a low-cost method which implies having a good identification and characterization of several acoustic modes to be able to follow its temporal evolution and to know about its growing and decreasing tendencies. This background allows to make a good prediction without numerically integrating over time: its detection tool analyzes the behavior of rates of variation and not modes, which is undoubtedly simpler and faster. The method consists in cataloging and linearly estimating of magnitudes of the mechanisms of amplification and attenuation. The application of linear approximations to nonlinear mechanisms allows, however, obtaining a reasonably com-

plete and manageable description for the purposes of the analysis. The author defines an index of stability, so that the imminent occurrence of an instability is anticipated when a certain value is exceeded. In this particular case, the oscillation is expected to occur when the value of the index exceeds one unit [9].

The goal of the method is to allow fast, low-cost decisions that can be made for a wide variety of design configurations and operating conditions without the complexity of other tools that require computational fluid dynamics. The proposed approach achieves moderate success by being tested on a basis of experimental data available in the literature as well as with new experiments, so it may also be useful to complement other methods already in use.

2.3. Experimental Diagnosis

Lee and Santavicca (2005) carry out an extensive discussion of the applicable methods for experimentally diagnosing, *i.e.* in operation, if instability is occurring in a combustion chamber [10]. Among the methods they discuss, brief comments are made here on some of them. Pressure measurements are usually the simplest ones, although it is necessary to take a set of precautions, for example about the location of the sensor or how to fix it, in order to obtain information in accordance with the objective. In addition to measuring pressure fluctuations in the combustion chamber, it is useful to simultaneously measure pressure fluctuations in the nozzle and in the fuel line. These fluctuations result in fluctuations in the rate of fuel flow, a phenomenon known as coupling of the feed system. Such measurements provide valuable information for evaluating the coupling role of the feed system in terms of its role as a mechanism in conducting or damping/aborting the effective occurrence of instability [10].

The effect of entropy waves on flow field instabilities is known since 1965, but their importance was supposed to be restricted only to low frequencies. More recent works (e.g., [4]) show that interference between entropy waves and pressure disturbances can be constructive or destructive, which can further aggravate the problem.

Fluctuations of heat release in the flame can cause acoustic waves that propagate upstream in the feed lines and in turn cause disturbances in the incoming air/fuel mixture. These disturbances can be carried by the mean flow and trigger a fluctuation in the flame controller, closing the instability loop. Several studies have addressed this possible mechanism and are considered of high potential to generate instability phenomena. The acoustic-convective waves are carried by the medium flow, such as eddies detached from the flame stabilizer and/or entropy waves that propagate downstream, and generate acoustic waves that propagate upstream.

There are also other possible sources of oscillatory combustion instability ranging from purely chemical-kinetic phenomena to other only fluid-mechanical phenomena. Their contributions vary with modes of oscillation. It is also possible that some of the modes of oscillation are caused by a combination of

perturbations (velocity, temperature, velocity of laminar flame, etc.).

Several mechanisms contribute to the occurrence of thermoacoustic instabilities [11]: fluctuations in the air/fuel ratio, acoustic-convective waves and entropy waves. Eddies detachment was suggested as the cause of combustion instabilities in 1956 by Rogers and Marble [12]. Instability is triggered when the vortices that are released from the flame stabilizer, entrain unburned mixture that spreads downstream and cause a sudden release of heat at some point in its path. This triggers an acoustic wave propagating upstream that closes the feedback loop.

A similar result would be found if these vortices affect an obstacle downstream (e.g. the outlet nozzle, a throttling, etc.), even if they carry no unburned mixture or if it is a non-reactive flow or a cold flow, causing the pressure oscillations to intensify. This result is purely acoustic and does not consider the contributions related to heat releasing.

Since hot spots are carried by the medium (usually low-speed) flow, it is assumed that entropy effects (if exist) are to occur at low frequencies. When these hot spots reach the entrance of a strangled nozzle, the propagation of an up-flow acoustic wave is triggered and it can cause an acoustic instability.

3. Experimental Findings

3.1. Measurements

A set of measurements were carried out to determine the acoustic power of eight large diesel engines (10 MW each). They were done according to UNE-EN-ISO 3744:2010 Standard [13]. A Class 1 Bruel & Kjaer sound pressure level meter (Model 2250) was used. Also the environmental sound pressure levels in the engines room were recorded during the tests.

All the figures in this section have been built using the experimental data registered during the tests; please notice that all graphics relate to only one engine operation.

3.2. High Frequencies' Findings

We found three kinds of phenomena that are to be called as cases A, B and C.

Case A refers to some high frequency components that became coherent from some time during the test (first presented at **Figure 1** and **Figure 2**).

Case B is related to some simultaneous jumps occurring also at high frequencies (first presented at **Figure 3**).

Case C show reduced variability and increasing sound pressure levels in some high frequency TOB (initially presented at **Figure 4** and **Figure 5**). They are preceded or accompanied by episodes of loss of chaos at low frequencies, mainly at 25 Hz.

The first case (Case A) shows a qualitative change at the highest frequency waves at about 11:15: they become coherent as shown by the pattern they exhibit from 10,000 Hz and upper frequencies. It doesn't happen at lower frequencies (**Figure 1** and **Figure 2**).

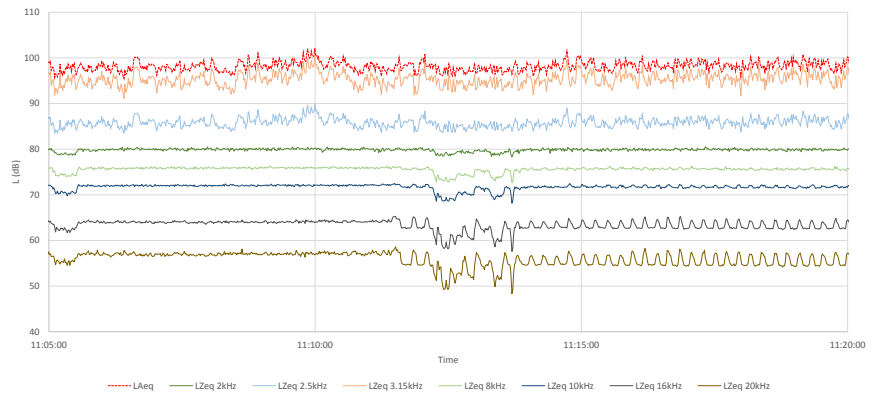


Figure 1. Time evolution of sound pressure levels in selected third-octave bands (Case A). Please note the change of shape occurring near 11:15 at the graphs of the highest frequencies.

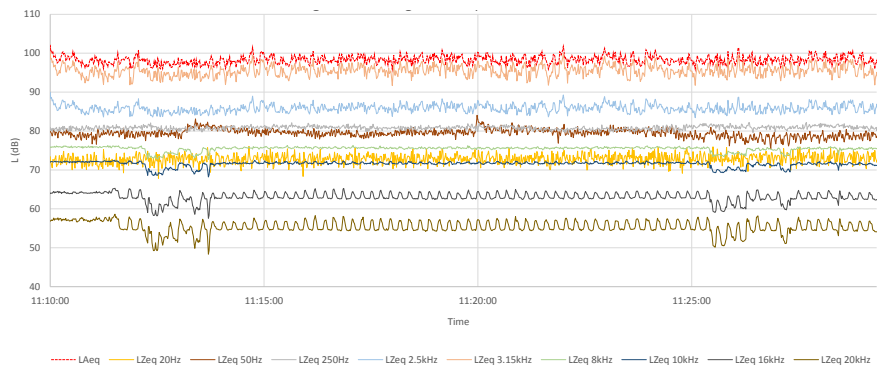


Figure 2. Loss of chaos at the highest audible frequencies (Case A).

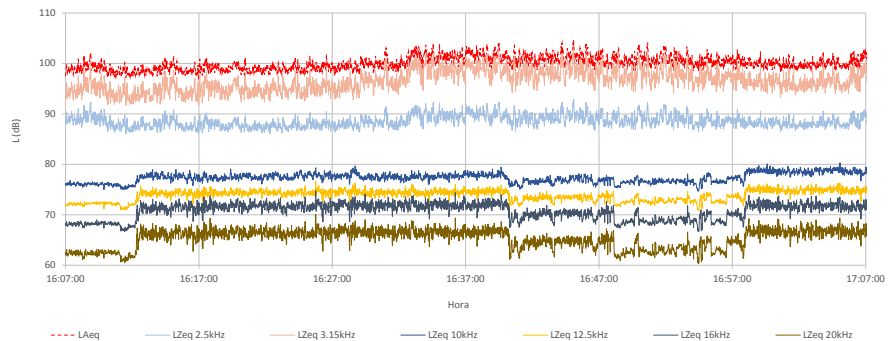


Figure 3. Time evolution of sound pressure levels in selected third-octave bands (Case B). Please note the simultaneous jumps occurring at the highest frequencies.

Another kind of phenomena appears at high frequencies in Case B. No coherence phenomena appear but there are some ascending and descending jumps that occur within some 3 to 5 minutes of difference. Although they are not reflected in the broad band levels, sound pressure levels jumps occur simultaneously in several TOBs (Figure 3).

The third case we found at high frequencies (Case C) is shown in Figure 4 and Figure 5. The sound pressure levels at high frequencies reduce their varia-

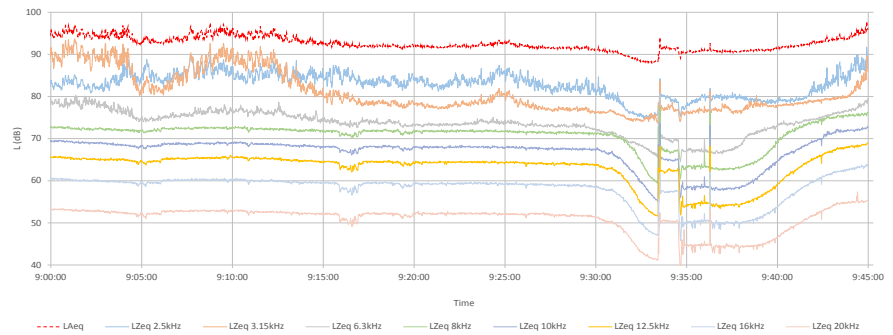


Figure 4. Time evolution of sound pressure levels in selected third-octave bands (Case C). Please note the decreasing variability of sound pressure levels at the highest audible frequencies.

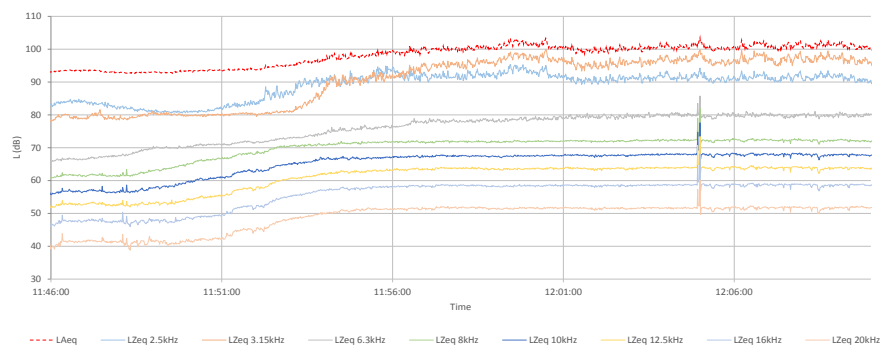


Figure 5. Time evolution of sound pressure levels in selected third-octave bands (Case C). Decreasing variability of sound pressure levels with increasing levels at the highest audible frequencies.

bility while increasing their value.

This occurs from 2500 Hz and upper frequencies. The sound pressure levels at 2000 Hz are rather constant over the time and have very few fluctuations.

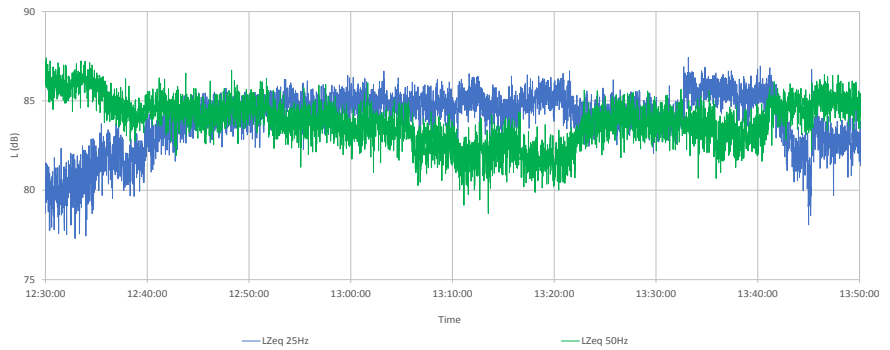
We have also registered interference phenomena during noise measures, as shown in **Figure 6**. Graphs show destructive interferences whether the components in different TOB appear almost in opposition of phase. It was found to happen both at harmonic frequencies (left) and at non-harmonic ones (right).

3.3. Related Phenomena at Low Frequencies: The Main Causes

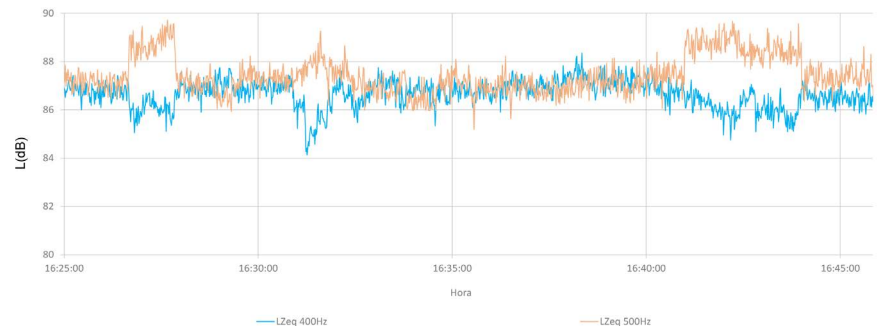
Once we have identified what was happening at high frequencies, we went on looking for regularities at other frequencies. We found that the root causes in the above-mentioned cases were linked to changes at low frequencies.

The changes in regime of acoustic emissions in TOB of 25 Hz but also 12.5 Hz and 50 Hz were always present during the recorded events.

We had only one measurement where Case A occurred (coherence in high frequencies components). For this particular case, we found that the component in 50 Hz was qualitatively less chaotic in the previous 10 minutes (**Figure 7**) and that was a consequence of an extended process which began about 50 minutes earlier (**Figure 8**).



(a)



(b)

Figure 6. Destructive interferences in selected third-octave bands. (a): low frequencies 25 Hz and 50 Hz; (b): middle frequencies 400 Hz and 500 Hz.

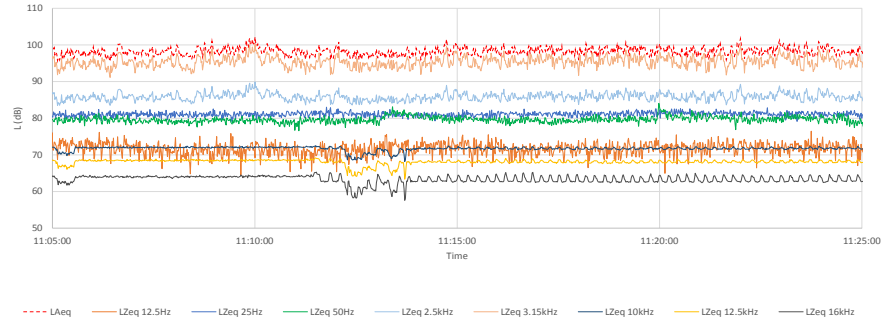


Figure 7. Previous changes in 16 Hz and 50 Hz about 10 minutes earlier than the beginning of Case A.

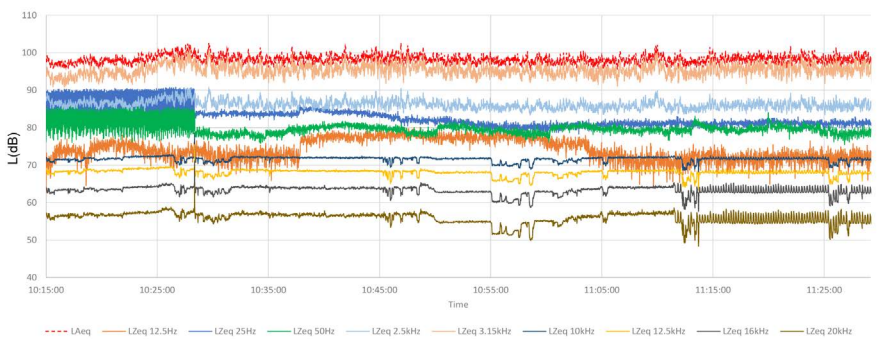


Figure 8. Different steps during Case A preparation: loss of coherence at 25 Hz (1 hour earlier) and sequence of different quasi-stationary states (about 10 minutes each one).

Case B was the most frequent during our measurements. It can be seen as a set of jumps in sound pressure levels occurring simultaneously in several TOB. There are at least three of these jumps in **Figure 9**. It corresponds to the whole event presented in **Figure 3**. It is possible to observe that jumps in high frequencies are anticipated by changes at lower frequencies expressed as episodes of loss of chaos.

Figures 10-13 show the same kind of phenomena occurring in other events.

The third group of cases we measured (Cases C) had the most unexpected behaviour at low frequencies.

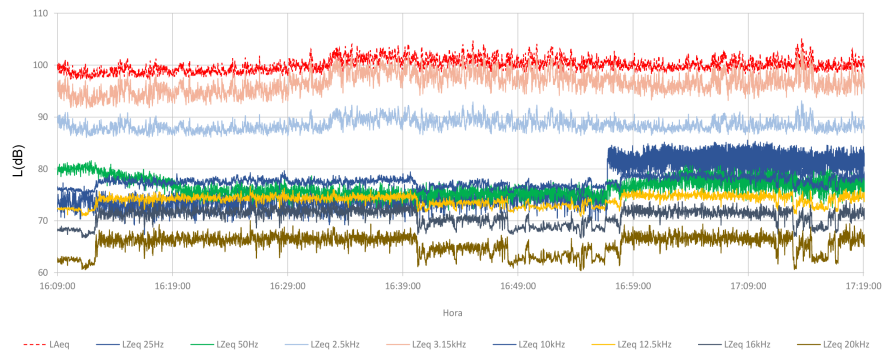


Figure 9. Simultaneous jumps in sound pressure levels at different TOB (Case B).

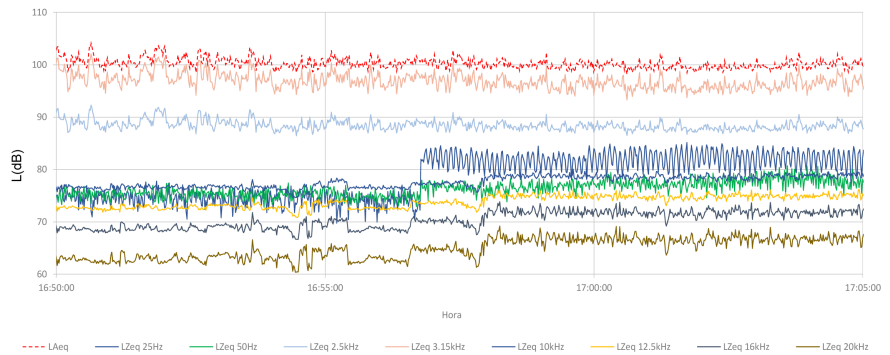


Figure 10. Measured sound pressure levels in selected TOB. Detail of Case B presented in **Figures 3-9**. Please note the great change at 25 Hz TBO.

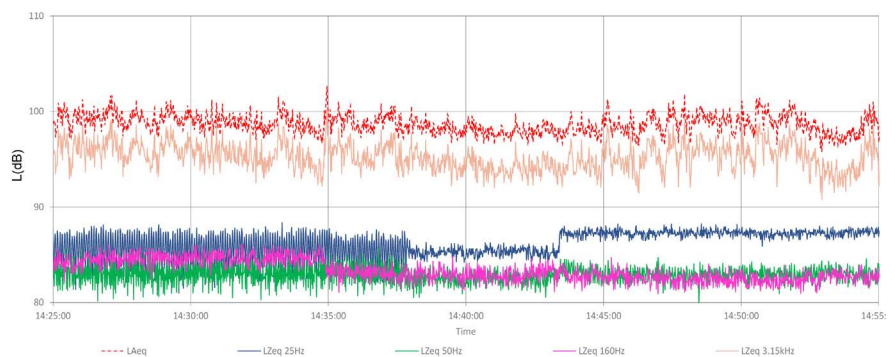


Figure 11. Examples of occurrence of Case B. Please note jumps at 25 Hz, 50 Hz and 160 Hz.

Figure 14 shows the evolution of some TOB during the whole event and Figure 15 presents a detail of what happens at TOB of 25 Hz and 50 Hz. When sound pressure levels and variability at 2.500 Hz begin to increase, low frequency bands return to a more chaotic condition. Note that sound pressure levels at certain middle TOB (e.g. 160 Hz and 315 Hz) show similar behavior than highest frequencies.

Another interesting example is shown in Figure 16 and Figure 17. The increase of sound pressure levels at high frequencies (e.g. 2500 Hz and 3150 Hz) is



Figure 12. Examples of occurrence of Case B. Jumps at 25 Hz, 50 Hz and 160 Hz are accompanied by smooth changes at 12.5 Hz, 125 Hz and 315 Hz.

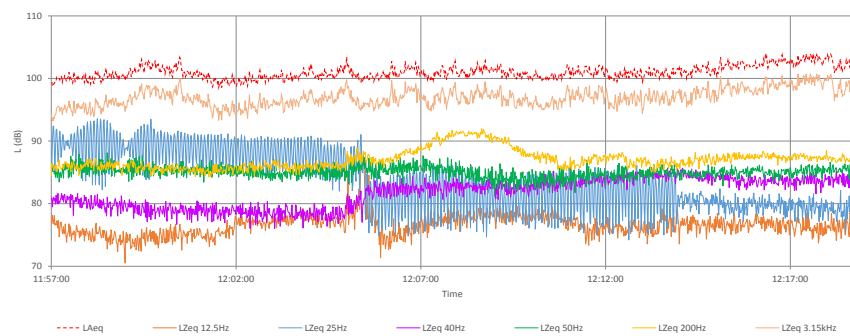


Figure 13. Examples of occurrence of Case B. Changes of behaviour at 25 Hz are accompanied by others at several TOB e.g. 12.5 Hz, 40 Hz and 200 Hz.

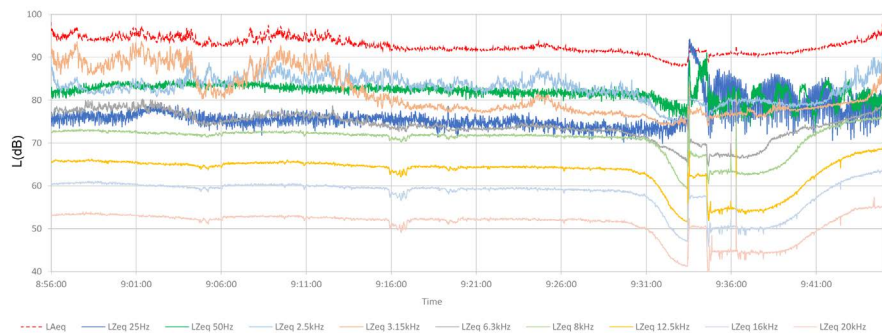


Figure 14. Example of occurrence of Case C. The phenomena at 25 Hz and 50 Hz occur after loss of variability and reduction of sound pressure levels at high frequencies; then, they begin to grow again.

very smooth; it lasts more than one hour since the beginning of the phenomenon at low frequencies (25 Hz and 50 Hz), as it can be seen in a closer approach shown at **Figure 17**.

Finally, **Figure 18** and **Figure 19** show the evolution of some TOB during the whole event introduced in **Figure 5**. **Figure 20** presents a closer approach of the retrieve of chaos at low frequencies. Two different scales seem to be involved in the phenomena: a quasi-periodic wave and a modulating one. This behaviour seems to appear in Case B, but in a less evident way.

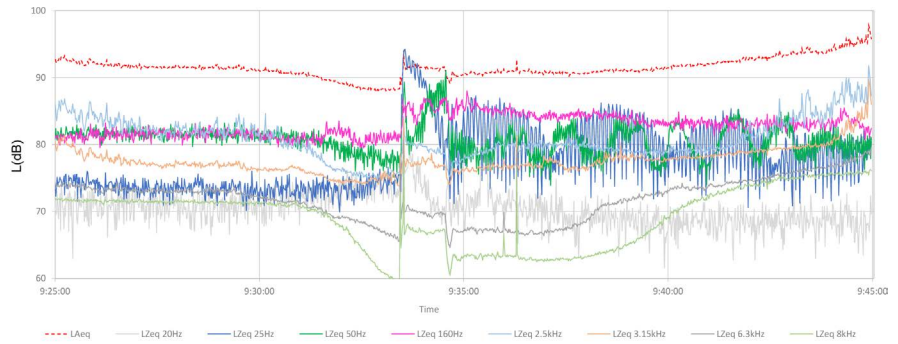


Figure 15. Measured sound pressure levels in selected TOB. Detail of Case C presented in **Figure 14**.



Figure 16. Examples of occurrence of Case C. The increase of sound pressure levels at high frequencies is very smooth.

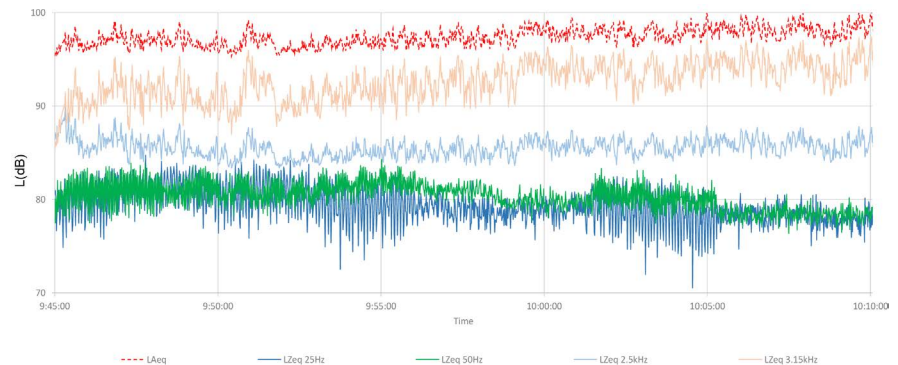


Figure 17. Measured sound pressure levels in selected TOB at the beginning of the episode. Detail of Case C presented in **Figure 16**.

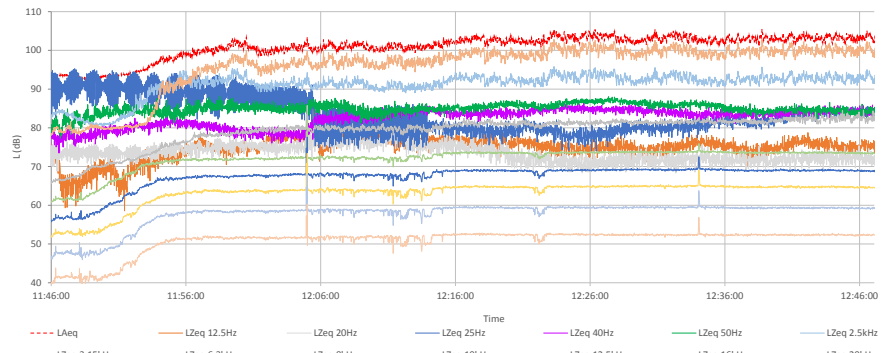


Figure 18. Examples of occurrence of Case C. Full event partially shown in **Figure 5** and **Figure 13**.

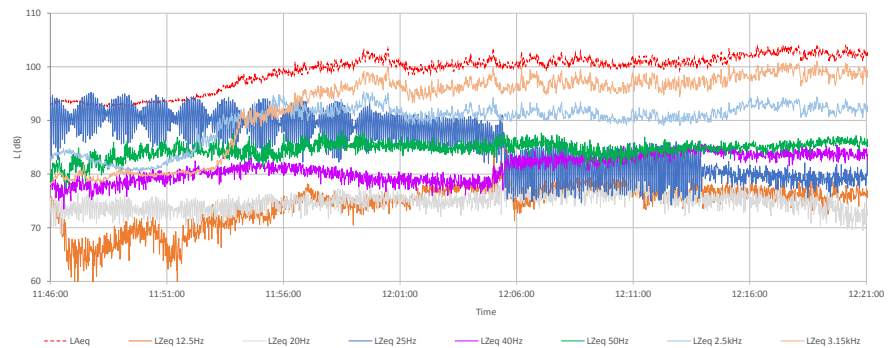


Figure 19. Measured sound pressure levels in selected TOB at the beginning of the event presented in **Figure 18**.

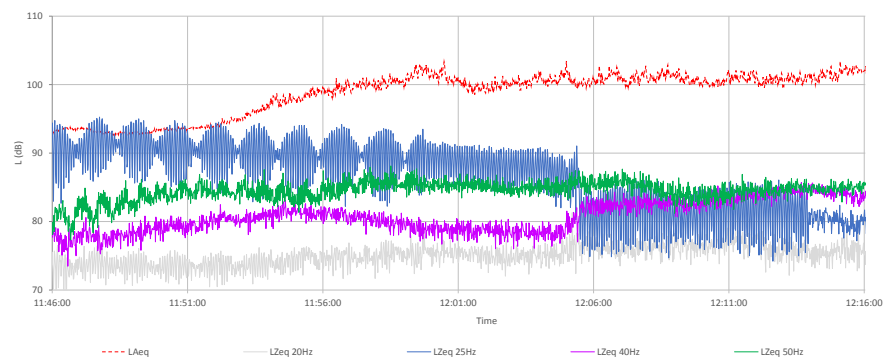


Figure 20. Measured sound pressure levels in selected TOB: 20 Hz, 25 Hz, 40 Hz and 50 Hz. Detail of the beginning of the Case C event presented in **Figure 18** and **Figure 19**. Please note that the process of retrieving of chaos lasts more than 25 minutes.

4. Conclusions

We have been able to measure the occurrence of several events of thermoacoustic instability in 10 MW engines.

These phenomena occur in large machines in which homogeneity of parameters and simultaneity of processes in the combustion chamber are not proper hypothesis. Small differences and/or fluctuations can generate disturbances and fluctuations in combustion parameters. In these conditions, for example, if a

coupling occurs with some geometric dimension, the system will go into resonance.

During the preparation of the instability events, processes of loss of chaos in low frequencies, especially in 25 Hz or 50 Hz, were observed. Also, a reduction of the variability of sound pressure levels in high frequencies occurred. After some minutes, the system retrieves the condition of randomness of the combustion.

Each of the “steady” states of operation lasts several minutes, as so the transition from one to another does.

Every quasi-stationary before and after the occurrence of a thermoacoustic instability episode last a few minutes, so active control systems seem to be a suitable solution to address such problems on large machines.

References

- [1] Strahle, W.C. (1978) *Journal of Progress in Energy and Combustion Science*, **4**, 157-176.
- [2] Schemel, C., Thiele, F. and Michel, U. (2004) Numerical Simulation of the Noise Generation at the Outlet Section of Combustion Chambers. CFD-DAGA2004, Strasbourg, Francia.
- [3] Litak, G., Taccani, R., Radu, R., Urbanowicz, K., Hołyst, J.A., Wendeker, M. and Giadrossi, A. (2005) *Chaos, Solitons and Fractals*, **23**, 1695-1701.
www.elsevier.com/locate/chaos
[https://doi.org/10.1016/S0960-0779\(04\)00434-5](https://doi.org/10.1016/S0960-0779(04)00434-5)
- [4] Polifke, W., Paschereit, C.O. and Döbbeling, K. (2001) *Journal of Acoustics and Vibration*, **6**, 135-146. <https://doi.org/10.20855/ijav.2001.6.382>
- [5] Cullick, F.E.C., Lin, W.H., Jahnke, C.C. and Sterling, J.D. (1991) Modeling for Active Control of Combustion and Thermally Driven Oscillations. American Control Conference, 2939-2948, 26-28 June 1991.
<http://ieeexplore.ieee.org/stamp/stamp.jsp?tp=&arnumber=4791942&isnumber=4791300>
- [6] Ghosh, A. (2008) The Role of Density Gradient in Liquid Rocket Engine Combustion Instability, Chapter 2: Literature Review.
- [7] Schuermans, B. (2003) Modeling and Control of Thermoacoustic Instabilities. Ph.D. Thesis, École Polytechnique Fédérale de Lausanne.
- [8] Nair, V., Thampi, G., Karuppusamy, S., Gopalan, S. and Sujith, R.I. (2013) *International Journal of Spray and Combustion Dynamics*, **5**, 273-290.
<https://doi.org/10.1260/1756-8277.5.4.273>
- [9] Ibrahim, Z.M.A. (2007) An Acoustic Energy Framework for Predicting Combustion-Driven Acoustic Instabilities in Premixed Gas-Turbines. UC San Diego Electronic Theses and Dissertations, Ph.D., UC San Diego. 123 p. Permalink.
<https://escholarship.org/uc/item/6wn0k48j>
- [10] Lee, J.G. and Santavicca, D.A. (2005) Experimental Diagnostics of Combustion Instabilities. Chapter 16. In: Lieuwen, T.C. and Yang, V., Eds., *Combustion Instabilities in Gas Turbine Engines. Operational Experience, Fundamental Mechanisms, and Modeling*, Volume 210, Progress in Astronautics and Aeronautics, American Institute of Aeronautics and Astronautics, Inc. (Frank K. Lu, Editor-in-Chief). Copyright c 2005 by the American Institute of Aeronautics and Astronautics.

- [11] Kabiraj, L. and Sujith, R.I. (2012) *Journal of Fluid Mechanics*, **713**, 376-397
- [12] Rogers, D.E. and Marble, F.E. (1956) *Jet Propulsion*, **1**, 456-462.
- [13] Asociación Española de Normalización y Certificación - Comité Europeo de Normalización. Norma UNE-EN-ISO 3744:2010. *Acústica: Determinación de los niveles de potencia acústica y de los niveles de energía acústica de fuentes de ruido utilizando presión acústica. Métodos de ingeniería para un campo esencialmente libre sobre un plano reflectante (ISO 3744:2010)*. 84 p. Julio, 2011.



Scientific Research Publishing

Submit or recommend next manuscript to SCIRP and we will provide best service for you:

Accepting pre-submission inquiries through Email, Facebook, LinkedIn, Twitter, etc.

A wide selection of journals (inclusive of 9 subjects, more than 200 journals)

Providing 24-hour high-quality service

User-friendly online submission system

Fair and swift peer-review system

Efficient typesetting and proofreading procedure

Display of the result of downloads and visits, as well as the number of cited articles

Maximum dissemination of your research work

Submit your manuscript at: <http://papersubmission.scirp.org/>

Or contact jmp@scirp.org

Sobolev Spaces, Schwartz Spaces, and a Definition of the Electromagnetic and Gravitational Coupling

Jean-Philippe Montillet

ESPlab, Ecole Polytechnique de Lausanne, Neuchâtel, Switzerland

Email: jeanfi montillet@yahoo.fr

How to cite this paper: Montillet, J.-P. (2017) Sobolev Spaces, Schwartz Spaces, and a Definition of the Electromagnetic and Gravitational Coupling. *Journal of Modern Physics*, 8, 1700-1722. <https://doi.org/10.4236/jmp.2017.810100>

Received: August 3, 2017

Accepted: September 3, 2017

Published: September 6, 2017

Copyright © 2017 by author and Scientific Research Publishing Inc.

This work is licensed under the Creative Commons Attribution International License (CC BY 4.0).

<http://creativecommons.org/licenses/by/4.0/>



Open Access

Abstract

The concept of *multiplicity of solutions* was developed in [1] which is based on the theory of energy operators in the Schwartz space $\mathcal{S}^-(\mathbb{R})$ and some subspaces called energy spaces first defined in [2] and [3]. The main idea is to look for solutions of a given linear PDE in those subspaces. Here, this work extends previous developments in $\mathcal{S}^-(\mathbb{R}^m)$ ($m \in \mathbb{Z}^+$) using the theory of Sobolev spaces. Furthermore, we also define the concept of *Energy Parallax*, which is the inclusion of additional solutions when varying the energy of a predefined system locally by taking into account additional smaller quantities. We show that it is equivalent to take into account solutions in other energy subspaces. To illustrate the theory, one of our examples is based on the variation of Electro Magnetic (EM) energy density within the skin depth of a conductive material, leading to take into account derivatives of EM evanescent waves, particular solutions of the wave equation. The last example is the derivation of the Woodward effect [4] with the variations of the EM energy density under strict assumptions in general relativity. It finally leads to a theoretical definition of an electromagnetic and gravitational (EMG) coupling.

Keywords

Electromagnetism, General Relativity, Schwartz Space, Sobolev Spaces, Multiplicity of Solutions, Energy Operators, Woodward Effect

1. Overview

Teager-Kaiser energy operator was defined in [5] and the family of Teager-Kaiser energy operators in [6]. Many applications in signal processing were

found over the past 25 years such as detecting transient signals [7], filtering modulated signals [8], image processing [9]. However, [2] and [10] introduced the conjugate Teager-Kaiser energy operator and associated family $(\Psi_k^+)_{k \in \mathbb{Z}}$. Subsequently using iterations of the Lie Bracket, [3] defined the generalized conjugate Teager-Kaiser energy operators $\left(\left[[\cdot]^p \right]_k^+ \right)_{k \in \mathbb{Z}}$ ($p \in \mathbb{Z}^+$). To abbreviate the notation, we sometimes use the generic name *energy operator* in order to refer to the conjugate Teager-Kaiser energy operators and the generalized conjugate Teager-Kaiser energy operators. Precision is made in the denomination when it is required. Furthermore, the purpose of the energy operators and generalized energy operators was the decomposition of the successive derivatives of a finite energy function f^n (n in $\mathbb{Z}^+ - \{0,1\}$) in the Schwartz space $\mathbf{S}^-(\mathbb{R})$. The generalized energy operators were introduced when decomposing the successive derivatives of a finite energy function of the form $\left(\left[[f]^p \right]_1^+ \right)^n$ (n in $\mathbb{Z}^+ - \{0,1\}$) in the Schwartz space. It then follows in [1] and [3] the definition of *Energy Spaces*, which are subspaces of the Schwartz Space $\mathbf{S}^-(\mathbb{R})$ associated with energy operators and generalized energy operators. This definition was used to define the concept of *multiplicity of solutions* in [1] (Theorem 2 and Corollary 1). The idea is to consider those energy spaces and functions associated with them when solving linear PDEs. More precisely, we look for solutions of a nominated linear PDE within those energy spaces (including the space reduced to $\{0\}$). The concept was further developed using the Taylor series of the energy of a solution $\mathbf{S}^-(\mathbb{R})$ for a nominated PDE. The work was based on finding when the successive derivatives, defined through the Taylor series coefficients, are also solutions of this particular PDE (see Section 4 in [1]).

This work first generalizes in $\mathbf{S}^-(\mathbb{R}^m)$ ($m \in \mathbb{Z}^+$) the theorems and lemmas established in [2] and [3] stated for $\mathbf{S}^-(\mathbb{R})$ using the properties of the L^2 space called here $L^2(\mathbb{R}^m)$ ($m \in \mathbb{Z}^+$) together with the general property of the Schwartz space $\mathbf{S}^-(\mathbb{R}^m) \subset L^2(\mathbb{R}^m)$ ($m \in \mathbb{Z}^+$) [11]. However, this work imposes the condition of the stability by Fourier transform for any functions in $\mathbf{S}^-(\mathbb{R})$ in order to use the Sobolev space (see **Appendix I**, Definition I.1). Thus, in this work we consider $\mathbf{S}^-(\mathbb{R})$ together with its dual: the tempered distributions $\mathbf{S}^{*-}(\mathbb{R})$. Secondly, the energy spaces \mathbf{M}_p^k ($p \in \mathbb{Z}^+$, $k \in \mathbb{Z}^+$) are also redefined as subspaces of $\mathbf{S}^-(\mathbb{R}^m)$. Furthermore, with the definition of the Sobolev spaces, and in particular the Hilbert spaces $\mathbf{H}^k(\mathbb{R}^m)$, it allows to show the inclusion $\mathbf{M}_p^k \subset \mathbf{H}^k(\mathbb{R}^m) \subset L^2(\mathbb{R}^m)$. Then, we finally redefine in \mathbb{R}^m the Theorem 3 established in [1] and the concept of *multiplicity of solutions*.

The next section together with **Appendix I** are reminders about some important definitions and properties for the Sobolev spaces, the Schwartz space and the L2-norm. Section 3 deals with the generalization of the work exposed in [2] and [3] in $\mathbf{S}^-(\mathbb{R}^m)$ and the redefinition of the energy spaces. Section 4

recalls the concept of *multiplicity of solutions* defined in [1] and generalized in $\mathbf{S}^-(\mathbb{R}^m)$ with Theorem 4. The last section focuses on some applications of this theory. The first application is the wave equation and the discussion of taking into account more solutions from other energy spaces. We then define another concept called *energy parallax* (i.e. mathematically in Definition 4, see discussion on the physical interpretation in **Appendix II**) which is directly related to *multiplicity of solutions*. In order to illustrate this concept, a second example is the variation of energy density in the skin depth of a conductor material. The idea is to show that the variation of energy density can lead to consider multiple derivatives of evanescent waves resulting from the electromagnetic field. The last section is dedicated to the derivation of the Woodward effect [4] from the Hoyle-Narlikar theory [12] [13] using the EM energy density and a discussion takes place about the relationship to the presented theory of energy spaces. It leads to a theoretical definition of an Electromagnetic and Gravitational coupling (EMG).

2. Definition of L-2 Norm and Schwartz Space

2.1. Notation and Symbols

In this work, several symbols are used. The set of integer numbers \mathbb{Z} is sometimes called only for the positive integer such as \mathbb{Z}^+ or \mathbb{Z}_+^m (for a space with dimension m). When the integer 0 is not included, it is explicitly mentioned such as $\mathbb{Z}^+ - \{0\}$. The set of natural numbers is \mathbb{N} , with only the positive numbers defined as \mathbb{N}^+ . \mathbb{R} is the set of real numbers. Also, the Schwartz space is here called $\mathbf{S}^-(\mathbb{R}^m)$ which is the notation used in previous works such as [1] and [2]. Several notations describe the relationship between spaces such as intersection (\cap), union (\cup), inclusion (\subset , inclusion without the equality \subsetneq , inclusion with equality \subseteq). Reader can refer to [14] or advanced mathematical textbooks for more explanations.

2.2. L-2 Norm and Schwartz Space

With the difference in **Appendix I** and the generalities with the Sobolev spaces, here the analysis focuses on the L-2 norm (p equal to 2 for the L^p norm). It allows to state the Plancherel identity $\forall f \in L^2(\mathbb{R}^m)$:

$$\int_{\mathbb{R}^m} f^2 dt = \int_{\mathbb{R}^m} \mathcal{F}(f)(\xi)^2 d\xi \tag{1}$$

We are here interested in the functions belonging to the Schwartz space $f \in \mathbf{S}^-(\mathbb{R}^m) \subset L^2(\mathbb{R}^m)$. The Schwartz space consists of smooth functions whose derivatives (including the function) are rapidly decreasing (e.g., the space of all bump functions [15]). The Schwartz space $\mathbf{S}^-(\mathbb{R}^m)$ is defined as (for $m \in [1, 2]$ in [1] [3], for $m \in \mathbb{Z}^+$ in [14] [16]):

$$\mathbf{S}^-(\mathbb{R}^m) = \left\{ f \in \mathbf{C}^\infty(\mathbb{R}^m) \mid f_{\alpha,\beta} < \infty, \forall \alpha, \beta \in \mathbb{Z}_+^m \right\} \tag{2}$$

where α, β are multi-indices and

$$f_{\alpha,\beta} = \sup_{t \in \mathbb{R}^m} |t^\beta D^\alpha f(t)| \tag{3}$$

Note that one can define $\mathbf{S}^-(\mathbb{R}^m)$ with $\forall \alpha, \beta \in \mathbb{R}^m$ according to [17], but we decide to use \mathbb{Z}_+^m following the development in the next sections. It is useful for the remainder of the work to remember some properties of the Schwartz functions in $\mathbf{S}^-(\mathbb{R}^m)$.

Properties 1. [18] Some Properties of $\mathbf{S}^-(\mathbb{R}^m)$.

- If $1 \leq p \leq \infty$, then $\mathbf{S}^-(\mathbb{R}^m) \subset L^p(\mathbb{R}^m)$
- $\mathbf{S}^-(\mathbb{R}^m)$ is a dense subspace of $H^{k,2}(\mathbb{R}^m)$ ($k \in \mathbb{N}$).
- (Stability with Fourier transform) The Fourier transform is a linear isomorphism $\mathbf{S}^-(\mathbb{R}^m) \rightarrow \mathbf{S}^-(\mathbb{R}^m)$.
- If $f \in \mathbf{S}^-(\mathbb{R}^m)$, then f is uniformly continuous on \mathbb{R}^m .

The proof of those properties are standard results with Schwartz spaces established in many harmonic analysis books (e.g., [17] [18]).

Remark (1) Note that in [1] [2] [3], the author used the general term of finite energy functions for Schwartz functions in $\mathbf{S}^-(\mathbb{R}^m)$, with m restricted to $[1, 2]$. It is a common definition in signal processing for the functions in $L^2(\mathbb{R}^m)$ and generally associated with the Plancherel identity.

Remark (2) One way to interpret the property that $\mathbf{S}^-(\mathbb{R}^m)$ is stable by Fourier transform is:

for $f \in \mathbf{S}^-(\mathbb{R}^m)$, $k \in \mathbb{N}$

$$\begin{aligned} & \sup_{\xi \in \mathbb{R}^m} \left\{ \left(1 + \xi^2\right)^{k/2} \mathcal{F}(f)(\xi) \right\} < \infty \\ \Leftrightarrow & \exists a \in \mathbb{R}, \left| \left(1 + \xi^2\right)^{k/2} \mathcal{F}(f)(\xi) \right| \leq \frac{a}{1 + \xi^2} \end{aligned} \tag{4}$$

Now, let us recall the definition of the Hilbert spaces $H^{k,p}(\mathbb{R}^m)$ (Sobolev spaces $W^{k,p}(\mathbb{R}^m)$ for $p = 2$, see **Appendix I**, Definition I.1) from (35) and drop the sup-script p in the remainder of this work:

$$\begin{aligned} W^k(\mathbb{R}^m) &= H^k(\mathbb{R}^m) \\ &:= \left\{ f \in \mathbf{S}^{*,-}(\mathbb{R}^m) \mid \left(1 + \xi^2\right)^{k/2} \mathcal{F}(f) \in L^2(\mathbb{R}^m) \right\} \end{aligned} \tag{5}$$

Note that $\mathbf{S}^{*,-}(\mathbb{R}^m)$ is the space of tempered distributions, dual of $\mathbf{S}^-(\mathbb{R}^m)$ via the Fourier transform. A function belongs to $L^2(\mathbb{R}^m)$ if and only if its Fourier transform belongs to $L^2(\mathbb{R}^m)$ and the Fourier transform preserves the L^2 -norm. As a result, the Fourier transform provides a simple way to define L^2 -Sobolev spaces on \mathbb{R}^m (including ones of fractional and negative order m [18]). Finally, the stability via Fourier transform is the key for $\mathbf{S}^-(\mathbb{R}^m) \subsetneq \mathbf{H}^k(\mathbb{R}^m)$.

Remark (3) Following the remark (Remark 3.4 in [19]) and the general properties of the Fourier transform, one can state the equivalence relationship in $L^2(\mathbb{R}^m)$

$$\begin{aligned}
 f \in \mathbf{H}^k(\mathbb{R}^m) &\leftrightarrow D^\alpha f \in L^2(\mathbb{R}^m) \forall \alpha \leq k \\
 &\leftrightarrow \mathcal{F}(D^\alpha f) \in L^2(\mathbb{R}^m) \forall \alpha \leq k \\
 &\leftrightarrow \xi^\alpha \mathcal{F}(f) \in L^2(\mathbb{R}^m) \forall \alpha \leq k \\
 &\leftrightarrow (1 + \xi^2)^{\alpha/2} \mathcal{F}(D^\alpha f) \in L^2(\mathbb{R}^m) \forall \alpha \leq k
 \end{aligned} \tag{6}$$

Using the definition of $\mathbf{H}^k(\mathbb{R}^m)$ and the properties of the Fourier transform, it is also possible to show that for $k > k'$, $\mathbf{H}^k(\mathbb{R}^m) \subset \mathbf{H}^{k'}(\mathbb{R}^m)$ [20], and the relationship $\mathbf{H}^0(\mathbb{R}^m) = L^2(\mathbb{R}^m)$. It is also possible to define $\mathbf{H}^\infty(\mathbb{R}^m) = \bigcap_{k \in \mathbb{N}} \mathbf{H}^k(\mathbb{R}^m)$ with $\mathbf{S}^-(\mathbb{R}^m) \subset \mathbf{H}^\infty(\mathbb{R}^m)$, and to extend this equality to $k \in \mathbb{R}$ following [19].

3. On Some Subsets of Schwartz Spaces: Energy Spaces

This section first recalls generalities on the Teager-Kaiser energy operator and its conjugate operator with the application to decompose Schwartz functions from the work developed in [2] and [3]. We call in this work *Energy operators* the families of operators based on the Teager-Kaiser energy operator. The definitions and theorems are here stated for the Schwartz space $\mathbf{S}^-(\mathbb{R}^m)$ ($m \in \mathbb{N}$) whereas the preliminary work in [2] and [3] stated the definitions and main theorems for $m \in [1, 2]$. For $m = 2$ in Section 6 in [3], a discussion takes place during the application of the theory to linear partial differential equations. Secondly, the energy spaces defined in [1] and [3] are here generalized on $\mathbf{S}^-(\mathbb{R}^m)$ with novel relationships with Sobolev spaces $\mathbf{H}^k(\mathbb{R}^m)$ ($k \in \mathbb{N}$).

3.1. Definition and Properties of the Energy Operators in $\mathbf{S}^-(\mathbb{R}^m)$

Let us call the set $\mathcal{F}(\mathbf{S}^-(\mathbb{R}^m), \mathbf{S}^-(\mathbb{R}^m))$ all Schwartz functions (or operators) defined such as $\gamma: \mathbf{S}^-(\mathbb{R}^m) \rightarrow \mathbf{S}^-(\mathbb{R}^m)$. For $f \in \mathbf{S}^-(\mathbb{R}^m)$, let us define $\partial_i^k f$ ($k \in \mathbb{Z}$, $i \in [1, \dots, m]$), with f defined with the vector parameter $\mathbf{T} = [t_1, t_2, \dots, t_m] \in \mathbb{R}^m$ such as

$$\begin{cases}
 \partial_i^k f = \frac{\partial^k f}{\partial t_i^k}, \forall i \in [1, \dots, m], \forall k \in \mathbb{Z}^+ - \{0\} \\
 \partial_i^k f = \int_{-\infty}^{t_i} \left(\dots \left(\int_{-\infty}^{\tau_1} f(t_1, t_2, \dots, \tau_1, t_{k+1}, t_m) d\tau_1 \right) \dots \right) d\tau_k, \forall i \in [1, \dots, m], \forall k \in \mathbb{Z}^- - \{0\} \\
 \partial_i^0 f = f, \forall i \in [1, \dots, m]
 \end{cases} \tag{7}$$

Combining multiple integrals and derivatives justify the use of the Schwartz space $\mathbf{S}^-(\mathbb{R}^m)$ and echoes the choice made previously in [2] (see equation (10)). The definitions and results given in [2] and [3] in the case $\mathbf{S}^-(\mathbb{R})$ are now formulated for $\mathbf{S}^-(\mathbb{R}^m)$. Section 2 in [2] and Section 4 in [3] defined the energy operators Ψ_k^+ , Ψ_k^- (k in \mathbb{Z}) and the generalized energy operators $[[\cdot]]_k^+$ and $[[\cdot]]_k^-$ (p in \mathbb{Z}^+). Following [3], let us define the energy

operators with multi-index derivative in (7):

$$\begin{aligned} \Psi_k^+(\cdot) &= \sum_{i=1}^m \partial_i^1 \cdot \partial_i^{k-1} \cdot + \partial_i^0 \cdot \partial_i^k \cdot \\ \Psi_k^+(\cdot) &= \sum_{i=1}^m \psi_{k,i}^+(\cdot) \\ [\cdot, \cdot]_k^+ &= \Psi_k^+(\cdot) \\ [\cdot, \cdot]_{k,i}^+ &= \psi_{k,i}^+(\cdot) \end{aligned} \tag{8}$$

Further more, we also use the short notation $[\cdot, \cdot]_k^+ = [\cdot]_k^+$ in the remainder of this work. Note that Ψ_k^- is the conjugate operator of Ψ_k^+ and $\psi_{k,i}^-$ respectively to $\psi_{k,i}^+$.

Remark (4) The families of (generalized) energy operators $\left([\cdot]_k^+\right)_{k \in \mathbb{Z}}$ and $\left([\cdot]_k^-\right)_{k \in \mathbb{Z}}$ (p in \mathbb{Z}^+) are also called families of differential energy operator (DEO) [2] [3].

Furthermore, [3] defined the generalized energy operators $[\cdot]_k^+$ and $[\cdot]_k^-$ ($k \in \mathbb{Z}$):

$$\begin{aligned} [\cdot, \cdot]_{k,i}^+, [\cdot, \cdot]_{k,i}^+ &= \partial_i^1 \psi_{k,i}^+(\cdot) \partial_i^{k-1} \psi_{k,i}^+(\cdot) + \partial_i^0 \psi_{k,i}^+(\cdot) \partial_i^k \psi_{k,i}^+(\cdot) \\ [\cdot, \cdot]_{k,i}^+, [\cdot, \cdot]_{k,i}^+ &= \partial_i^1 [\cdot]_{k,i}^+ \partial_i^{k-1} [\cdot]_{k,i}^+ \\ &\quad + \partial_i^0 [\cdot]_{k,i}^+ \partial_i^k [\cdot]_{k,i}^+ \\ [\cdot, \cdot]_k^+, [\cdot, \cdot]_k^+ &= \sum_{i=1}^m [\cdot, \cdot]_{k,i}^+, [\cdot, \cdot]_{k,i}^+ \\ [\cdot, \cdot]_k^+, [\cdot, \cdot]_k^+ &= \sum_{i=1}^m [\cdot]_{k,i}^+ = [\cdot]_k^+ \end{aligned} \tag{9}$$

By iterating the bracket $[\cdot]$, [3] defined the generalized operator $[\cdot]_{k,i}^-$ and the conjugate $[\cdot]_{k,i}^+$ with p in \mathbb{Z}^+ . Note that $[[f]^p]_{1,i}^- = 0 \quad \forall p$ in \mathbb{Z}^+ and i in \mathbb{Z} .

Now, the derivative chain rule property and bilinearity of the energy operators and generalized operators (for i in $[1, 2]$) are shown respectively in [2], Section 2 and [3], Proposition 3. The generalisation of this property to i in $[1, \dots, m]$ for the operators $\psi_{k,i}^+(\cdot)$, $\psi_{k,i}^-(\cdot)$, $[\cdot]_{k,i}^-$ and $[\cdot]_{k,i}^+$ ($k \in \mathbb{Z}$, $p \in \mathbb{Z}^+$) is trivial due to the linearity of the derivatives and integrals when defining ∂_i^k in (7). Due to the linearity of the sum, the bilinearity property is also generalized to $\Psi_k^+(\cdot)$, $\Psi_k^-(\cdot)$, $[\cdot]_k^+$ and $[\cdot]_k^-$ ($k \in \mathbb{Z}$, $p \in \mathbb{Z}^+$).

Definition 1. [2] $\forall f$ in $\mathbf{S}^-(\mathbb{R}^m)$, $\forall v \in \mathbb{Z}^+ - \{0\}$, $\forall n \in \mathbb{Z}^+$ and $n > 1$, the

family of operators $(G_k)_{k \in \mathbb{Z}}$ (with $(G_k)_{k \in \mathbb{Z}} \subseteq \mathcal{F}(\mathbf{S}^-(\mathbb{R}^m), \mathbf{S}^-(\mathbb{R}^m))$) decomposes $\partial_i^v f^n$ in \mathbb{R}^m ($i \in [1, \dots, m]$), if it exists $(N_j)_{j \in \mathbb{Z}^+ \cup \{0\}} \subseteq \mathbb{Z}^+$,

$(C_l)_{l=-N_j}^{N_j} \subseteq \mathbb{R}$, and it exists (α_j) and r in $\mathbb{Z}^+ \cup \{0\}$ (with $r < v$) such as

$$\partial_i^v f^n = \sum_{j=0}^{v-1} \binom{v-1}{j} \partial_i^{v-1-j} f^{n-r} \sum_{u=-N_j}^{N_j} C_u G_u (\partial_i^{\alpha_u} f).$$

In addition, one has to define $\mathbf{s}^-(\mathbb{R}^m)$ as:

$$\mathbf{s}^-(\mathbb{R}^m) = \left\{ f \in \mathbf{S}^-(\mathbb{R}^m) \mid f \notin \left(\bigcup_{k \in \mathbb{Z}} \text{Ker}(\Psi_k^+) \right) \cup \left(\bigcup_{k \in \mathbb{Z} - \{1\}} \text{Ker}(\Psi_k^-) \right) \right\} \quad (10)$$

or with the energy operators $\psi_{k,i}^+$ and $\psi_{k,i}^-$ defined in (8)

$$\mathbf{s}^-(\mathbb{R}^m) = \left\{ f \in \mathbf{S}^-(\mathbb{R}^m) \mid f \notin \bigcup_{i \in [1, \dots, m]} \left(\bigcup_{k \in \mathbb{Z}} \text{Ker}(\psi_{k,i}^+(f)) \cup \left(\bigcup_{k \in \mathbb{Z} - \{1\}} \text{Ker}(\psi_{k,i}^-(f)) \right) \right) \right\} \quad (11)$$

$\text{Ker}(\cdot)$ is the notation for the kernel associated here with the operators Ψ_k^+ , Ψ_k^- , $\psi_{k,i}^+$ and $\psi_{k,i}^-$ (k in \mathbb{Z}) (see [2], Properties 1 and 2). By definition, one can state that $\mathbf{s}^-(\mathbb{R}^m) \subsetneq \mathbf{S}^-(\mathbb{R}^m)$. Following Definition 1, the *uniqueness* of the decomposition in $\mathbf{s}^-(\mathbb{R}^m)$ with the families of differential operators can be stated as:

Definition 2. [2] $\forall f$ in $\mathbf{s}^-(\mathbb{R}^m)$, $\forall v \in \mathbb{Z}^+ - \{0\}$, $\forall n \in \mathbb{Z}^+$ and $n > 1$, the families of operators $(\Psi_k^+)_{k \in \mathbb{Z}}$ and $(\Psi_k^-)_{k \in \mathbb{Z}}$ ($(\Psi_k^+)_{k \in \mathbb{Z}}$ and $(\Psi_k^-)_{k \in \mathbb{Z}} \subseteq \mathcal{F}(\mathbf{s}^-(\mathbb{R}^m), \mathbf{S}^-(\mathbb{R}^m))$) decompose uniquely $\partial_i^v f^n$ in \mathbb{R}^m , if for any family of operators $(S_k)_{k \in \mathbb{Z}} \subseteq \mathcal{F}(\mathbf{S}^-(\mathbb{R}^m), \mathbf{S}^-(\mathbb{R}^m))$ decomposing $\partial_i^v f^n$ in \mathbb{R}^m , there exists a unique couple (β_1, β_2) in \mathbb{R}^{2m} such as:

$$S_k(f) = \beta_1 \Psi_k^+(f) + \beta_2 \Psi_k^-(f), \quad \forall k \in \mathbb{Z} \quad (12)$$

Two important results shown in [2] are:

Lemma 1 For f in $\mathbf{S}^-(\mathbb{R}^m)$, the family of DEO Ψ_k^+ ($k \in \mathbb{Z}$) decomposes $\partial_i^v f^n$, $\forall v \in \mathbb{Z}^+ - \{0\}$, $n \in \mathbb{Z}^+ - \{0, 1\}$ and $i \in [1, \dots, m]$.

Theorem 1. For f in $\mathbf{s}^-(\mathbb{R}^m)$, the families of DEO Ψ_k^+ and Ψ_k^- ($k \in \mathbb{Z}$) decompose uniquely $\partial_i^v f^n$, $\forall v \in \mathbb{Z}^+ - \{0\}$, $n \in \mathbb{Z}^+ - \{0, 1\}$ and $i \in [1, \dots, m]$.

The Lemma 1 and Theorem 1 were then extended in [3] to the family of generalized operator with :

Lemma 2. For f in $\mathbf{S}_p^-(\mathbb{R}^m)$, p in \mathbb{Z}^+ , the families of generalized energy operators $\left[[\cdot]^p \right]_k^+$ ($k \in \mathbb{Z}$) decompose $\partial_i^v \left(\left[[f]^{p-1} \right]_1^+ \right)^n$ $\forall v \in \mathbb{Z}^+ - \{0\}$, $n \in \mathbb{Z}^+ - \{0, 1\}$ and $i \in [1, \dots, m]$.

Theorem 2. For f in $\mathbf{s}_p^-(\mathbb{R}^m)$, for p in \mathbb{Z}^+ , the families of generalized operators $\left[[\cdot]^p \right]_k^+$ and $\left[[\cdot]^p \right]_k^-$ ($k \in \mathbb{Z}$) decompose uniquely $\partial_i^v \left(\left[[f]^{p-1} \right]_1^+ \right)^n$ $\forall v \in \mathbb{Z}^+ - \{0\}$, $n \in \mathbb{Z}^+ - \{0, 1\}$ and $i \in [1, \dots, m]$.

$\mathbf{S}_p^-(\mathbb{R}^m)$ and $\mathbf{s}_p^-(\mathbb{R}^m)$ (p in \mathbb{Z}^+) are energy spaces in $\mathbf{S}^-(\mathbb{R}^m)$ defined in the next section.

Remark (5) One can extend the Theorem 1, Theorem 2, Lemma 1 and Lemma 2 for f^n with n in \mathbb{Z} following previous discussions in [2] (Section 3, p.74) and [3] (Section 4). n is here restricted to $\mathbb{Z}^+ - \{0,1\}$ in order to easy the whole mathematical development.

3.2. Energy Spaces in $\mathbf{S}^-(\mathbb{R}^m)$

Let us introduce the energy spaces and some properties.

Definition 3. ([1], Definition 3) The energy space $\mathbf{E}_p \subsetneq \mathbf{S}^-(\mathbb{R}^m)$, with p in \mathbb{Z}^+ , is equal to $\mathbf{E}_p = \bigcup_{v \in \mathbb{Z}^+ \cup \{0\}} \mathbf{M}_p^v$.

With $\mathbf{M}_p^v \subsetneq \mathbf{S}^-(\mathbb{R}^m)$ for v in \mathbb{Z}^+ defined as

$$\mathbf{M}_p^v = \left\{ g \in \mathbf{S}^-(\mathbb{R}^m) \mid g = \partial_i^k \left(\left[[f]^p \right]_1^+ \right)^n, \left[[f]^p \right]_1^+ \in \mathbf{S}^-(\mathbb{R}^m), k \in \mathbb{Z}^+, \right. \\ \left. \forall k \leq v, n \in \mathbb{Z}^+ - \{0\}, i \in [1, \dots, m] \right\} \tag{13}$$

The energy spaces, $\mathbf{S}_p^-(\mathbb{R}^m)$ and $\mathbf{s}_p^-(\mathbb{R}^m)$ ($p \in \mathbb{Z}^+$), cited in Lemma 2 and Theorem 2 are defined:

$$\mathbf{S}_p^-(\mathbb{R}^m) = \left\{ \mathbf{E}_p = \bigcup_{i \in \mathbb{Z}^+ \cup \{0\}} \mathbf{M}_p^i \right\} \\ \mathbf{s}_p^-(\mathbb{R}^m) = \left\{ f \in \mathbf{S}_p^-(\mathbb{R}^m) \mid f \notin \bigcup_{i \in [1, \dots, m]} \left(\bigcup_{k \in \mathbb{Z}} \text{Ker} \left(\left[[f]^p \right]_{k,i}^+ \right) \right) \right. \\ \left. \cup \left(\bigcup_{k \in \mathbb{Z} - \{1\}} \text{Ker} \left(\left[[f]^p \right]_{k,i}^- \right) \right) \right\} \tag{14}$$

Remark (6) Definition 3 does not follow completely Definition 3 in [1], because the energy space \mathbf{M}_p^v is defined here $\forall k \leq v$, and only for $k = v$ in [1].

Remark (7) In the previous definition, $\mathbf{M}_p^\infty = \{0\}$ ($\forall p \in \mathbb{Z}^+$). Also, $\mathbf{M}_p^\infty \subset \mathbf{S}_p^-(\mathbb{R}^m)$, whereas $\mathbf{M}_p^\infty \not\subset \mathbf{S}_p^-(\mathbb{R}^m)$ in [1] and [3]. The inclusion does not change Lemma 2 and Theorem 2 (i.e. $\mathbf{M}_p^\infty \not\subset \mathbf{s}_p^-(\mathbb{R}^m)$). The justification of not including this space was only based on the applications of the theory in [1] and [3] which is not justified in this work.

We can now state some properties associated with the energy spaces on $\mathbf{S}^-(\mathbb{R}^m)$.

Properties 2. $\forall v$ in \mathbb{Z}^+ , and in particular v_1, v_2 in \mathbb{Z}^+ (with $v_1 < v_2$), p in \mathbb{Z}^+ , we have the following inclusions:

- $\mathbf{M}_p^v \subsetneq \mathbf{H}^v(\mathbb{R}^m)$
- $\mathbf{M}_p^{v_2} \subsetneq \mathbf{M}_p^{v_1}$
- $\mathbf{E}_p = \bigcup_{v \in \mathbb{Z}^+ \cup \{0\}} \mathbf{M}_p^v \subsetneq \mathbf{H}^0(\mathbb{R}^m)$

Proof.

1) Let us recall the definition of the Hilbert space on \mathbb{R}^m according to **Appendix I**, Definition I.1 and Definition 1.

$$\mathbf{H}^v(\mathbb{R}^m) = \left\{ f \in L^2(\mathbb{R}^m) \mid D^\alpha f \in L^2(\mathbb{R}^m), \forall \alpha \leq v \right\} \quad (15)$$

Looking at the definition of the energy space \mathbf{M}_p^v and $\mathbf{H}^v(\mathbb{R}^m)$, one can notice the similitude. However, the multi-index derivative D^α ([21], chap. 1.1) contains also the cross-derivatives (e.g., $\frac{\partial^2}{\partial t_1 \partial t_2}$), whereas there are no cross-

derivatives in the definition of ∂_i^v at the beginning of **Appendix I**. Thus, the energy spaces \mathbf{M}_p^v ($p \in \mathbb{Z}^+$, $v \in \mathbb{Z}^+ - \{0\}$) is defined without the cross-derivatives. In addition with Properties 1, $\mathbf{S}^-(\mathbb{R}^m) \subsetneq L^2(\mathbb{R}^m)$. Thus, by definition we have the relationship $\mathbf{M}_p^v \subsetneq \mathbf{H}^v(\mathbb{R}^m)$:

2) With Remark (3), we know that for $v_1 < v_2$, $\mathbf{H}^{v_2}(\mathbb{R}^m) \subset \mathbf{H}^{v_1}(\mathbb{R}^m)$. Now, with 1), $\mathbf{M}_p^{v_1} \subsetneq \mathbf{H}^{v_1}(\mathbb{R}^m)$ and $\mathbf{M}_p^{v_2} \subsetneq \mathbf{H}^{v_2}(\mathbb{R}^m)$. Now by definition of $\mathbf{M}_p^{v_1}$ and $\mathbf{M}_p^{v_2}$, $\mathbf{M}_p^{v_1} \mathbf{H}^{v_2}(\mathbb{R}^m) = \mathbf{M}_p^{v_2}$. Finally, $\mathbf{M}_p^{v_2} \subsetneq \mathbf{M}_p^{v_1}$.

3) From Remark (3), $\mathbf{H}^0(\mathbb{R}^m) = L^2(\mathbb{R}^m)$, $\mathbf{S}^-(\mathbb{R}^m) \subset L^2(\mathbb{R}^m)$ and (by definition of the energy space) $\mathbf{E}_p = \bigcup_{v \in \mathbb{Z}^+ - \{0\}} \mathbf{M}_p^v \subsetneq \mathbf{S}^-(\mathbb{R}^m)$ ($p \in \mathbb{Z}^+$). Thus, $\mathbf{E}_p = \bigcup_{v \in \mathbb{Z}^+ - \{0\}} \mathbf{M}_p^v \subsetneq \mathbf{H}^0(\mathbb{R}^m)$ ($p \in \mathbb{Z}^+$).

Furthermore, **Appendix III** discusses the relationship between the subspaces \mathbf{M}_p^v and \mathbf{M}_{p-1}^v ($p \in \mathbb{Z}^+$). Finally, because we are studying functions and operators in subspaces of $\mathbf{S}^-(\mathbb{R}^m)$ with $\mathbf{S}^-(\mathbb{R}^m) \subset L^2(\mathbb{R}^m)$, one need to extend Proposition 1 in [1] and [3].

Proposition 1. *If for $n \in \mathbb{Z}^+$, $f^n \in \mathbf{S}^-(\mathbb{R}^m)$ and analytic; for any $(p_i, q_i) \in \mathbb{R}^2$ and $\tau_i \in [q_i, p_i]$ ($\forall i \in [1, \dots, m]$), and $\mathcal{E}(f^n)$ is analytic, where*

$$\mathcal{E}(f^n(\tau_i)) = \int_{q_i}^{\tau_i} f^n(t_i)^2 dt_i < \infty \quad (16)$$

then

$$\mathcal{E}(f^n(p_i)) = \mathcal{E}(f^n(q_i)) + \sum_{k=0}^{\infty} \partial_{t_i}^k (f^n(q_i))^2 \frac{(p_i - q_i)^k}{k!} < \infty \quad (17)$$

is a convergent series.

Proof. The proof of Proposition 1 for i equal 1 is given in [1] (p.4). The extension of the proof for the case i equal m is straightforward with the general definition for any $(p_i, q_i) \in \mathbb{R}^2$ and $\tau_i \in [q_i, p_i]$ ($\forall i \in [1, \dots, m]$).

4. Multiplicity of the Solutions in $\mathbf{S}^-(\mathbb{R}^m)$

To recall [1], a possible application of the theory of the energy operators is to look at solutions of a given partial differential equation for solutions in $\mathbf{S}^-(\mathbb{R}^m)$ of the form $\partial_i^v(f^n)$. Instead of solving the equation for specific values (e.g., boundary conditions), the work in [1] ([1], Theorem 1 and corollary) defines the concept of *multiplicity* of solutions in $\mathbf{S}^-(\mathbb{R}^m)$ ($m \in [1, 2]$) such as the study of the multiple solutions of a PDE based on the definition of the energy spaces \mathbf{E}_p

($p \in \mathbb{Z}^+$). One way to understand this concept, is to study the convergence of the development in Taylor series of the energy function associated to a nominated energy space. It was shown in [1] that taking into account additional terms of the Taylor series leads to define additional solutions of the wave equation (see Section 4 [1]). In this section, we extend this concept to $\mathbf{S}^-(\mathbb{R}^m)$ ($m \in \mathbb{N}_0$) and we reformulate the results from [1] for the solutions in the subspaces

$$\mathbf{M}_p^v \subset \mathbf{E}_p \subset \mathbf{S}^-(\mathbb{R}^m) \subset L^2(\mathbb{R}^m) \quad (p \in \mathbb{Z}^+, v \in \mathbb{Z}^+).$$

Let us define any PDEs of the form:

$$\begin{cases} \sum_{j \in \mathbb{Z}^+} \sum_{i \in [0, \dots, m]} a_{ij} \partial_i^{v_j} g = 0, \\ \forall g \in \mathbf{A}(\mathbb{R}^m) \subseteq \mathbf{S}^-(\mathbb{R}^m), \\ \forall a_{ij} \in \mathbb{R}, \quad v_j \in \mathbb{Z}^+ \end{cases} \quad (18)$$

Thus, all the solutions are here defined in $\mathbf{A}(\mathbb{R}^m) \subseteq \mathbf{S}^-(\mathbb{R}^m)$. Now, we are interested in the solutions which can be defined on the energy spaces \mathbf{E}_p ($p \in \mathbb{Z}^+$). In other words, $\mathbf{A}(\mathbb{R}^m) \cap_{p \in \mathbb{Z}^+} \mathbf{E}_p \neq \{\emptyset\}$. In particular, we choose the solution $g = 0 \in \mathbf{A}(\mathbb{R}^m) \cap_{p \in \mathbb{Z}^+} \mathbf{E}_p$. Furthermore, one can define

$g \in \mathbf{A}(\mathbb{R}^m) \cap_{p \in \mathbb{Z}^+} \mathbf{E}_p$, such as $\exists v \in \mathbb{Z}^+$ for $g \in \mathbf{A}(\mathbb{R}^m) \cap_{p \in \mathbb{Z}^+} \mathbf{M}_p^v$. In other words, $\exists f \in \mathbf{S}^-(\mathbb{R}^m)$ and $n \in \mathbb{Z}^+ - \{0\}$, such as $g = \left(\left[[f]^p \right]_1^+ \right)^n$. Now, one can

then state a general theorem of *multiplicity of solutions* based on [1]. It follows:

Theorem 3. (*Multiplicity of Solutions in \mathbb{R}^m*) If $\mathbf{A}(\mathbb{R}^m) \subseteq \mathbf{S}^-(\mathbb{R}^m)$ is a subspace of all the solutions of a nominated linear PDE. For $p \in \mathbb{Z}^+$, g is in \mathbf{E}_p . Then, g is a solution for this linear PDE if and only if:

- 1) (General condition to be a solution) $\mathbf{A}(\mathbb{R}^m) \cap \mathbf{E}_p \neq \{\emptyset\}$.
- 2) (Solutions in $\mathbf{S}^-(\mathbb{R}^m)$) $g \in \mathbf{A}(\mathbb{R}^m) \cap \mathbf{E}_p$, $\exists m \in \mathbb{R}^+$ such as $m = \sup(\mathcal{E}(g))$.
- 3) (Multiplicity of the solutions) If $g \in \mathbf{M}_p^v$ ($v \in \mathbb{Z}^+$), $\exists f \in \mathbf{S}^-(\mathbb{R}^m)$ and $n \in \mathbb{Z}^+ - \{0\}$, such as $g = \partial_i^v \left(\left[[f]^p \right]_1^+ \right)^n$ ($i \in [0, \dots, m]$) and $\forall k \geq v, k \in \mathbb{Z}^+$, $\partial_i^k \left(\left[[f]^p \right]_1^+ \right)^n \in \mathbf{A}(\mathbb{R}^m) \cap \mathbf{E}_p$.
- 4) (Superposition of solutions and energy conservation) If $F \in \mathbf{A}(\mathbb{R}^m) \cap \mathbf{E}_p$, with $F = \sum_{k \in \mathbb{Z}^+, \forall k \geq v} \partial_i^k \left(\left[[f]^p \right]_1^+ \right)^n$ such as $\partial_i^k \left(\left[[f]^p \right]_1^+ \right)^n \in \mathbf{M}_p^k$ ($i \in [0, \dots, m]$), then $\mathcal{E}(F) < \infty$.

Proof. The proof is the generalization of what was already written in [1] (see Theorem 2 in [1]) for the case m equal 1. Here is the generalization to m .

- 1) This is the definition of a solution for a nominated PDE with solutions in $\mathbf{A}(\mathbb{R}^m)$ and in the energy space \mathbf{E}_p .
- 2) $g \in \mathbf{A}(\mathbb{R}^m) \cap \mathbf{E}_p \subset L^2(\mathbb{R}^m)$, thus $\mathcal{E}(g) < \infty$. With Proposition 1, it

means that for any $(p_i, q_i) \in \mathbb{R}^2$ and $\tau_i \in [q_i, p_i]$ ($\forall i \in [1, \dots, m]$)

$$\mathcal{E}(g(\tau_i)) = \int_{q_i}^{\tau_i} g(t_i)^2 dt_i < \infty \tag{19}$$

Thus, following [18], one can define $m_i \in \mathbb{R}$ such as $m_i = \sup_{\tau_i \in [q_i, p_i]} \mathcal{E}(g(\tau_i))$ and then we define $m = \max_{i \in [1, \dots, m]} m_i$. With our notation, it is equivalent to write $m = \sup(\mathcal{E}(g))$.

3) It is sufficient to show that for $v \in \mathbb{Z}^+$, $\forall k \geq v$, $\mathbf{A}(\mathbb{R}^m) \cap \mathbf{M}_p^k \neq \{\emptyset\}$.

Now, with the definition $\mathbf{A}(\mathbb{R}^m) \cap \mathbf{E}_p \neq \{\emptyset\}$, and $\mathbf{A}(\mathbb{R}^m) \cap \mathbf{M}_p^k \neq \{\emptyset\}$. In addition, $\mathbf{M}_p^\infty = \{0\}$, $\mathbf{M}_p^\infty \subset \mathbf{M}_p^k$ ($\forall k \geq v$) and $0 \in \mathbf{A}(\mathbb{R}^m) \cap \mathbf{M}_p^k$. The interest of this statement is the function $\partial_i^v h \in \mathbf{S}^-(\mathbb{R}^m)$ such as $\exists k \in \mathbb{Z}^+$ with $k \geq v$ and $\partial_i^k h = 0$. In particular, if we introduce a numerical approximation in order to get the condition $\partial_i^k h \sim 0$. In other words,

$$\partial_i^k h \sim 0 \Leftrightarrow \left\{ \exists \epsilon \in \mathbb{R}^+, \epsilon \ll 1, \forall k \in \mathbb{Z}^+, k > 0, \text{ such as } |\partial_i^k h| \leq \epsilon \right\} \tag{20}$$

In some examples in Section 4 in [1] and Section 6 in [3], it is shown that the evanescent waves when solving the wave equation for specific solutions, is a particular example of those functions.

4) The proof follows [1] (Theorem 2). This statement is to guarantee that there is a finite sum of energy with the superposition of multiple solutions. Thus with the development in statement (2.), one can use the Minkowski inequality (e.g, [22], Theorem 202) for τ_i in $[p_i, q_i]$ ($\forall i \in [1, \dots, m]$)

$$\begin{aligned} \mathcal{E}(F(\tau_i)) &= \int_{p_i}^{\tau_i} \left| \sum_{k \in \mathbb{Z}^+, \forall k \geq v} \partial_i^k \left(\left[[f(t_i)]^p \right]_1^+ \right)^n \right|^2 dt_i \\ (\mathcal{E}(F(\tau_i)))^{0.5} &\leq \sum_{k \in \mathbb{Z}^+, \forall k \geq v} \left(\int_{p_i}^{\tau_i} \left| \partial_i^k \left(\left[[f(t_i)]^p \right]_1^+ \right)^n \right|^2 dt_i \right)^{0.5} \\ (\mathcal{E}(F(\tau_i)))^{0.5} &\leq \sum_{k \in \mathbb{Z}^+, \forall k \geq v} \left(\mathcal{E} \left(\partial_i^k \left(\left[[f(\tau_i)]^p \right]_1^+ \right)^n \right) \right)^{0.5} \\ (\mathcal{E}(F(\tau_i)))^{0.5} &\leq \sum_{k \in \mathbb{Z}^+, \forall k \geq v} m_k^{0.5} \end{aligned} \tag{21}$$

with $m_k = \sup_{\tau_i \in [q_i, p_i]} \left(\mathcal{E} \left(\partial_i^k \left(\left[[f(\tau_i)]^p \right]_1^+ \right)^n \right) \right)$. Thus, (4.) stands if and only if

$\sum_{k \in \mathbb{Z}^+, \forall k \geq v} m_k^{0.5} < \infty$. As $\forall k \in \mathbb{Z}^+$, $\forall k \geq v$, m_k is in \mathbb{R}^+ , it then exists $M = \sup \sum_{k \in \mathbb{Z}^+, \forall k \geq v} m_k^{0.5}$. One possibility is $\exists k_o$ in \mathbb{Z}^+ such as $\forall k > k_o$, then $m_k = 0$.

5. Some Applications

This section focuses on the application of the energy space theory. The first section is the study of the concept of *multiplicity of solutions* with a simple mathematical example using the wave equation. Then, the second section is

discussing the application of this concept within the Woodward effect [4] [13]

5.1. Energy Variation and Wave Equation

As a simple case of linear PDE, the wave equation with the particular solutions of the form of evanescent waves, was already discussed in Section 6 of [3] and [1]. However, it is an interesting example to apply and understand the concept of multiplicity stated in Theorem 3. From [23], the wave equation can be formulated in \mathbb{R}^2 (with t and r the time and space variables):

$$\begin{cases} \partial_r^2 g(r,t) - \frac{1}{c^2} \partial_t^2 g(r,t) = 0, \\ t \in [0, T], \quad r \in [r_1, r_2], \quad (r_1, r_2, T) \in \mathbb{R}^3, \quad r_1 < r_2 \\ t_0 \in [0, T], \quad r_0 \in [r_1, r_2] \end{cases} \quad (22)$$

c is the speed of light. Note that the values of t and r are restricted to some interval, because it is conventional to solve the equation for a restricted time interval in \mathbb{R}^+ and a specific region in space. According to the previous section, we are here interested in the solutions in the energy (sub)space \mathbf{M}_p^k , of the kind $g(r,t) = \partial_t^k \left(\left[[f]^p \right]_1^+ \right)^n (r,t)$ (n in $\mathbb{Z}^+ - \{0\}$, p in \mathbb{Z}^+ , k in \mathbb{Z}^+).

Furthermore, the relationship $\mathbf{M}_p^k \subset \mathbf{S}^-(\mathbb{R}^2) \subset L(\mathbb{R}^2)$ imposes that the solutions should be finite energy functions, decaying for large values of r and t . It was previously underlined in [1] and [3] that planar waves should be rejected, because this type of solutions does not belong to $L(\mathbb{R}^2)$. However, evanescent waves are a type of solutions included in $\mathbf{S}^-(\mathbb{R}^2)$ and considered in this work. They are here defined such as:

$$\begin{cases} f(r,t) = \text{Real} \{ A \exp(u_2 r) \exp(i(\omega t - u_1 r)) \}, \\ t \in [0, T], \quad r \in [r_1, r_2], \quad (r_1, r_2) \in \mathbb{R}^2, \quad r_1 < r_2 \end{cases} \quad (23)$$

$i^2 = -1$, u_1 and u_2 are the wave numbers, ω is the angular frequency and A is the amplitude of this wave [23]. Assuming ω and (u_1, u_2) known, one can add some boundary conditions in order to estimate u_1 , u_2 and A . Furthermore, a traveling wave solution of (19) should satisfy the dispersion relationship between u_1 , u_2 and ω [23]. However, our interest is just the general form assuming that all the parameters are known. For $p = 0$, the type of solutions in \mathbf{M}_0^k are:

$$\begin{cases} \partial_t^k f^n(r_0, t) = (i\omega n)^k f^n(r_0, t), \\ \partial_r^k f^n(r, t_0) = (n(u_2 - iu_1))^k f^n(r, t_0), \\ t \in [0, T], \quad r \in [r_1, r_2], \quad (r_1, r_2, T) \in \mathbb{R}^3, \quad r_1 < r_2 \\ t_0 \in [0, T], \quad r_0 \in [r_1, r_2], \quad n \in \mathbb{Z}^+ - \{0\}, \quad k \in \mathbb{Z}^+ - \{0\} \end{cases} \quad (24)$$

In \mathbf{M}_1^k , one can then write the type of solutions

$$\begin{aligned}
 \partial_t^k \Psi_{1,r}^+(f)(r_0, t) &= \partial_t^k \left(\left[[f(r_0, t)]^+ \right]_{1,r} \right) \\
 \partial_t^k \Psi_{1,r}^+(f)(r_0, t) &= \text{Real} \{ (i2k\omega) f^2(r_0, t) \} \\
 \partial_r^k \Psi_{1,r}^+(f)(r, t_0) &= \text{Real} \{ (2k(u_2 - iu_1)) f^2(r, t_0) \} \\
 t \in [0, T], \quad r \in [r_1, r_2], \quad (r_1, r_2, T) \in \mathbb{R}^3, \quad r_1 < r_2 \\
 t_0 \in [0, T], \quad r_0 \in [r_1, r_2], \quad n \in \mathbb{Z}^+ - \{0\}, \quad k \in \mathbb{Z}^+ - \{0\}
 \end{aligned} \tag{25}$$

Let us consider the form of solutions which propagates in a closed cavity (e.g., closed wave guide [23]). One possible solution is the evanescent wave described in (20). Now, if f and $\mathcal{E}(f)$ are analytic in \mathbb{R}^2 , with Proprsition 1 we can assume that f is finite energy (and more generally in $\mathbf{S}^-(\mathbb{R}^2)$) with a wise choice on the parameters A , u_1 , u_2 and ω . One can estimate the difference of energy in time over dt inside the cavity at a specific location r_0 (r_0 in $[r_1, r_2]$) such as

$$\begin{aligned}
 \mathcal{E}(f(r_0, T)) &= \int_0^T (f(r_0, h))^2 dh < \infty \\
 \mathcal{E}(f(r_0, T + dt)) &= \mathcal{E}(f(r_0, T)) + \sum_{k=0}^{\infty} \partial_t^k (f^2(r_0, T)) \frac{(dt)^k}{k!} < \infty \\
 \mathcal{E}(f(r_0, T + dt)) &= \mathcal{E}(f(r_0, T)) + f^2(r_0, T) dt + \sum_{k=1}^{\infty} \partial_t^{k-1} \Psi_{1,r}^+(f)(r_0, T) \\
 \mathcal{E}(f(r_0, T + dt)) &= \mathcal{E}(f(r_0, T)) + f^2(r_0, T) dt
 \end{aligned} \tag{26}$$

Here the symbol ‘ \simeq ’ means that

$$\exists \epsilon \in \mathbb{R}^+, \quad \epsilon \ll 1, \quad \forall k \in \mathbb{Z}^+, \quad k > 0 \mid \left| \partial_t^{k-1} (\Psi_{1,r}^+(f)(r_0, T)) \right| < \epsilon \mid f^2(r_0, T) \mid \tag{27}$$

Now, let us do a hypothesis that $\mathcal{E}(f(r_0, T + dt))$ increases significantly over dt modifying the approximation in (24)

$$\exists \epsilon \in \mathbb{R}^+, \quad \epsilon \ll 1, \quad \forall k \in \mathbb{Z}^+, \quad k > 1 \mid \left| \partial_t^{k-1} \Psi_{1,r}^+(f)(r_0, T) \right| < \epsilon \mid \Psi_{1,r}^+(f)(r_0, T) \mid \tag{28}$$

and then,

$$\mathcal{E}(f(r_0, T + dt)) \simeq \mathcal{E}(f(r_0, T)) + f^2(r_0, T) dt + \Psi_{1,r}^+(f)(r_0, T) \frac{dt^2}{2} \tag{29}$$

To recall that $f^2(r, t) \in \mathbf{M}_0^0$, $\partial_t f^2(r, t) \in \mathbf{M}_0^1$ and $\Psi_{1,r}^+(f)(r, t) \in \mathbf{M}_1^0$, and using Theorem 3, one can take into account solutions in those subspaces. The multiplicity of the solutions due to the variation of energy can be formulated as an approximation for taking into account additional solutions produced by the wave equation.

Remark (8): In [1], the general idea was to look for the solutions of linear PDEs in $\mathbf{S}^-(\mathbb{R})$ associated with energy subspaces $\mathbf{s}_p^-(\mathbb{R})$ ($p \in \mathbb{Z}^+$) in order to apply Theorem 1 in [1], which is here generalized in Theorem 3 for \mathbb{R}^m ($m \in \mathbb{N}^+$). The purpose was to find the subspaces reduced to $\{0\}$ when studying the convergence of the Taylor series of the energy functions. However, the redefinition of the energy subspaces \mathbf{M}_p^k within the Sobolev spaces defined

in Section 3 allows us to look for solutions in $\mathbf{S}_p^-(\mathbb{R}^m)$ in order to use Lemma 2. Because of the inclusion of the energy spaces shown in Properties 2 using the Sobolev embedding (e.g., Theorem I.1 in Appendix I) such as $\mathbf{M}_p^{k+1} \subset \mathbf{M}_p^k$ ($k \in \mathbb{Z}^+$, $p \in \mathbb{Z}^+$), $\mathbf{M}_p^\infty = \{0\} \subset \mathbf{M}_p^k$.

Definition 4. (Energy Parallax) Considering a linear PDE with some solutions in $\mathbf{A}(\mathbb{R}^m)$ such as $\mathbf{A}(\mathbb{R}^m) \cap \mathbf{S}^-(\mathbb{R}^m) \neq \{\emptyset\}$. Furthermore, if it exists p and $v \in \mathbb{Z}^+$ such as $\mathbf{A}(\mathbb{R}^m) \cap \mathbf{M}_p^v \neq \{\emptyset\}$, then we associate the energy $\mathcal{E}(f)$ for $f \in \mathbf{A}(\mathbb{R}^m) \cap \mathbf{M}_p^v$, such as one can estimate the variation

$d\mathcal{E}(f) = (\mathcal{E}(f(q+dq)) - \mathcal{E}(f(q)))dq$ over an elementary quantity dq (e.g., space or time). If $d\mathcal{E}(f)$ is not negligible ($\exists \epsilon \in \mathbb{R}^m$ such as $\epsilon \gg 1$ and $d\mathcal{E}(f) > \epsilon$), then one can consider additional solutions in $\mathbf{A}(\mathbb{R}^m) \cap \mathbf{M}_p^{v+1}$.

5.2. Variation of EM Energy Density and the Woodward Effect

In this section, the theory of energy space is applied to the possible variations of electromagnetic energy density due to, for example, skin depth effect [23] inside some conductive material. Beyond this application, the interest is to give a physical meaning of taking into account those additional solutions in various energy spaces. The second part is dedicated to the Woodward effect and the possible relationship with the variation of EM energy density in some specific settings.

5.2.1. Variation of EM Energy Density

Thus, let us formulate the variation in time of energy density (u) at the second order with a Taylor series development such as:

$$du = \partial_t u dt + \partial_t^2 u \frac{dt^2}{2} + o(dt^2) \tag{30}$$

o is the Landau notation to omit higher order quantities. Note that at the first order $\frac{du}{dt} = \partial_t u$. The higher orders term are based on the assumptions that

the EM waves inside the skin layer of the copper plate are evanescent waves and thus functions in the Schwartz space ($\mathbf{S}^-(\mathbb{R}^4)$ -with 3 dimension variables and considering also the time) [23]. As discussed before, those solutions are finite energy functions and in $L(\mathbb{R}^4)$ (i.e. following [1] and [3],

$u = \mathcal{E}(f(x_0, y_0, z_0, T)) < \infty$ at some given point in the skin layer defined by the coordinates (x_0, y_0, z_0) . Now, using the Lemma 1 and the space \mathbf{M}_0^k in Section 3, we can state in $\mathbf{S}^-(\mathbb{R}^4)$

$$\begin{aligned} \mathbf{M}_0^k &= \left\{ g \in \mathbf{S}^-(\mathbb{R}^4) \mid g = \partial_t^k f^n(x_0, y_0, z_0, t) \right. \\ &= \alpha_n \partial_t^{k-1} f^{n-2}(x_0, y_0, z_0, t) (\Psi_1^+(f(x_0, y_0, z_0, t))), \\ &\left. f \in \mathbf{S}^-(\mathbb{R}^4), n \in \mathbb{Z}^+ - \{0\}, \alpha_n \in \mathbb{R}, z_0 \in [0, L], (x_0, y_0) \in [0, a]^2 \right\} \end{aligned} \tag{31}$$

Here f is either the electric or magnetic field (i.e. the absolute norm of \vec{E}

and \bar{B} respectively). With the concept of *multiplicity of solutions* (e.g., Theorem 3). If g is a general solution of some linear PDEs, then f^n can be identified as a special form of the solution (conditionally to its existence).

Now considering the wave equation, the electric field and magnetic field are solutions and belong to the subspace M_0^k and associated with the variation of energy density $\partial_t u$. Furthermore, we can consider the solutions in M_0^1 associated with the variation of energy density $\partial_t^2 u$, which can be explained with the concept of *multiplicity of solutions*. The solutions of interest in M_0^1 are for the electric field $g = \partial_t E$ and the magnetic field $g = \partial_t B$. The Taylor Series development of the energy of (for example) the electric field on a nominated position in space (i.e., x_0, y_0, z_0) and in an increment of time dt :

$$\begin{aligned} \mathcal{E}(E(x_0, y_0, z_0, T + dt)) &= \mathcal{E}(E(x_0, y_0, z_0, T)) + \sum_{k=0}^{\infty} \partial_t^k (E^2(x_0, y_0, z_0, T)) \frac{(dt)^k}{k!} < \infty \\ d\mathcal{E}(E(x_0, y_0, z_0, T + dt)) &= \sum_{k=0}^{\infty} \partial_t^k (E^2(x_0, y_0, z_0, T)) \frac{(dt)^k}{k!} \end{aligned} \quad (32)$$

Finally one can write the relationship with the energy density following (26) and the previous Taylor series development for the electric and magnetic field:

$$\begin{aligned} &0.5 \left(\epsilon_0 \frac{d\mathcal{E}(E(x_0, y_0, z_0, T + dt))}{dt} + \frac{1}{\mu_0} \frac{d\mathcal{E}(B(x_0, y_0, z_0, T + dt))}{dt} \right) \\ &= 0.5 \left(\epsilon_0 E^2(x_0, y_0, z_0, T) + \frac{1}{\mu_0} B^2(x_0, y_0, z_0, T) \right) + \partial_t u \frac{dt}{2} + \partial_t^2 u \frac{dt^2}{6} + o(dt^2) \end{aligned} \quad (33)$$

Therefore, taking into account the second order term of the energy density $\partial_t^2 u$ means that additional solutions should also be considered in the EM modeling. Note that in **Appendix IV**, we are taking an example of evanescent waves inside a copper wall (i.e. skin depth effect [23]) and try to give further meaning to the consideration of higher order derivatives of the EM energy density where the additional solutions are defined with the energy spaces (e.g., $\partial_t E$ and $\partial_t B$ in M_0^1).

5.2.2. Derivation of the Woodward Effect Using the Electromagnetic Energy Density

This section focuses on the derivation of the Woodward effect created in a asymmetric EM cavity (i.e. frustum) due to EM waves reflected on the cavity's wall. Thus, the assumption is that the EM energy density variation results from the evanescent waves taking place in the skin depth of the asymmetric EM cavity's walls.

1) Assumptions with the energy momentum relationship

When the Woodward effect was established in [4] [13], the authors implicitly assumed the rest mass of the piezoelectric material via the famous Einstein's relation in special relativity $\mathcal{E} = mc^2$ (\mathcal{E} the rest energy associated with the rest mass m) and its variation via electrostrictive effect.

Here, the system is the asymmetric EM cavity. The rest mass is all the particles

within it at time t_0 when no charges are on the cavity's walls. It excludes the photons considered with a null mass. Thus, the main assumption is that the EM excitation on the walls creates electric charges (*i.e.* electrons) which makes the rest mass varying with time. This assumption is the same as the mass variation of a capacitor between the charge and discharge times [24]. It allows us to state the variation of rest energy such as:

$$d\mathcal{E} = \mathcal{E}(t + dt) - \mathcal{E}(t) = (m(t + dt) - m(t))c^2 = dmc^2 \tag{34}$$

Finally, the variation of rest energy $d\mathcal{E}$ is assumed to be equal to the variation of EM energy density (du) resulting from the charges within the skin depth of the walls. We neglect any electrostrictive effects compared to the variation of EM energy density.

Note that at the particle level, the rest mass should satisfy the energy momentum relationship (u_e) for a free body in special relativity [25]:

$$u_e^2 = (pc)^2 + (m_e c^2)^2$$

$$p = v \frac{u_e}{c^2} \tag{35}$$

with p the momentum and m_e the rest mass of the particle associated with the total energy u_e . The particle is accelerated via the Lorentz force applied to the whole cavity with obviously $v \ll c$. Thus, we have also the relationship $p^2 < (u_e/c)^2$. In the remainder, we also use the elementary variation δ which becomes d for an infinitesimally small variation.

2) Derivation of the Woodward effect and relationship with EM energy density

If we define the mass density such as $\rho = m/V$, then from [13], one can write the elementary mass variation per unit of volume

$$\delta\rho = \frac{\delta m}{V} \sim d\rho \quad (\text{infinitesimally small variation})$$

$$d\rho = \frac{1}{4\pi G} \left[\frac{1}{\rho} \partial_i^2 \rho - \frac{1}{\rho^2} (\partial_i \rho)^2 \right] \tag{36}$$

Let us define the the rest energy $\mathcal{E} = \rho c^2$, then

$$d\rho = \frac{1}{4\pi G} \left[\frac{1}{\rho c^2} \partial_i^2 \mathcal{E} - \frac{1}{(\rho c^2)^2} (\partial_i \mathcal{E})^2 \right]$$

$$d\rho = \frac{1}{4\pi G} \left[\frac{1}{\mathcal{E}} \partial_i^2 \mathcal{E} - \frac{1}{(\mathcal{E})^2} (\partial_i \mathcal{E})^2 \right] \tag{37}$$

In some particular cases such as an EM cavity, we assume that the variation in time of the rest energy is equal to the variation of EM energy density u (*i.e.* $\partial_i \mathcal{E} \approx \partial_i u$), but the rest energy is much bigger than the EM energy density $\mathcal{E} \gg u$. It allows then to state the relationship between the Woodward effect and the EM energy density

$$d\rho = \frac{1}{4\pi G} \left[\frac{1}{\mathcal{E}} \partial_i^2 u - \frac{1}{(\mathcal{E})^2} (\partial_i u)^2 \right] \tag{38}$$

The EM energy density u follows the general definition of the sum of energy density from the electric (u_E) and magnetic (u_B) fields [23]. Finally, (38) can be seen as the definition of the EMG coupling.

6. Conclusions

This work generalizes in the Schwartz space $\mathbf{S}^-(\mathbb{R}^m)$, the framework on conjugate Teager-Kaiser energy operators established in [2] and [3] for the case m in [1,2]. The concept of *multiplicity of solutions* defined in [1] is also redefined here in Theorem 3. However, this concept uses the notion of energy spaces (\mathbf{M}_p^v ($p \in \mathbb{Z}^+$, $v \in \mathbb{Z}^+$), subspaces of $\mathbf{S}^-(\mathbb{R}^m)$ defined previously in [1] and [3]. In order to generalize their definition as subspaces of $\mathbf{S}^-(\mathbb{R}^m)$, the theory has been extended to some properties on the Hilbert spaces ($\mathbf{H}_1^v(\mathbb{R}^m)$) on $L^2(\mathbb{R}^m)$. In particular, we show in Properties 2 that $\mathbf{M}_{p_2}^v \subsetneq \mathbf{M}_{p_1}^v$ ($v_1 < v_2$) and the inclusion $\mathbf{M}_{p_1}^v \subsetneq \mathbf{H}_1^v(\mathbb{R}^m) \subsetneq L^2(\mathbb{R}^m)$.

The concept of *multiplicity of solutions* focuses on, generally speaking, looking for solutions of a given linear PDE specifically in the energy spaces. In this way, it is not following the classical way of solving a linear PDE with boundary conditions. Three examples illustrate this concept. The first one investigates some type of solutions (e.g., evanescent waves) of the wave equation when analysing the Taylor series development of the energy function associated with an evanescent wave. We then formulate another concept: the *energy parallax*. It is defined mathematically in Definition 4. Under some specific circumstances (e.g., the energy function exists), we show that the variations of energy locally in a predefined system, should lead to include additional solutions in the energy spaces with higher order v (in \mathbb{Z}^+). The second example is based on the local variations of EM energy density, which allows to define waves which are first order derivative of the EM field. This example is further explored in **Appendix IV**. Finally, the last example is the derivation of the Woodward effect with some strong hypothesis in order to include the EM energy density in the specific case of asymmetric EM cavity. We introduce in the Woodward effect, the first and second order derivative of the EM energy density, which can be interpreted such as a theoretical definition of an Electromagnetic and Gravitational coupling.

Acknowledgements

The author would like to acknowledge the important discussions with Dr. José Rodal and Prof. Heidi Fearn (California State University Fullerton, physics department) on the Woodward effect and its derivation from general relativity. In addition, we thank Prof. Paul Jolissaint (Université de Neuchâtel, Institute of Mathematics) for his kind advices on the Sobolev spaces, and Prof. Marc

Troyanov together with Dr. Luigi Provenzano (Ecole Polytechnique Fédérale de Lausanne, Institute of Mathematics) for the corrections on the Sobolev spaces and the Schwartz space. Finally, we acknowledge the constructive comments from the anonymous reviewers improving this work.

References

- [1] Montillet, J.P. (2017) *Bulletin of Mathematical Analysis and Applications*, **9**, 134-150. <http://bmathaa.org/repository/docs/BMAA9-1-13.pdf>
- [2] Montillet, J.P. (2013) *Acta Applicandae Mathematicae*, **129**, 61-80.
- [3] Montillet, J.P. (2015) *Acta Applicandae Mathematicae*, **140**.
<https://doi.org/10.1007/s10440-014-9978-9>
- [4] Woodward, J.F. (2001) *Foundations of Physics*, **31**, 819.
<https://doi.org/10.1023/A:1017500513005>
- [5] Kaiser, J.F. (1990) On a Simple Algorithm to Calculate the “Energy” of a Signal. *Proceedings of IEEE Conference on Acoustics, Speech, and Signal Processing*, Vol. 1. <https://doi.org/10.1109/ICASSP.1990.115702>
- [6] Maragos, J.F. and Potamianos, A. (1995) *IEEE Signal Processing Letters*, **2**, 152-154.
<https://doi.org/10.1109/97.404130>
- [7] Dunn, R.B., Quatieri, T.F. and Kaiser, J.F. (1993) Detection of Transient Signals using the Energy Operator. *Proceedings of IEEE Conference on Acoustics, Speech, and Signal Processing*, Minneapolis, 27-30 April 1993, Vol. 3, 145-148.
- [8] Bovik, A.C., Havlicek, J.P. and Desai, M.D. (1993) Theorems for Discrete Filtered Modulated Signals. *Proceedings of IEEE Conference on Acoustics, Speech, and Signal Processing*, Minneapolis, 27-30 April 1993, Vol. 3, 153-156.
- [9] Cexus, J.C., Boudraa, A., Ardeyeh, F.H. and Diop, E.H.S. (2010) 2D Cross-ΨB-Energy Operator for Images Analysis. *Proceedings of International Symposium on Communications, Control and Signal Processing*, Limassol, 3-5 March 2010, 1-4.
- [10] Montillet, J.P. (2010) *International Mathematical Forum*, **5**, 2387-2400.
<http://www.m-hikari.com/imf-2010/45-48-2010/montilletIMF45-48-2010.pdf>
- [11] Hunter, J.K. (2009) Lecture Notes, Chapter 5.
https://www.math.ucdavis.edu/~hunter/m218a_09/ch5A.pdf
- [12] Fearn, H. (2015) *Journal of Modern Physics*, **6**, 260-272.
- [13] Woodward, J.F. (2004) *AIP Conference Proceedings*, **699**, 1127.
<https://doi.org/10.1063/1.1649682>
- [14] Adams, R. and Fournier, J. (2003) Sobolev Spaces. Elsevier Academic Press.
- [15] Johnson, S.G. (2015) Saddle-Point Integration of C “Bump” Functions.
<https://arxiv.org/abs/1508.04376>
- [16] Keyl, M., Kiukas, J. and Werner, R.F. (2016) *Reviews in Mathematical Physics*, **28**, Article ID: 1630001. <https://doi.org/10.1142/S0129055X16300016>
- [17] Folland, G.B. (1999) Real Analysis: Modern Techniques and Their Applications. Wiley-Interscience Series of Texts, Monographs and Tracts.
- [18] Hunter, J.K. (2012) Introduction to Real Analysis. Lecture Notes, Chapter 7.
https://www.math.ucdavis.edu/~hunter/m125a/intro_analysis_ch7.pdf
- [19] Reiter, M. and Schuster, A. (2008) Fourier Transform and Sobolev Spaces. Lecture Notes, Summer Term.

- http://www.mat.univie.ac.at/~stein/lehre/SoSem08/sobolev_fourier.pdf
- [20] Van den Ban, E. and Crainic, M. (2013) Analysis on Manifolds, Lecture 4: Fourier Transforms.
https://www.staff.science.uu.nl/~ban00101/anman2013/anman2013_ch4.pdf
- [21] Saint Raymond, X. (1991) Elementary Introduction to the Theory of Pseudo Differential Operators. CRC Press, Boca Raton.
- [22] Hardy, G.H., Littlewood, J.E. and Plya, G. (1952) Inequalities. Cambridge University Press, Cambridge.
- [23] Petit, R. (1993) Ondes Electromagnetiques en Radioélectricité et en Optique, Masson.
- [24] Porcelli, E.B. and Filho, V.S. (2016) *Physics Essays*, **29**.
<https://doi.org/10.4006/0836-1398-29.1.002>
- [25] Moller, C. (2011) The Theory of Relativity. Nabu Press.
- [26] Evans, L.C. (2010) Partial Differential Equations. American Mathematical Society.
<https://doi.org/10.1090/gsm/019>
- [27] Feynman, R. (1964) The Feynman Lectures on Physics.
<http://www.feynmanlectures.caltech.edu/>
- [28] Vinogradov, I.M. (1977) Encyclopedia of Mathematics. Kluwer Academic Publishers.

Appendix I: Generalities on Sobolev Spaces

A Sobolev space is a vector space of functions equipped with a norm that is a combination of L^p -norms of the function itself and its derivatives up to a given order. Intuitively, a Sobolev space is a space of functions with sufficiently many derivatives for some application domain, such as partial differential equations, and equipped with a norm that measures both the size and regularity of a function. Sobolev spaces are named after the Russian mathematician Sergei Sobolev.

Definition I.1. [14] Let $\Omega \subseteq \mathbb{R}^m$ ($m \in \mathbb{N}^+$) be open. The Sobolev space $W^{k,p}(\Omega)$ ($k \in \mathbb{N}$, $p \in [1, \infty]$) is defined as:

$$W^{k,p}(\Omega) = \left\{ f \in L^p(\Omega) \mid D^\alpha f \in L^p(\Omega), \forall \alpha \leq k \right\} \quad (39)$$

with $D^\alpha f$ the α -th partial derivative in multi index notation,

$D^\alpha f = \frac{\partial^{|\alpha|} f}{\partial t_1^{\alpha_1} \dots \partial t_n^{\alpha_n}}$. The Sobolev space $W^{k,p}(\Omega)$ is the space of all locally

integrable functions f in Ω such as their partial derivatives $D^\alpha f$ exist in the weak sense for all multi index $\alpha \leq k$ and belongs to $L^p(\Omega)$ (i.e. $f_{L^p} < \infty$) ([26], chap. 5). If f lies in $W^{k,p}(\Omega)$, we define the $W^{k,p}$ norm of f by the formula

$$f_{W^{k,p}(\Omega)} = \sum_{|\alpha| \leq k} D^\alpha f_{L^p(\Omega)} \quad (40)$$

Now, let us introduce the Fourier transform $\mathcal{F}: L^1(\mathbb{R}^m) \rightarrow \mathcal{C}_b(\mathbb{R}^m)$ as in [19]

$$\mathcal{F}(f) = \int_{\Omega} f(x) e^{-ix \cdot \xi} dx = \mathcal{F}(f)(\xi) \quad (41)$$

Here $\mathcal{C}_b(\mathbb{R}^m)$ is the space of bounded and continuous functions in \mathbb{R}^m [17]. Note that \cdot is the scalar product (with x and ξ in \mathbb{R}^m). One can then define the Sobolev spaces for $\Omega = \mathbb{R}^m$, $W^{k,p}(\mathbb{R}^m)$ using the Bessel potentials and the Fourier transform such as [14] or [17] (chap. 9):

$$W^{k,p}(\mathbb{R}^m) = H^{k,p}(\mathbb{R}^m) := \left\{ f \in L^p(\mathbb{R}^m) \mid \mathcal{F}^{-1} \left[(1 + \xi^2)^{k/2} \mathcal{F}(f) \right] \in L^p(\mathbb{R}^m) \right\} \quad (42)$$

The Bessel potential spaces are defined when replacing k by any real number s . They are Banach spaces and, for the special case $p = 2$, Hilbert spaces. Now, one can state an important result with Sobolev spaces [14]

Theorem I.1.: $W^{k,p}(\mathbb{R}^m) \subseteq W^{l,q}(\mathbb{R}^m)$, whenever $k > l \geq 0$ and $1 \leq p < q < \infty$ are such that $(k - l)p < m$

Proof. The proof of this theorem is rather long and technically delicate which is not our focus. Readers interested in this matter should refer to [14] [26] (Chap. 5)

Appendix II: Possible Interpretation of the Energy Parallax in Modern Physics

In Section 4, we define mathematically the notion of *multiplicity of solutions* for a given PDE. Through the various examples in Section 5, we define the concept

of *energy parallax*. The general meaning is that additional solutions should be taken into account when varying the amount of energy. Those solutions should be defined based on the associated energy spaces (e.g., \mathbf{E}_p , $p \in \mathbb{Z}^+$). Now, if we replace this concept in modern physics, what is the meaning behind it?

In modern physics, *Energy* is a global concept across the whole science. The definition varies with for example kinetic energy and potential energy in classical mechanics. It relates respectively to the object's movement through space and function of its position within a field [27]. Chemical energy can be defined broadly such as the electrical potential energy among atoms and molecules. In quantum mechanics, energy is defined in terms of energy operators (e.g., Hamiltonian) as a time derivative of the work function. It allows to define particles at nominated energy levels associated with an EM waves emitted at frequencies defined by the Planck's relation. In General Relativity, energy results from the product of a varying mass and the square of the speed of light. Energy can describe the behavior of a system of two particles (and more). For example, the electron-positron annihilation in which rest mass (invariant mass) is destroyed. At the opposite, the inverse process (creator) in which the rest mass of the particle is created from energy of two (or more) annihilating photons [28].

Energy parallax is here defined such as the concept of using additional wave functions. For example in Section 5.2.2 increasing the higher order derivatives of the EM energy density leads to the consideration of additional waves. The energy parallax concept can then help us to state that those additional waves are additional excited photons that we must take into account to vary the EM energy density.

Appendix III: Discussion on the Possible Relationship between the Energy Spaces \mathbf{M}_p^v and \mathbf{M}_{p+1}^{v-1}

This section follows the development in Section 3.2 and especially Properties 2. First, $\forall p \in \mathbb{Z}^+$, $\mathbf{M}_{p+1}^v \cap \mathbf{M}_p^v \neq \{\emptyset\}$, because $0 \in \mathbf{S}^-(\mathbb{R}^m)$, and $(\forall p \in \mathbb{Z}^+, v \in \mathbb{Z}^+) 0 \in \mathbf{M}_{p+1}^v$. Thus, $0 \in \mathbf{M}_{p+1}^v \cap \mathbf{M}_p^v$.

To recall Definition 2 and Lemma 2, $\partial_i^v \left(\left[[f]^p \right]_1^+ \right)^n$ can be decomposed with the family of energy operators $\left(\left[[\cdot]^{p+1} \right]_k^+ \right)_{k \in \mathbb{Z}}$ ($\forall n \in \mathbb{Z}^+ - \{0, 1\}$, $i \in [1, \dots, m]$, $p \in \mathbb{Z}^+$, $v \in \mathbb{Z}^+ - \{0\}$). Thus, one can write ($l < v$):

$$\partial_i^v \left(\left[[f]^p \right]_1^+ \right)^n = \sum_{j=0}^{v-1} \binom{v-1}{j} \partial_i^{v-1-j} \left(\left[[f]^p \right]_1^+ \right)^{n-l} \sum_{u=-N_j}^{N_j} C_u \left[\left[\partial_i^u f \right]^{p+1} \right]_1^+ \quad (43)$$

Thus, for $n > 1$, Lemma 2 allows to state that $\mathbf{M}_{p+1}^v \cap \mathbf{M}_p^v = \{ \mathbf{M}_p^{v,n>1} \}$, with $\mathbf{M}_p^{v,n>1}$ the subspace of \mathbf{E}_p , but restricted for $n \in \mathbb{Z}^+$ and $n > 1$.

Furthermore, let us define the space $\mathbf{s}_p^{-,*}(\mathbb{R}^m)$:

$$\mathbf{s}_p^{-,*}(\mathbb{R}^m) = \left\{ f \in \mathbf{S}_p^-(\mathbb{R}^m) \mid f \notin \bigcup_{i \in [1, \dots, m]} \left(\bigcup_{k \in \mathbb{Z}} \text{Ker} \left(\left[[f]^p \right]_{k,i}^+ \right) \right) \right\} \quad (44)$$

Note that $\mathbf{M}_p^\infty \not\subseteq \mathbf{s}_p^{v,*}(\mathbb{R}^m)$, but the bump functions [15] are included in $\mathbf{s}_p^{v,*}(\mathbb{R}^m)$. We can also recall the discussion on $n=1$ in [1] and [3], with the definition

$$\left\{ \forall f \in \mathbf{s}_p^{v,*}(\mathbb{R}^m), p \in \mathbb{Z}^+ \mid \exists g \in \mathbf{S}^-(\mathbb{R}^m), g = \frac{1}{\left(\left[[f]^p\right]_1^+\right)^n}, \forall n \in \mathbb{Z}^+, n > 1 \right\} \quad (45)$$

On can also state that $\partial_i^k \left(\left[[f]^p\right]_1^+\right) = \partial_i^k \left(\frac{\left(\left[[f]^p\right]_1^+\right)^3}{\left(\left[[f]^p\right]_1^+\right)^2}\right)$ ($k \in \mathbb{Z}^+$) and use the

Leibniz’s rule for derivations in order to expand the multiple derivatives or the decomposition stated in Lemma 2. If we call $\mathbf{M}_p^{v,*}$ ($p \in \mathbb{Z}^+$), the subspaces of $\mathbf{s}_p^{v,*}(\mathbb{R}^m)$. For all g_1 in $\mathbf{M}_p^{v,*}$ can be written as a non linear sum of g_2 in $\mathbf{M}_{p+1}^{v,*}$. Finally, we can conclude that $\mathbf{M}_p^{v,*} \subsetneq \mathbf{M}_{p+1}^{v,*}$. With the specific extension of \mathbf{M}_p^v to the case $n=1$, we can also conclude $\mathbf{M}_p^v \subsetneq \mathbf{M}_{p+1}^v$. In addition, $\mathbf{s}_p^{v,*}(\mathbb{R}^m) \subsetneq \mathbf{s}_{p+1}^{v,*}(\mathbb{R}^m)$ by definition.

Appendix IV: Consequences in Terms of EM Theory

We are taking the example of the variation of EM energy density inside a copper wall due to planar waves reflecting and refracting on it [23]. To recall Section 5.2, the EM field is now including $(\mathbf{E}, \delta\mathbf{E})$ and $(\mathbf{B}, \delta\mathbf{B})$, contribution of the subspaces M_0^0 and M_0^1 respectively when using the concept of multiplicity of the solutions (*i.e.* Theprem 3) for the higher order derivatives of the energy density (see (26)). We call the total EM field \mathbf{E}_{tot} and \mathbf{B}_{tot} inside the copper plate (skin layer) with associated permittivity ϵ and permeability μ . They are solutions of the Maxwell equations:

$$\left. \begin{aligned} \nabla \cdot \mathbf{E}_{tot} &= \frac{\rho_{tot}}{\epsilon}, \\ \nabla \times \mathbf{E}_{tot} &= -\partial_t \mathbf{B}_{tot}, \\ \nabla \cdot \mathbf{B}_{tot} &= 0, \\ \nabla \times \mathbf{B}_{tot} &= \mu\epsilon\partial_t \mathbf{E}_{tot} + \mu\mathbf{j}, \end{aligned} \right\} \quad (46)$$

with the principle of charge conservation:

$$\partial_t \rho_{tot} + \nabla \cdot \mathbf{j} = 0 \quad (47)$$

Now, the variation of energy density (26) together with the equation of charge conservation is formulated such as:

$$\frac{du}{dt} + \nabla \cdot \mathbf{P}_{tot} = \nabla \cdot \mathbf{E}_{tot} \quad (48)$$

$\mathbf{P}_{tot} = \frac{\mathbf{E}_{tot} \times \mathbf{B}_{tot}}{\mu}$ is the Poynting vector. Now, writing $\mathbf{E}_{tot} = \mathbf{E} + \delta\mathbf{E}$, $\mathbf{B}_{tot} = \mathbf{B} + \delta\mathbf{B}$ and δ is the first derivative in time (∂_t) (*i.e.* solutions in M_0^1),

then following [23]

$$(\mathbf{E} + \partial_t \mathbf{E}) \cdot \mathbf{j} = (\mathbf{E} + \partial_t \mathbf{E}) \cdot \left[\frac{1}{\mu} \nabla \times (\mathbf{B} + \partial_t \mathbf{B}) - \epsilon \partial_t (\mathbf{E} + \partial_t \mathbf{E}) \right] \quad (49)$$

using the equalities $\nabla \cdot (\mathbf{E} \times \mathbf{B}) = \mathbf{B} \cdot \nabla \times \mathbf{E} - \mathbf{E} \cdot \nabla \times \mathbf{B}$ and the Maxwell equation $\nabla \times \mathbf{E} = -\partial_t \mathbf{B}$, $\nabla \times \partial_t \mathbf{E} = -\partial_t^2 \mathbf{B}$ the previous equation reduces to:

$$\begin{aligned} & \mathbf{E} \cdot \mathbf{j} + \nabla \cdot \left(\frac{\mathbf{E} \times \mathbf{B}}{\mu} \right) + \partial_t u + \partial_t \mathbf{E} \cdot \mathbf{j} + \nabla \cdot \left(\frac{\partial_t \mathbf{E} \times \partial_t \mathbf{B}}{\mu} \right) + \partial_t^2 u \\ & + \nabla \cdot \left(\frac{\partial_t \mathbf{E} \times \mathbf{B}}{\mu} \right) + \nabla \cdot \left(\frac{\mathbf{E} \times \partial_t \mathbf{B}}{\mu} \right) + \frac{\partial \mathbf{B} \cdot \partial \mathbf{B}}{\mu} + \epsilon \partial_t \mathbf{E} \cdot \partial_t \mathbf{E} = 0 \end{aligned} \quad (50)$$

We can separate in three groups,

$$\left. \begin{aligned} \partial_t u + \nabla \cdot \left(\frac{\mathbf{E} \times \mathbf{B}}{\mu} \right) &= -\mathbf{j} \cdot \mathbf{E} \\ \partial_t^2 u + \nabla \cdot \left(\frac{\partial_t \mathbf{E} \times \mathbf{B}}{\mu} \right) + \nabla \cdot \left(\frac{\mathbf{E} \times \partial_t \mathbf{B}}{\mu} \right) &= -\mathbf{j} \cdot \partial_t \mathbf{E} \\ \nabla \cdot \left(\frac{\partial_t \mathbf{E} \times \partial_t \mathbf{B}}{\mu} \right) &= -\frac{\partial_t \mathbf{B} \cdot \partial_t \mathbf{B}}{\mu} - \epsilon \partial_t \mathbf{E} \cdot \partial_t \mathbf{E} \end{aligned} \right\}$$

The Poynting vector is defined as $\mathbf{P} = \frac{\mathbf{E} \times \mathbf{B}}{\mu}$ and its derivative

$$\partial_t \mathbf{P} = \frac{\partial_t \mathbf{E} \times \mathbf{B}}{\mu} + \frac{\mathbf{E} \times \partial_t \mathbf{B}}{\mu}.$$

Thus, the second order term of the energy density is the contribution of the EM field generated by $\partial_t \mathbf{E}$ and $\partial_t \mathbf{B}$ is:

$$\left. \begin{aligned} \partial_t u + \nabla \cdot \mathbf{P} &= -\mathbf{j} \cdot \mathbf{E} \\ \partial_t^2 u + \nabla \cdot (\partial_t \mathbf{P}) &= -\mathbf{j} \cdot \partial_t \mathbf{E} \\ \nabla \cdot \left(\frac{\partial_t \mathbf{E} \times \partial_t \mathbf{B}}{\mu} \right) &= -\frac{\partial_t \mathbf{B} \cdot \partial_t \mathbf{B}}{\mu} - \epsilon_0 \partial_t \mathbf{E} \cdot \partial_t \mathbf{E} \end{aligned} \right\}$$

The last line is the contribution from only the fields $\partial_t \mathbf{E}$ and $\partial_t \mathbf{B}$.

Finally, the creation of the wave defined by the EM field $(\partial_t \mathbf{E}, \partial_t \mathbf{B})$ means that some material properties may allow to create two type of EM waves namely (\mathbf{E}, \mathbf{B}) and $(\partial_t \mathbf{E}, \partial_t \mathbf{B})$.

Curvature Energy and Their Spectrum in the Spinor-Twistor Framework: Torsion as Indicium of Gravitational Waves

Francisco Bulnes¹, Yuri Stropovskiy², Igor Rabinovich²

¹Research Department in Mathematics and Engineering, TESCHA, IINAMEI, Chalco, Mexico

²Mathematics Department, Lomonosov Moscow State University, Moscow, Russia

Email: francisco.bulnes@tesch.edu.mx

How to cite this paper: Bulnes, F., Stropovskiy, Y. and Rabinovich, I. (2017) Curvature Energy and Their Spectrum in the Spinor-Twistor Framework: Torsion as Indicium of Gravitational Waves. *Journal of Modern Physics*, 8, 1723-1736.
<https://doi.org/10.4236/jmp.2017.810101>

Received: August 3, 2017

Accepted: September 9, 2017

Published: September 12, 2017

Copyright © 2017 by authors and Scientific Research Publishing Inc.

This work is licensed under the Creative Commons Attribution International License (CC BY 4.0).

<http://creativecommons.org/licenses/by/4.0/>



Open Access

Abstract

The twistor kinematic-energy model of the space-time and the kinematic-energy tensor as the energy-matter tensor in relativity are considered to demonstrate the possible behavior of gravity as gravitational waves that derive of mass-energy source in the space-time and whose contorted image is the spectrum of the torsion field acting in the space-time. The energy of this field is the energy of their second curvature. Likewise, it is assumed that the curvature energy as spectral curvature in the twistor kinematic frame is the curvature in twistor-spinor framework, which is the mean result of this work. This demonstrates the lawfulness of the torsion as the indicium of the gravitational waves in the space-time. A censorship to detect gravitational waves in the space-time is designed using the curvature energy.

Keywords

Censorship Condition, Contorted Surface, Curvature Energy, Gravitational Waves, Matter-Energy Tensor, 3-Dimensional Sphere, Spinor Fields, Twistor Kinematic-Energy Model, Weyl Curvature

1. Introduction

The twistor kinematic energy model could establish to the future-null-infinity in the space-time, a quasi-local matter model represented through gravitational waves of cylindrical type considering the condition on the spinor fields respective, in the null-infinity. Here, is obtained the asymptotical flat space-time far away of the mass-energy source.

We consider the Penrose's definition of the kinematic twistor associated to a

2-surface in a general curved space when the total momentum of energy and angular momentum to a system in special relativity and in linearized general relativity can be characterized geometrically. Of fact, the geometrical evidence of torsion through a contorted surface is wanted.

We consider a source as total charge depending of k^a , (Killing vector) of the Minkowski space background, modeled this as $\mathbb{M} \cong S^2 \otimes C^2 \otimes M$, which has an important analytic system of twistor solution in the same space-time $M \cong S^+ \oplus S^-$. Then their system has a complex 4-dimensional solutions family ($\cong C^2$) and the family defines the 2-surface twistor space $\mathbb{T}(S)$.

But, in a surface of arbitrary genus g , and of index $4(1-g)$, the solution is a general twistor solution, which can be given though a model problem between bosonic fields deduced of the dual problem given by the relation:

$$A_{\alpha\beta} I^{\beta\gamma} \Sigma_{\gamma\alpha} = A_{\alpha'\gamma} I^{\beta'\gamma'} \Sigma_{\gamma'\alpha'}, \tag{1}$$

to the energy-matter tensors T^{ab} , and the integral solution given to the kinematic tensor $A_{\alpha\beta}$, through the energy-matter tensor,

$$A_{\alpha\beta} Z_1^\alpha Z_2^\beta = \frac{1}{4\pi G} \int_{\Sigma} R_{abcd} f^{ab} d\sigma^{cd} = \int_{\Sigma} T_{ab} k^a d\sigma^b, \tag{2}$$

The exhibition of the kinematic tensor happens when the special surface inside space-time background \mathbb{M} , results to be the product $S^+ \otimes S^-$, of the twistor 2-surface $\mathbb{T}(S^1)$, and also (2) defines a kinematic twistor tensor $A_{\alpha\beta}$, as element of this symmetrized product of two 2-surfaces

$A_{\alpha\beta} \in (\mathbb{T}(S) \otimes \mathbb{T}(S))^*$, which is a twistor space of (valence-2) and symmetric dual twistor.

Proposition 1.1. The twistor kinematic tensor $A_{\alpha\beta}$, is an element in duality of the energy-mass tensor T^{ab} .

We observe the following figure establishing the duality signed in the proposition 1.1. (see **Figure 1**).

Proof. Their demonstration is given considering the relation $A_{\alpha\beta} I^{\beta\gamma} \Sigma_{\gamma\alpha} = A_{\alpha'\gamma} I^{\beta'\gamma'} \Sigma_{\gamma'\alpha'}$, where the second member can be had as a spinor using the integral (2):

$$A_{\alpha\beta} Z_1^\alpha Z_2^\beta = \frac{1}{4\pi G} \int R_{ABcd} \omega_1^A \omega_2^B d\sigma^{cd}, \tag{3}$$

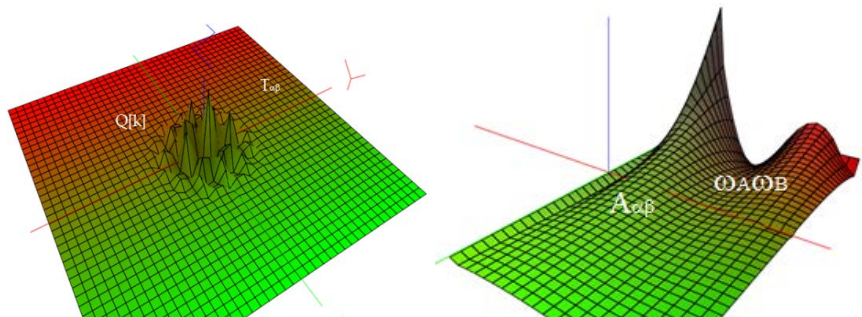


Figure 1. Duality between tensors $A_{\alpha\beta}$, and T^{ab} .

which, using the spinor framework [1] [2] inside the integral (3) we have:

$$A_{\alpha\beta}Z_1^\alpha Z_2^\beta = \frac{1}{4\pi G} \int \{(\phi_{01} - \psi_1)\omega_1^A \omega_2^B + (\phi_{11} + \Lambda - \psi_2)(\omega_1^0 \omega_2^1 + \omega_1^1 \omega_2^0) + (\phi_{21} - \psi_3)\omega_1^1 \omega_2^1\} dS, \quad (4)$$

which is simplified using the spinor frame equations¹:

$$\begin{aligned} \wp \pi_{\nu'} + \rho \pi_{\nu'} &= i(\psi_2 - \phi_{11} - \Lambda)\omega^1 + i(\psi_1 - \phi_{01})\omega^0, \\ \wp' \pi_{\nu'} + \rho' \pi_{\nu'} &= i(\psi_3 - \phi_{21})\omega^1 + i(\psi_2 - \phi_{11} - \Lambda)\omega^0, \end{aligned} \quad (5)$$

to the integral

$$A_{\alpha\beta}Z_1^\alpha Z_2^\beta = \frac{-i}{4\pi G} \int (\pi_1^0 \pi_{\nu'}^2 + \pi_{\nu'}^1 \pi_{\nu'}^2) dS, \quad (6)$$

which establishes the required duality. \blacklozenge

Of the integral involved in (6), we note that the twistor kinematic tensor $A_{\alpha\beta}$, depends of S , which has more mean, that is to say, depends on the first and second fundamental forms of S .

This means the presence of curvature inside spinor terms in the integrating of (6). This explains only the dependence of the energy due to curvature. Then to spinor fields of the form $(\omega^A, \pi_{A'})$, we have the quantity [1]:

$$\Sigma = \omega^A \bar{\pi}_{A'} + \bar{\omega}^{A'} \pi_{A'}, \quad (7)$$

which is constant to constant curvature space. However, for a 2-surface in a general space-time \mathbb{M} , there is no reason to that (7) could be constant. Likewise, we have the following proposition:

Proposition 1.2. (7) is constant for every 2-surface twistor if and only if the 2-surface with their field $(\omega^A, \pi_{A'})$, is embedded in a conformally flat space-time modulo certain genericity conditions.

Then in little words, the proposition 1.2. prepares a detection condition from a contorted property of the 2-surface when is affected by the presence of a field source. This in the conformally conditions detects curvature which is measured and modeled in the spinor waves as is showed in **Figure 1** in the 2-surface twistor of the twistor kinematic tensor $A_{\alpha\beta}$. In our study of spectral curvature we can define this measure as curvature energy obtained through twistor frame of the energy-mass tensor, as in the integrals (3) and (6). These have involved a curvature tensor, which has curvature energy as spinor field energy or spinor wave, this last understood as energy manifestation in the kinematic tensor space $(\mathbb{T}(S) \otimes \mathbb{T}(S))^*$.

Likewise, the curvature energy as spectral curvature in the twistor kinematic frame is the curvature in twistor-spinor framework.

¹The twistor equations to valence-2 on symmetric spinor ω^{AB} , can be written as:

$$\nabla_A^A \omega^{BC} = -i \epsilon^{AB} k_{A'}^C,$$

which has a 10-dimensional complex solutions space. Their solution space is spanned by fields ω^{AB} , of the form $\omega_1^{(A} \omega_2^{B)}$, (such and is showed in **Figure 1**), where each ω_1^A , satisfies the twistor equation

$$\nabla_A^A \omega^B = -i \epsilon^{AB} \pi_{A'},$$

whose solutions defines a 4-dimensional complex vector space which is the twistor space \mathbb{T} .

Def. 1.1. A 2-surface S , is contorted if their embedding involves one component of the twistor space $\mathbb{T}(S)$.

Remember that $A_{\alpha\beta}$, is the twistor kinematic tensor of the given source. Due to that the twistor equations to spinor fields ω^{AB} , have a 10-dimensional complex solution space, $A_{\alpha\beta}$, apparently has too much information in it. To curvature we want solutions provided of the energy-mass tensor. Then for simplification and the spinor framework is obtained the linearized general relativity context where the tensor T^{ab} , must satisfy the equation

$$\nabla^a T^{ab} = 0, \tag{8}$$

thought out as a source for a linearized gravitational field. This will bring a linearized Riemann tensor, which will be agreed to the spinor frame considering the components $f_{ab} = \omega_{AB} \in_{A'B'}$, which relates the spinor field ω_{AB} , with the Killing vector k^a , in the twistor equations to twistors of valence-2. Then using divergence theorem when S , is a 2-surface on the 3-surface Σ , as given in (7) surrounding the source, we have several censorship conditions designed through dominating energy condition of curvature.

Then the energy of the twistor kinematic tensor that will the energy substantive to measure curvature energy in the case of the twistor-spinor framework, is given in energy domain $M_N \geq A_{\alpha\beta} Z^\alpha I^{\beta\gamma} \bar{Z}_\gamma \geq 0$.

The inequality written in the last paragraph conforms the inequalities family of Hilbert type in twistor theory required to explain the range or domain of energy where can be censured the existence of the massive object that will produce the torsion of the space. Then of this torsion will be produced the gravitational waves in the space-time far of the massive source, but whose asymptotic behavior helps to the understanding the post-Newtonian limit after of the horizon of events of the massive source, when the space-time tends to de Sitter Universe.

2. Curvature and Twistor-Spinor Framework

A result of the curvature digression as an observable of an object obtained through integral transform on cycles is the following theorem.

Theorem 2. 1 (Y. Stropovskyy, F. Bulnes, I. Rabinovich). We consider the embedding $\sigma: \Sigma \rightarrow (\mathbb{T}(S) \otimes \mathbb{T}(S))^*$. The space $\sigma(\Sigma)$, is smoothly embedded in the twistor space $(\mathbb{T}(S) \otimes \mathbb{T}(S))^*$. Then their curvature energy is the energy given in the interval $M_N \geq A_{\alpha\beta} Z^\alpha I^{\beta\gamma} \bar{Z}_\gamma \geq 0$.

Some considerations on the curvature of twistor-spinor framework in a complex Riemannian manifold are necessary to clarify. After we realize the demonstration of the theorem 2. 1, which is the central goal of the chapter.

We consider the twistor fields Ψ_{ABCD} , and $\tilde{\Psi}_{A'B'C'D'}$, satisfying the twistor equations

$$\nabla^{AA'} \Psi_{ABCD} = 0, \nabla^{AA'} \tilde{\Psi}_{A'B'C'D'} = 0, \tag{9}$$

whose solutions are given by the twistor contour integrals

$$\Psi_{ABCD} = \oint_{\partial_{\omega} 2\pi=S^1} \frac{\partial}{\partial \omega^A} \frac{\partial}{\partial \omega^B} \frac{\partial}{\partial \omega^C} \frac{\partial}{\partial \omega^D} f(z) dz, \tag{10}$$

and

$$\tilde{\Psi}_{A'B'C'D'} = \oint_{\partial_{\omega} 2\pi=S^1} \pi_A \pi_{B'} \pi_C \pi_{D'} \tilde{f}(z) dz, \tag{11}$$

which could be deformed by the presence of an incurved section of the space having the energy-stress-mass tensor condition given by Einstein in conformally. Here $f(z)$, is a function of homogeneous degree +2, and $\tilde{f}(z)$, is a function of homogeneous degree-6².

We can consider the linearized gravity framework (which can be complex) where we have the curvature, then considering the deforming contributions of the contour integrals given on (10) and (11), we have:

$$K_{abcd} = \Psi_{ABCD} \epsilon_{A'B'} \epsilon_{C'D'} + \epsilon_{AB} \epsilon_{CD} \tilde{\Psi}_{A'B'C'D'}, \tag{12}$$

where $\Psi_{ABCD} \epsilon_{A'B'} \epsilon_{C'D'}$, is the anti-self-dual component and $\epsilon_{AB} \epsilon_{CD} \tilde{\Psi}_{A'B'C'D'}$, is the self-dual part. Here Ψ_{ABCD} , and $\tilde{\Psi}_{A'B'C'D'}$, both symmetric if K_{abcd} , is real, due that Ψ_{ABCD} , and $\tilde{\Psi}_{A'B'C'D'}$, are both complex conjugate.

The differential of the integrals (10) and (11) comes given as:

$$\delta Z = \epsilon^{A'B'} \pi_A d\pi_{B'}, \tag{13}$$

Likewise, f , and \tilde{f} , are representatives of cohomology. Here, we have the spectral curvature considering their spectra in the twistor space $(\mathbb{T}(S) \otimes \mathbb{T}(S))^*$. But is necessary consider all cases that are presented in the complex Riemannian manifold \mathbb{M} , to curvature study. Likewise in general relativity, to the flat space we can consider the duality between the spaces $\mathbb{C}\mathbb{M}$, and $\mathbb{C}\mathbb{P}^3$, having a null separation dual to meeting lines (see **Figure 2**).

Also in deformation theory, the anti-self-dual complex space-time has correspondence in duality with the general Ricci-flat space $\mathbb{C}\mathbb{P}^1$, where circles of the deformed tube have images in a π -space. These deformed tubes could be geometrical representations of 2-dimensional superstrings whose circles of their diameter are points of the infinite line or π -space. Then the anti-self-dual complex space-time and the Ricci-flat space are equivalent to the parallelism for π_A - spinors (locally), that is to say,

$$[\nabla_{AA'}, \nabla_{BB'}] \pi_C = 0, \tag{14}$$

taking place a curvature classification due the products of the summation indices [1]. Likewise, the curvature in Ψ_{ABCD} , represents the non-existence of holomorphic planes³ in the twistor space to the tube (twistor tube) $\subset \mathcal{T}$, then is required the twistor component due to the homogeneous degree-6, $\tilde{\Psi}_{A'B'C'D'}$,

²Left-handed graviton with f , homogeneous with degree +2. And right-handed graviton with \tilde{f} , homogeneous with degree -6.

³Def. A β -plane is a holomorphic plane in the twistor space $\subset \mathcal{T}$.

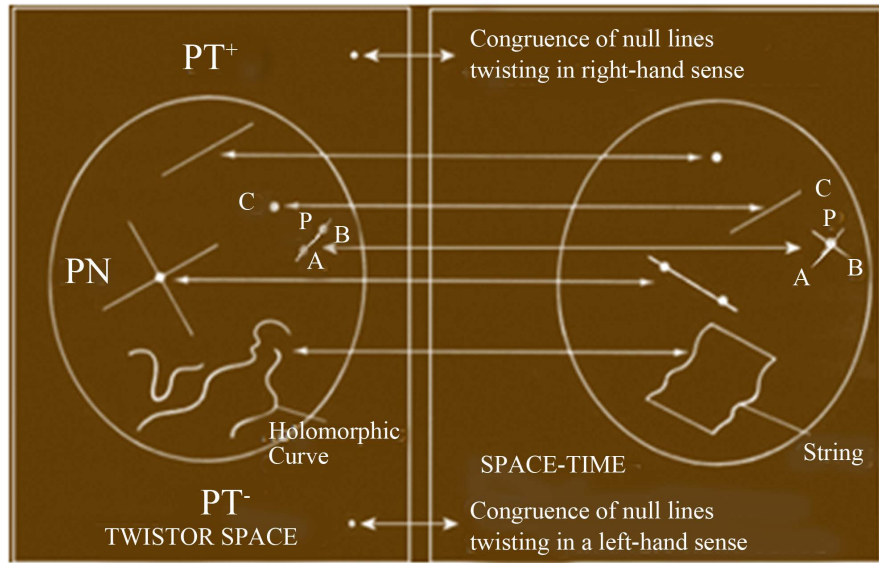


Figure 2. Dualities between the twistor space elements and space-time elements [1].

which involves a torsion energy (second curvature energy) and the Ricci-flat space condition.

The appearing necessity of torsion as special factor of curvature detection in the deforming of the microscopic space-times in \mathbb{M} , is a condition of existence of curvature in these spaces. Likewise, in [2] is obtained a particular solution, which could establish curvature in spinor-twistor terms through of the second component of curvature given in (12).

Here the problem is to see the cause of second curvature to K_{abcd} , which are the elements mentioned before.

Let \mathbb{M} , a complex Riemannian manifold. We have the following natural conjecture.

Conjecture 2.1. The curvature in spinor-twistor framework can be perceived with the appearing of the torsion and the anti-self-dual fields.

Proof. We consider the complex Minkowski space \mathbb{M} . Then their Weil curvature is anti-self-dual given place to the α -planes where could to exist distortion or twists. But this exists to a space-time referred to the group $U_c(4)$, in gravity. Under these conditions the complex Minkowski space can present a torsion as the candidate to produce distortions as second curvature in the space \mathbb{M} , (locally). But the spinor model of torsion can be write as:

$$S_{ab}{}^c = \chi_{AA'}^{CC'} \in_{A'B'} + \tilde{\chi}_{A'B'}^{CC'} \in_{AB}, \tag{15}$$

where spinors $\chi_{A'B'}$, and $\tilde{\chi}_{A'B'}$, are symmetric in AB, and A'B', respectively and linearly independents. Likewise, re-written the spinor equation to torsion (15), in the twistor-spinor framework we have⁴:

⁴ $\forall X, Y \in \mathfrak{X}(\mathbb{M})$, with connection ∇ , we have the torsion expression [3]:

$$[X, Y] = \nabla_X Y - \nabla_Y X - 2S(X, Y),$$

If we consider the fields defined as $X^a = \lambda^a \pi^{a'}$, and $Y^a = \eta^a \pi^{a'}$, then the twistor-spinor model of torsion is given.

$$\pi^{A'}(\nabla_{AA'}\pi_{B'}) = \xi_A\pi_{B'} - 2\pi^{A'}\pi^C\tilde{\chi}_{A'B'AC'}, \tag{16}$$

Then we must to do that the anti-self-dual complex space-time and the Ricci-flat space are equivalent to the parallelism for π_A -spinors (locally) that are had with the formalisms (15) and (16). This condition is an integrability condition necessary to the existence of solutions to equation types as (14). Here arise several tensors considering different spinor indices bracket products. Likewise, the curvature tensor written through spinors tools, using the spinor Ricci identities stays as:

$$\begin{aligned} R_{abcd} = & \phi_{ABCD} \epsilon_{A'B'}\epsilon_{C'D'} + \tilde{\phi}_{A'B'C'D'} \epsilon_{AB}\epsilon_{CD} + \Phi_{ABCD'} \epsilon_{A'B'}\epsilon_{CD} + \tilde{\Phi}_{A'B'CD} \epsilon_{AB}\epsilon_{C'D'} \\ & + \Delta_{AB} \epsilon_{A'B'}\epsilon_{CD}\epsilon_{C'D'} + \tilde{\Delta}_{A'B'} \epsilon_{AB}\epsilon_{CD}\epsilon_{C'D'} + \Omega(\epsilon_{AC}\epsilon_{BD} + \epsilon_{AD}\epsilon_{BC}) \epsilon_{A'B'}\epsilon_{C'D'} \tag{17} \\ & + \tilde{\Omega}(\epsilon_{A'C'}\epsilon_{B'D'} + \epsilon_{A'D'}\epsilon_{B'C'}) \epsilon_{AB}\epsilon_{CD}, \end{aligned}$$

and the torsion through integrability condition (15):

$$[\nabla_{C(A'}\nabla_{B')}^C - 2\tilde{\chi}_{A'B'}\nabla_{HH'}]\pi^{C'} = \phi_{A'B'E}^C\pi^{E'} - 2\tilde{\Omega}\pi_{(A}\epsilon_{B')}C' + \tilde{\Delta}_{A'B'}\pi^{C'}, \tag{18}$$

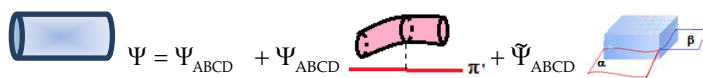
where is clear the appearing of torsion in the terms $\phi_{A'B'E}^C\pi^{E'} - 2\tilde{\Omega}\pi_{(A}\epsilon_{B')}C'$, and the integrability condition to α -surfaces also is appeared considering $\lambda_A\lambda^A = \pi_A\pi^{A'} = 0$. ♦

Then a total spinor field Ψ , that detect distortions due to curvature existence in the microscopic level can be written as:

$$\Psi = \oint_{S^1} \frac{\partial}{\partial\omega^A} \frac{\partial}{\partial\omega^B} \frac{\partial}{\partial\omega^C} \frac{\partial}{\partial\omega^D} \epsilon_{AB}\epsilon_{BC} \pi d\pi + \oint_{S^1} \pi_A\pi_B\pi_C\pi_D \epsilon_{A'B'}\epsilon_{B'C'} d\pi, \tag{19}$$

where are perceived these distortions with right-handed gravity (see **Figure 3**).

Then we have the combining of two deformations with one component with two interaction planes. Likewise, in both components are considered the spinor fields Ψ_{ABCD} , and $\tilde{\Psi}_{ABCD}$, where the component $\tilde{\Psi}_{ABCD}$, is really the principal contribution of the distortions:

$$\Psi = \Psi_{ABCD} + \Psi_{ABCD} \pi + \tilde{\Psi}_{ABCD} \tag{20}$$


But in the component Ψ_{ABCD} , also happens certain distortion understood as twistor waves with image in spinors, where to the twistor function $f(z)$, the degree +2 has the infinitesimal shunt to wave-spinor $\hat{\omega}^A = \omega^A + \epsilon\eta^{AB} \frac{\partial f}{\partial\omega^B}$,

and $\hat{\pi}_A = \pi_A$, with vector field $\eta^{AB} \frac{\partial f}{\partial\omega^B} \frac{\partial}{\partial\omega^A}$, agreeing with the integral:

$$\Psi_{ABCD} = \oint \frac{\partial}{\partial\omega^A} \dots \frac{\partial}{\partial\omega^D} \pi d\pi,$$

Then the field $\tilde{\Psi}_{ABCD}$, is incorporated as was signed in (20) using this field may be, with the differential form in major dimension. But necessarily has that be incorporated in a 3-dimensional space which is inside an energy state space which will give a censorship condition to the detection and measure of first and

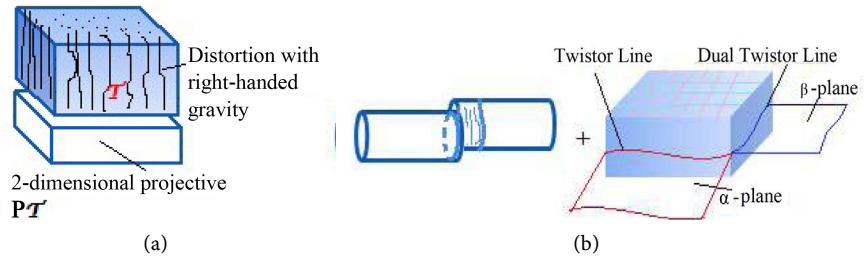


Figure 3. (a) Distortions with right-handed gravity by spinor $\Psi_{ABCD}\alpha + \bar{\Psi}_{ABCD}\beta$; (b) Distorted tube more right-handed gravity given by (19).

second curvature considering the twistor-spinor waves used in the field frame-work.

Likewise, with this spirit of ideas, will be necessary incorporate a 3-forms of Sparling type to use the adequate Hamiltonian vector density where their \mathcal{H} -space is equal to ASD space-time whose the non-linear graviton twistor space is the space $\mathbb{P}\mathcal{T}$, of twistor lines Z .

3. The Kinematic Tensor and the Dominating Energy Condition to Torsion Indicium

Remember that the wanted positivity condition can be expressed as (using Hermitian matrix):

$$A_{\alpha\beta} \bar{I}_{\bar{\alpha}}^{\beta} Z^{\alpha} \bar{Z}^{\alpha} \geq 0, \tag{21}$$

$\forall Z^{\alpha}$, a constant field, that is to say, the Hermitian matrix $A_{\alpha\beta} \bar{I}_{\bar{\alpha}}^{\beta}$, could be positive semi-definite.

Likewise, considering that the exhibition of curvature energy can be written through the energy densities obtained for twistor fields and their dual, the spinor frame, we can write the dominating energy condition as the integral:

$$\begin{aligned} A_{\alpha\beta} \bar{I}_{\bar{\alpha}}^{\beta} Z^{\alpha} \bar{Z}^{\alpha} &= \frac{i}{8\pi G_S} \int \bar{\pi}^A d\pi^{A'} \wedge \theta_{AA'} \\ &= \frac{i}{8\pi G_{\mathcal{H}}} \int d\bar{\pi}_A \wedge d\pi_{A'} \wedge \theta^{AA'} - \frac{1}{2} G_{ab} \bar{\pi}^A \pi^{A'} \mathbf{X}^b, \end{aligned} \tag{22}$$

$\forall \mathbf{X}^b$, a Hamiltonian vector density:

$$\mathbf{X}^b = \frac{1}{6} \epsilon_{abc}^b \theta^c \wedge \theta^d \wedge \theta^e, \tag{23}$$

which is the 3-form mentioned in **Table 1**.

In the conformally flat space-time (Ricci-flat space) we have solutions to the equation $\nabla_A^A \omega^B = -i \epsilon^{AB} \pi_{A'}$, and any 2-surface twistor arises by restriction of a “4-space-time” such as in the FRW-cohomology⁵. Then the kinematic twistor is again written in terms of the flux integrals.

Considering the scalar “observable” due the twistor kinematic tensor $A_{\alpha\beta}$, given by, M_N , we have:

⁵Friedman-Robertson-Walker cohomology.

Table 1. Differential forms to different objects in twistor-spinor theory.

#	Physical Object	Differential Forms	
		N-dimension al form	Locally Expression in M.
1	Deformed Line	1-form: $\ell (= \delta Z)$	$\delta Z = I_{\alpha\beta} Z^\alpha dZ^\beta = \epsilon^{\Lambda\Lambda'} \pi_{\Lambda'} \pi_{\Lambda}$
2	2-Dimensional Waving Space (for example Figure 4(b))	2-form: $\tau = \frac{1}{2} dL$	$\tau = \frac{1}{2} I_{\alpha\beta} dZ^\alpha \wedge dZ^\beta = \epsilon^{\Lambda\Lambda'} d\pi_{\Lambda'} \wedge d\pi_{\Lambda}$
	\mathcal{H} -Spaae	3-form: θ	$\theta = \frac{1}{6} \epsilon_{\alpha\beta\gamma\delta} Z^\alpha dZ^\beta \wedge dZ^\gamma \wedge dZ^\delta$ $= Z^0 dZ^1 \wedge dZ^2 \wedge dZ^3 - Z^1 dZ^0 \wedge dZ^2 \wedge dZ^3$ $+ Z^2 dZ^0 \wedge dZ^1 \wedge dZ^3 - Z^3 dZ^0 \wedge dZ^1 \wedge dZ^2$
4	Spin Bundle	4-form: $\phi = \frac{1}{4} d\theta$	$\phi = \frac{1}{24} \epsilon_{\alpha\beta\gamma\delta} dZ^\alpha \wedge dZ^\beta \wedge dZ^\gamma \wedge dZ^\delta$ $= dZ^0 \wedge dZ^1 \wedge dZ^2 \wedge dZ^3$
5	Field Distorsion Components	Euler form: $Y = \theta : \phi$ $da \wedge \theta = Y(a)\phi$	$Y = Z^\alpha \frac{\partial}{\partial Z^\alpha}$

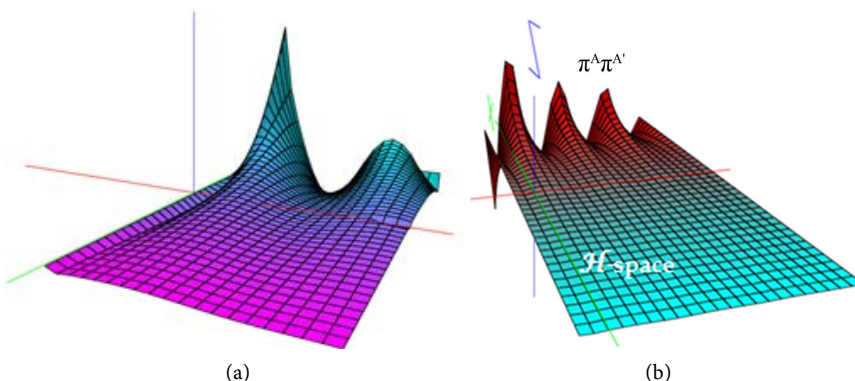


Figure 4. (a) Positive definite condition applied in the spinor $\omega_A \omega_B$, and $\pi^\Lambda \pi^{\Lambda'}$, in the 2-dimensional model of the space-time kinematic twistor. In the model (b); is included the perturbations in the \mathcal{H} -space, that is to say, is the \mathcal{H} -space model of the twistor kinematic space.

$$M_N^2 = \frac{1}{2} A_{\alpha\beta} \bar{A}^{\alpha\beta}, \tag{24}$$

which can be written on a 3-surface as:

$$M_N^2 = \frac{1}{2} A_{\alpha\beta} \bar{A}^{\alpha\beta} \Sigma^{\alpha\alpha'} \Sigma^{\beta\beta'}, \tag{25}$$

Likewise, we find that the 3-surface twistor equation has a complex 4-dimensional family of solutions (a 3-surface twistor space $\mathbb{T}(\Sigma)$) if and only if Σ , with their first and second fundamental forms are embedded in a conformally-flat space-time (see **Figure 5**).

The nature of the $\mathbb{T}(\Sigma)$, from a point of view of QFT, are fermionic sources (currents) whose fermionic fields are Grassman numbers satisfying anti-commutation relations where bosonic fields and currents commute.

We consider the following main result, which is the culmination of this research.

Theorem 3.1 (F. Bulnes, I. Verkelov, Y. Stropovskiy, I. Rabinovich). Spinor wave $S^{AA'}$, in the non-commutative ring algebra (Clifford algebra type) has as Spec in the kinematic-twistor space-time as rotating embedding surfaces (waving) in the \mathcal{H} -space given by $\Pi_{AA'}$.

Proof. We consider the theorem 2.1, of the section 2, and considering the proposition 1. 2, to the contorted 2-surfaces embedded with values in the \mathcal{H} -space as $(T(S) \otimes T(S))^*$, we demonstrate that the deformed category of the moduli stack to the elements that acted in the space-time are the of non-commutative algebra whose spectrum⁶ (see the scheme of derived categories) is in the corresponding twistor kinematic space-time. This proves the asseveration of the theorem 3.1. The elements in the \mathcal{H} -space are bosonic fields commuting with currents. The waving is of type as **Figure 6**.

The moduli stack comes given by the gravitational waves given by the dualities between spinors and kinematic tensors.

These are gravitational waves in the space-time, since come of the torsion which is a second curvature, and by the arguments of fermion interactions and fermionic sources (and particle helicities), these produce torsion from microscopic level until the conforming of the macroscopic behaviour of the space-time near of massive source.

Then the evolution of the space from the Big Bang until the Universe that we know, have two periods of particles interacting, the first called leptogenesis where the Universe conforms the base of the fermions in different types of neutrinos. Then these new fermionic interacting and due to the particle helicities that go arising of the fermionic sources, generate the torsion modelled geomet-

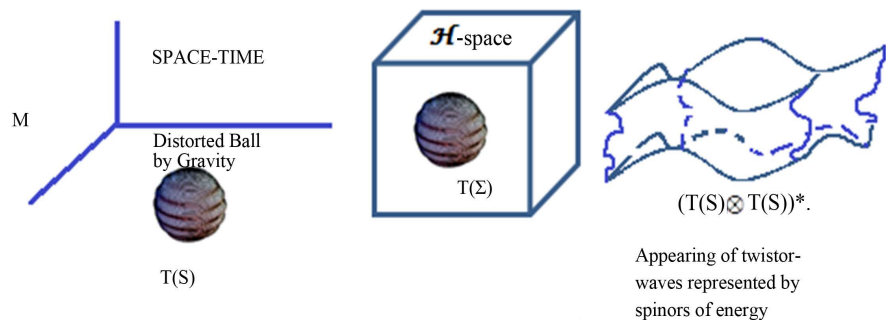


Figure 5. The appearing of the twistor image due to the twistor kinematic tensor acting on space-time from the twistor space $T(\Sigma)$.

⁶Theorem (I. Verkelov, F. Bulnes) [4] [5]. Considering the functors Φ, Ψ , with the before properties $\text{Moduli}_n \xrightarrow[\text{GP}_n]{\Phi_n F} \text{Alg}_{\text{aug}}^{(n)}$, the corresponding homotopy equivalence, and their canonical homotopy,

likewise, the relation $\text{Alg}_{\text{aug}}^{(n)} \xrightarrow{\Phi^{-1}} \text{Moduli}_n \subseteq \text{Fun}(\text{Alg}_{\text{sm}}^{(n)}, \mathbb{S})$, we have the following scheme

$$\text{Hom}_{\text{Moduli}_n}(X, \text{Spec}(B)) \cong \text{Hom}_{\text{CAlg}(\text{Sp})}(B, \mathbb{S}).$$

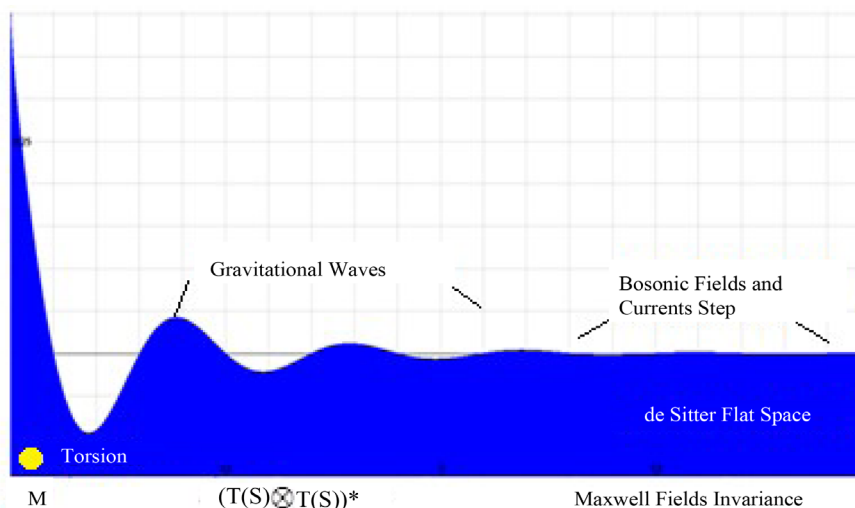


Figure 6. Bose-Einstein distribution to the gravitational waving evolution. The fermionic sources happened before of the flatness of the space-time far of the massive object M (yellow source). The torsion component creates the waving on space-time.

rically by the space $\tau(\Sigma)$, then this produce a baryon-genesis whose action on the space-time produce the initial condiment of matter-energy, which finally gives the gravitational waves and after the bosonic fields and currents (see the **Figure 7**).

4. Spectrum of Kinematic Tensor to Curvature and Design Curvature Censorships to Quantum Gravity Sensors

Through consider the field study framework realized in this chapter we could determine and design a censorship condition with possibilities to their application in sensor technology [7].

In addition, we can consider the models of the space-time influenced for the fields on each particle of this, that is to say, consider the light cone of each particle intersects with the infinity nullity of the gravitational field that creates the deformation of the space-time [7].

In these intersections exist the detectable and measurable part that can be measured through microscopic electromagnetic fields and for the other side, that has the gravitational nature that provokes the curvature, generating enough energy to be bounded by the cosmic censorship of Penrose [8].

But the proper movements of the space-time from the 3-invariance in 4-dimensional complex space-time, and the expansion of the space-time studied in field theory frame considering gravitational fields, we can have the kinematic models given by the spaces that are asymptotically de Sitter and anti-de Sitter [9] [10]. These could give a fine censorship condition in the kinematic twistor models explained before.

Through a gauge field (electromagnetic type field as photons) acting on the background radiation of the Minkowski space \mathbb{M} , where the energy of the matter will be related with this gauge field through equation

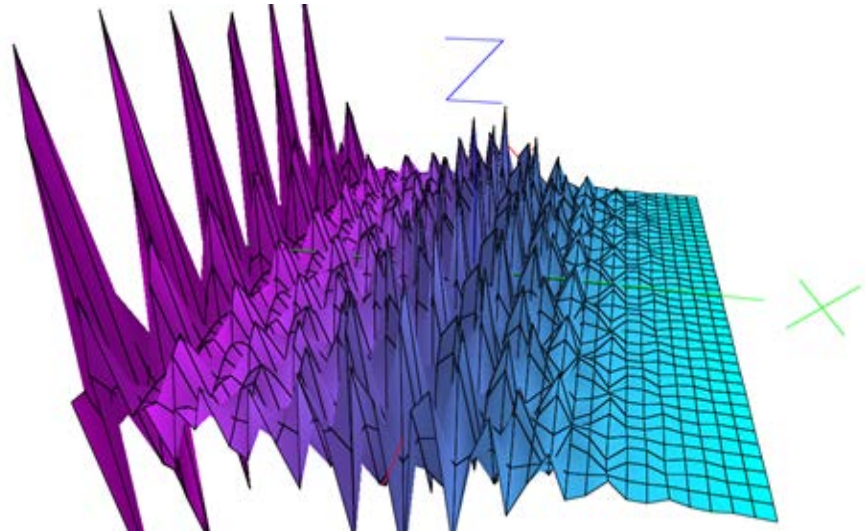


Figure 7. The torsion is represented in the clear purple waving [6] in the space-time.

$$J^\alpha = k^\alpha T^{\alpha\beta}, \tag{26}$$

(where k^α) can represent the density of background radiation which establishes for the curved part of the space (*that in this case has spherical symmetry*) together with the energy and matter tensor that (see the **Figure 8**)

$$\frac{1}{4\pi G} \int_{S^2} T_{\alpha\beta} k^\alpha d\sigma^\beta \geq \int_{S^2} J^\alpha d\sigma^\beta \geq 2\pi\chi \tag{27}$$

Then of the dominating energy condition normed by the twistor kinematic tensor given by the 3-dimensional ball affected (electromagnetic fields in $SU(2)$, which is isomorphic to S^3) by gravitation in the 4-dimensional space, we can have the image of the twistor space of sphere in $(\mathbb{T}(S) \otimes \mathbb{T}(S))^*$, whose condition is had as:

$$16\pi M^2 \geq A, \tag{28}$$

which is the Penrose censorship⁷ [11] for a singularity detected of spherical type [12] [13] [14] [15]. But from this idea can be designed and developed a sensor that use the torsion energy as second curvature energy. Because the fundamental conclusion of the end of the Section 3, is that the torsion energy obtained by movement of the 3-dimensional ball inside the \mathcal{H} -space, is curvature energy and thus gravitational energy.

5. Conclusion

Curvature energy as image of the twistor kinematic-energy tensor applied to 3-dimensional sphere as surface to the cosmic censorship and the obtaining of curvature through gravitational waves can be very useful in quantum gravity theory to creation of advanced sensor devices that can measure the deformation

$$\int_{S^2} \left(\int_{S^2} \Omega (1 - \nabla^2 \log \Omega) \right)^2 \geq 4\pi \int \Omega^2.$$

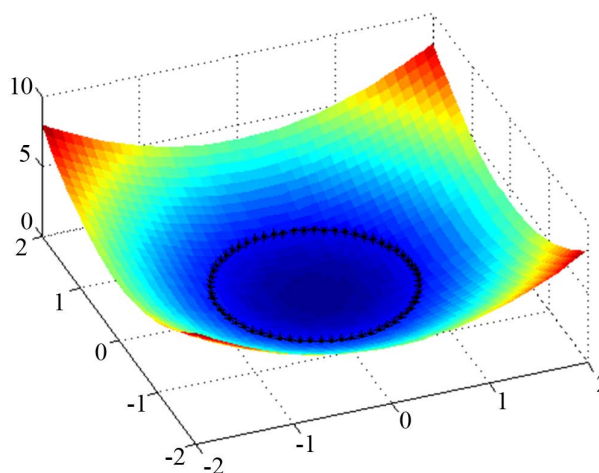


Figure 8. Degenerated neutrinos energy, which will be persistent to space-time background, being a strong indicium of the torsion (rest of the leptogenesis/baryogenesis process. This low energy signed in the circle is the represented in the right extreme of the inequality (27). Then gravitational waves appear.

on surfaces affected to micro-local level by the energy-matter-momentum tensor variations. One of these variations is the torsion energy, which is the curvature energy. Likewise, theoretically the integral representation given to the electrical charge depending of the momenta, establishes through analysis realized in duality that the gravitational energy condition required is to detect curvature in terms of energy. This is obtained with a censorship condition on cylindrical gravitational waves. These gravitational waves are produced from a 3-dimensional sphere located inside the background model of the space-time, whose values are in the space $(\mathbb{T}(S) \otimes \mathbb{T}(S))^*$. This obeys to a topological space as complex Riemannian manifold with local structure, which is isomorphic to a Hilbert space to this dominated energy in the space. Then the energy condition in this case is established for the existence of the sources, which is given by gravitational waves (source detection). These gravitational waves are solutions of a twistor equation whose spinor equivalent is the solution to the dominated energy by the presence of matter of a massive object whose existence in the space-time is given by this energy condition [13] [14]. This study is bounded to the curvature energy extended to the field torsion, using the spinor technology to create waves from field interactions. Studies realized on dilatons used as gauge particles to measure gravitational distortions has been proposed in several works [6] [8]. The idea of use fields to measure other fields is extended to other field formalisms considering tropical geometries in a complex Riemannian model of the space-time, that they can be carried to the technological design of sensor devices to detect quantum gravity [16]. The following step will be the application of the \mathcal{H} -states [7] [16] to produce that technology.

Acknowledgements

I am very grateful with Rene Rivera Roldan, Eng, Head of Electronic Engineer-

ing Division for your support to give facilities in time and electronic laboratory devices to the research. Also, I am very grateful with Evaristo Vázquez, C. B, Finance Department, TESCHA, and Edgar Daniel Sánchez Balderas, L. B, General Director of TESCHA, for the financing support.

References

- [1] Penrose, R. and Rindler, W. (1986) *Spinors and Space-Time*, Vol. 2. Cambridge University Press. <https://doi.org/10.1017/CBO9780511524486>
- [2] Esposito, G. (1992) *Fortschritte der Physik/Progress of Physics*, **40**, 1-30. <https://doi.org/10.1002/prop.2190400102>
- [3] Kobayashi, K. and Nomizu, K. (1969) *Foundations of Differential Geometry*. Vol. 2, Wiley and Sons, New York.
- [4] Verkelov, I. (2014) *Pure and Applied Mathematics Journal. Special Issue: Integral Geometry Methods on Derived Categories in the Geometrical Langlands Program*, **3**, 12-19. <https://doi.org/10.11648/j.pamj.s.2014030602.13>
- [5] Bulnes, F. (2017) *Integral Geometry Methods in the Geometrical Langlands Program*, SCIRP, USA.
- [6] Guivenchy, E. (2015) *Journal on Photonics and Spintronics*, **4**, 14-22.
- [7] Bulnes, F. (2017) Detection and Measurement of Quantum Gravity by a Curvature Energy Sensor: H-States of Curvature Energy, Recent Studies in Perturbation Theory. In: Uzunov, D., Ed., InTech, <https://www.intechopen.com/books/recent-studies-in-perturbation-theory/detection-and-measurement-of-quantum-gravity-by-a-curvature-energy-sensor-h-states-of-curvature-energy> <https://doi.org/10.5772/68026>
- [8] Bulnes, F. (2012) *Journal of Electromagnetic Analysis and Applications*, **4**, 252-266. <https://doi.org/10.4236/jemaa.2012.46035>
- [9] Gibbons, G.W. (1984) The Isoperimetric and Bogomolny Inequalities for Black Holes. In: Willmore, T.J. and Hitchin, N.J., Eds., *Global Riemannian Geometry*, Ellis Horwood, Halsted Press, Chichester, New York, 194-202.
- [10] Geroch, R. (1977) Asymptotic Structure of Space-Time. In: Esposito, F.P. and Witten, L., Eds., *Asymptotic Structure of Spacetime, Proceedings of a Symposium on Asymptotic Structure of Space-Time (SOASST)*, University of Cincinnati, Ohio, 14-18 June 1976, 1-105. https://doi.org/10.1007/978-1-4684-2343-3_1
- [11] Kelly, R.M. (1985) Asymptotically Anti-de Sitter Space-Time. *Twistor Newsletter*, No. 20, 11-23.
- [12] Frauendiener, J. (2001) *Physical Review Letters*, **87**, Article ID: 101101. <https://doi.org/10.1103/PhysRevLett.87.101101>
- [13] Penrose, R. (1982) *Proceedings of the Royal Society of London A*, **381**, 53-63.
- [14] Tod, K.P. (1985) *Classical and Quantum Gravity*, **2**, L65-L68.
- [15] Dougan, A.J. (1992) *Classical and Quantum Gravity*, **9**, 2461-2475. <https://doi.org/10.1088/0264-9381/9/11/012>
- [16] Bulnes, F. (2014) Design of Quantum Gravity Sensor by Curvature Energy and Their Encoding. *Science and Information Conference*, London, 27-29 August 2014, 855-861.

Resonant Modes of One-Dimensional Metamaterial Containing Helmholtz Resonators with Point Defect

Dongbao Gao*, Xinwu Zeng, Xuanjun Liu, Kaifeng Han

Academy of Ocean Science and Engineering, National University of Defense Technology, Changsha, China

Email: *gaodongbao@nudt.edu.cn

How to cite this paper: Gao, D.B., Zeng, X.W., Liu, X.J. and Han, K.F. (2017) Resonant Modes of One-Dimensional Metamaterial Containing Helmholtz Resonators with Point Defect. *Journal of Modern Physics*, 8, 1737-1747.

<https://doi.org/10.4236/jmp.2017.810102>

Received: July 17, 2017

Accepted: September 22, 2017

Published: September 25, 2017

Copyright © 2017 by authors and Scientific Research Publishing Inc. This work is licensed under the Creative Commons Attribution International License (CC BY 4.0).

<http://creativecommons.org/licenses/by/4.0/>



Open Access

Abstract

The metamaterial constructed by Helmholtz resonators (HR) has low-frequency acoustic forbidden bands and possesses negative mass density and effective bulk modulus at particular frequencies. The resonant modes in one-dimensional HR structure with point defect were studied using finite element method (FEM). The results show that the acoustic energy is localized between the resonant HR and the opening in the local-resonant-type gap. There is a high pressure area around the defect resonator at the frequency of defect mode. In the Bragg type gap, the energy mainly distributes in the waveguide with harmonic attenuation due to the multi-scattering. Phase opposition demonstrates the existence of negative dynamic mass density. Local negative parameter is observed in the pass band due to the defect mode. Based on further investigation of the acoustic intensity and phase distributions in the resonators corresponding to two different forbidden bands, only one local resonant mode is verified, which is different from the three-component local resonant phononics. This work will be useful for understanding the mechanisms of acoustic forbidden bands and negative parameters in the HR metamaterial, and of help for designing new functional acoustic devices.

Keywords

Helmholtz Resonator Metamaterial, Resonant Mode, Point Defect, Local Negative Parameters, Phase Distribution

1. Introduction

Helmholtz resonator (HR) is normally constructed by a large cavity with a short

neck [1]. Due to its resonance, the resonator possesses capability of low-frequency sound absorption and elimination [2]. Recently, with the increasing research on phononic crystals and acoustic metamaterials, the structure based on HRs has been reconsidered for its property of sound forbidden [3]-[8]. Furthermore, it is found that the structure possesses negative effective bulk modulus [4] and negative dynamic mass density [5] in its band gap, and therefore it is considered as a possible material to realize new functional devices of transformation acoustics [9].

Based on the different mechanisms, there are two kinds of acoustic forbidden bands in the HR metamaterial. One is called Bragg type gap (BG), which is appeared due to the Bragg scattering in the material with periodically arrayed cells [10]. The BG can only forbid the sound waves with wavelength comparable or shorter than the lattice constant. It is unpractical to control low frequency sound using this kind of metamaterial for its huge sizes. On the other hand, the second type acoustic forbidden band is brought by local resonance of HR [11], which can be called local-resonant-type gap (LRG). The LRG exists around the eigenfrequency of the resonator. As the sound wavelength corresponding to the eigenfrequency is usually some times of magnitude larger than the geometric parameters of the resonator, low frequency sound waves can be well controlled.

The band structure is much richer when defect exists [7] comparing that of perfect periodical case. Localized mode can be observed due to the coupling of the defect units and perfect units [12] [13] as well as several new gaps of BG and/or LRG. A localized mode is that, at a particular frequency, the linear free oscillations are trapped around the defect resonators and decay exponentially away from them [7]. In this case, the acoustic energy can be captured by the point defect or limited directionally transmitting along the line defect and area defect. With this character, wave-control devices can be designed [14] [15]. Recently, Fey *et al.* [8] indicated that a wide bandgap material could be get with a subwavelength collection of detuned HRs which are considered as a series of defects. However, the problem turns complicated with the increase of the number of defects.

Comparing with two- and three-dimensional metamaterials, one-dimensional (1D) systems can be calculated with higher accuracy [1] [4]. It is also understood that the results of 1D system are helpful for understanding the property of more complex cases. In previous researches, theoretical studies on the 1D HR structures were based on the theory of Bloch wave and scattering [1] [2]. However, due to its strict periodicity assumption, this method is infeasible to deal with more complicated composites with quasiperiodicity or disperiodicity. Recently, some reduced methods were developed to analyze the acoustic transmission property of the HR structure. Cheng *et al.* [5] analyzed the acoustic transmission properties of 1D HR metamaterial by means of acoustic transmission line method (ATLM). Based on the interface response theory (IRT), Wang *et al.* [7] studied 1D phononic crystals containing HRs systematically, especially on the acoustic

transmission properties of structure with point defect.

So far, these studies gave more attention to the transmission property of the HR metamaterial with simplified parameters than the details inside the structure. We believe that, with full view of distribution of the oscillation modes in the structure, a clear understanding on the mechanisms about the acoustic band gaps and negative parameters can be obtained, which is useful for designing new acoustic energy concentrator and creating high pressure environment for acoustic experiments.

In practice, since the complex geometry is simplified in former theoretical methods which are unable to investigate the detailed field distribution in the structure, an accurate approach must be introduced to analyze the resonant modes property of the HR metamaterial. The Finite Element Method (FEM) is an appropriate approach to minutely study the characteristics of the acoustic field for complex structures. On the basis of FEM, the distributions of acoustic intensity and phase for different oscillation modes in the 1D metamaterial with HRs were studied in this paper. Local resonant modes were also investigated for different forbidden gaps.

2. Model and Verification of the Method

Figure 1 shows the schematic diagram of a Helmholtz resonator which is connected with a section of waveguide forming a unit cell of the metamaterial. As a numerical example, here we consider a model with 11 HR unit cells, and the 6th one is abnormal which can be considered as a defect. The overall geometric parameters are $L = 0.09$ m, and $d_1 = 0.025$ m. For the cells, the geometrical parameters of the ten perfect units are $a_2 = 0.02$ m, $d_2 = 0.02$ m, $V = a_3 \times l_3 \times d_3 = 0.03 \times 0.04 \times 0.05$ m³, while the only difference for the defect unit is that $d_2 = 0.04$ m. The background media is water ($\rho_0 = 998$ kg/m³, $c_0 = 1483$ m/s). Here, we analyzed the acoustic band gap structure of the metamaterial in the region of 1 - 10 kHz.

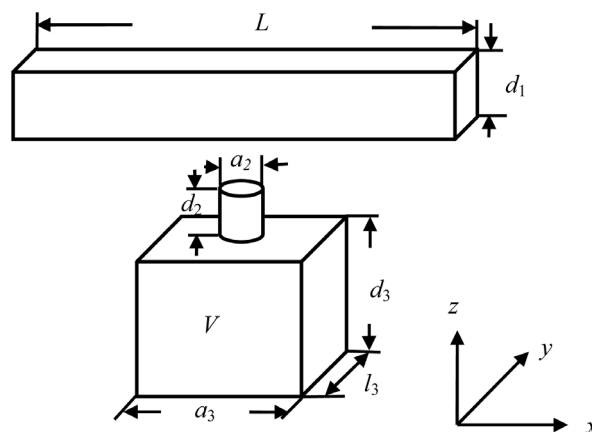


Figure 1. Schematic diagram of a Helmholtz resonator and a section of waveguide.

We studied the 3-dimensional model using COMSOL Multiphysics software (Version 4.2) which is based on the Finite Element Method (FEM). We set up the boundary conditions as shown in **Figure 2**, in which a perfect matched layer (PML) was used at the end of the waveguide to simulate the absorbing boundary condition. All the other boundaries were set to be hard walls, except that a radiation boundary condition with a harmonic wave was used as the incident wave. The host medium in the waveguide and the resonators is water.

To the computational mesh, in our simulation, at least 8 elements per wavelength were used, which guaranteed the accuracy of the method, and also satisfied the general six-element-per-wavelength rule in acoustic mesh [16]. All elements are hexahedral.

To validate the feasibility of the software using FEM, we first made a comparison between the results of FEM and ATLM [5] [17] for the acoustic transmission property of the metamaterial.

In ATLM, based on the transformation relationship between acoustic impedances of the inlet and outlet, the transmission coefficient can be obtained by applying this formula recursively.

The impedance transfer formula [16] of ATLM can be written as

$$Z_1 = Z_0 \times \frac{Z_r + jZ_0 \tan(kL)}{Z_0 + jZ_r \tan(kL)} \tag{1}$$

where, Z_1 (Z_r) is the effective impedance of the inlet (outlet) of the unit cell. $Z_0 = \rho_0 c_0 / S_g$ is the distributed impedance of the duct. S_g is the cross-section area of the waveguide. k is the wave vector of the host medium. L is the distance between two adjacent HRs.

With the assumption of long-wavelength, the transfer impedance of the waveguide parallels to the HR impedance Z_h [16]. The parallel impedance is

$$Z_c = Z_l \parallel Z_h \tag{2}$$

which can be considered as the terminal-end impedance of its left neighbor.

By repeating this process over the N units, the effective acoustic impedance (Z_{effect}) of 1D metamaterial with N unit cells can be obtained. Then, the sound pressure reflection coefficient can be calculated as

$$r_p = \frac{Z_{\text{effect}} - Z_0}{Z_{\text{effect}} + Z_0} \tag{3}$$

The sound intensity reflection coefficient and intensity transmission coefficient are

$$r_I = |r_p|^2, T = 1 - r_I \tag{4}$$

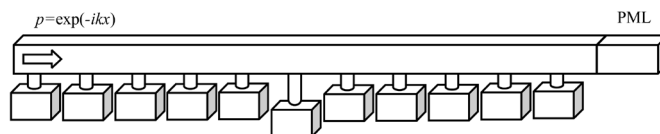


Figure 2. Finite element model of the metamaterial.

In Equation (4), the band gap exists only if $T = 0$, which means $|r_p| = 1$, and therefore $Z_{\text{effect}} = 0$ or ∞ . It indicates that Z_1 or/and Z_b vanishes in Equation (2). $Z_1 = 0$ corresponds to that the real and imaginary parts of Equation (1) equal zero simultaneously, which is mathematically impossible. In fact, based on Equation (1), we get that, when $KL = n\pi$, viz. $f = nc/2L$, the value of Z reaches its minimum (equals to Z_r). This frequency corresponds to the central frequency of BG. On the other hand, when $Z_b = 0$, the incident wave frequency equals to the resonant frequency of the HR, which means the appearance of LRG in this case.

Figure 3 shows the acoustic transmission coefficient curves for both perfect metamaterial and structure with point defect basing on FEM and ATLM, respectively. Despite small differences, the results obtained based on FEM can also show all the properties of the HR metamaterial with point defect, such as transmission bands, forbidden bands and defect mode. **Figure 3** demonstrates the feasibility of FEM, which can be a further approach to analyze the resonant

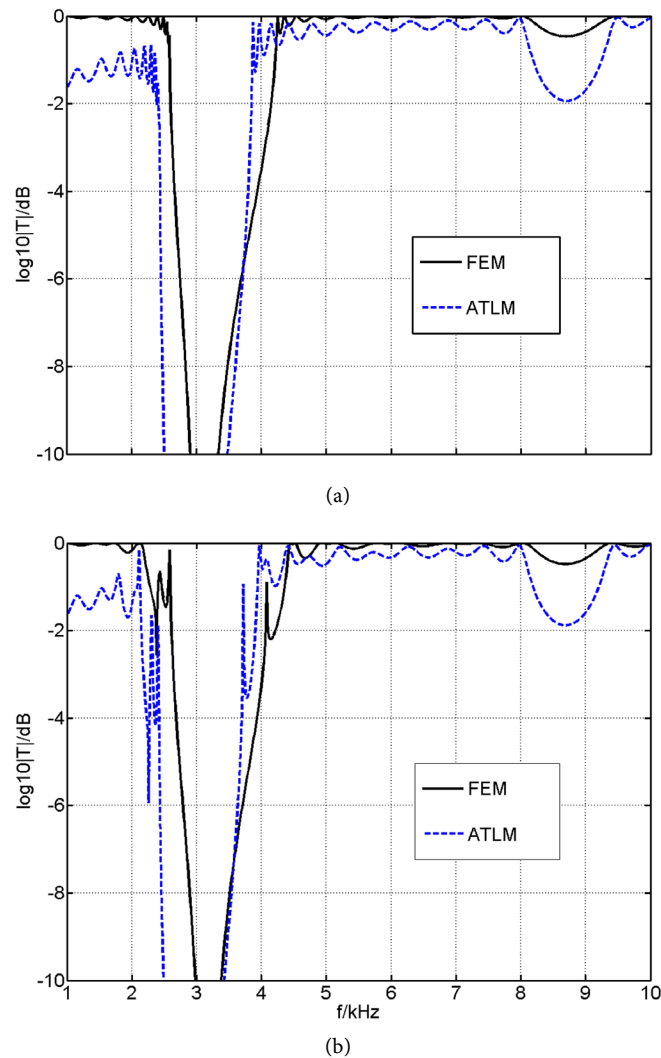


Figure 3. Comparison of acoustic transmission coefficient spectra based on FEM and ATLM for structures with (a) only perfect cells and (b) a point defect, respectively.

modes of the structure. It is also observed that the depth and width of the band calculated by FEM are much narrower and shallower than that obtained by ATLM. These characters are attributed to the inherent difference of FEM and ATLM. The main reason might be that the complex geometry of the structure is simplified by lumped parameters in ATLM, which ignores the wall effect in pipes. While in the well meshed FEM, details caused by the structure could be captured.

3. Simulation Based on FEM

Now we take a detail observation on the acoustic intensity distributions of the structure with point defect for several specified frequencies using the results with full-wave simulation based on FEM. The choice of the frequencies was based on FEM results in **Figure 3(b)**. The acoustic intensity distributions are displayed in **Figure 4**.

In **Figure 4**, point (a) locates at 1.5 kHz in the low-frequency pass band, where the acoustic intensity distributes periodically in the waveguide. Since the frequency does not reach the resonant frequency of HRs, the resonators are in the state of “pre-resonance”, and the acoustic energy is being localized by the resonator. In **Figure 4(b)** (2.38 kHz), energy is localized between the defect HR and the incident opening with small amount of acoustic energy penetrating. The acoustic intensity in the waveguide is obviously weaker than that in the resonators. As we know, point (b) corresponds to the resonant frequency of the defect HR, which indicates that, in the LRG, the resonant HR can localize almost all the energy passing across it. Point (c) (2.52 kHz) is another dip between the two LRGs. Comparing with **Figure 4(b)**, the energy in the defect HR has been already released in **Figure 4(c)**. This is because that with the increase of frequency, the resonant mode of the defect HR vanishes. In this case, the sound is no

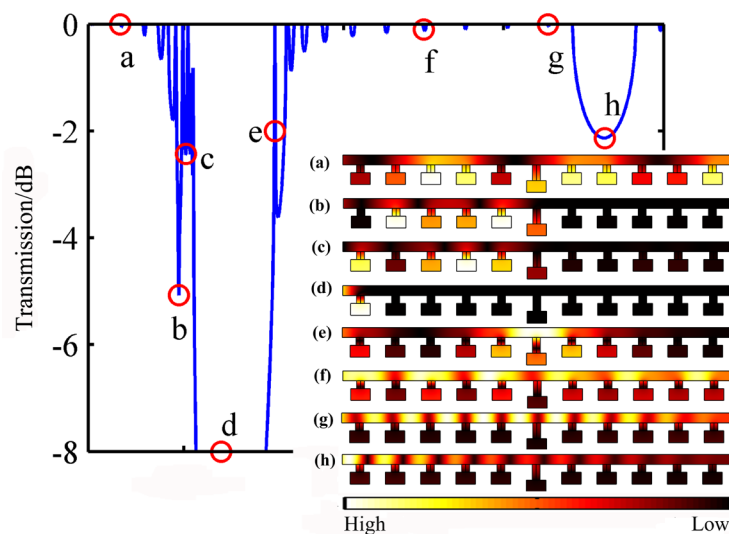


Figure 4. Acoustic pressure intensity distribution for different oscillation modes, which are corresponding to the special frequencies selected from (a) to (h), respectively.

longer localized in the resonator, and the resonators are in the state of “after-resonance”. On the other hand, point (c) is also close to the resonant frequency of perfect HR. The wave oscillation in the perfect resonators becomes strong, and therefore the energy is still localized in few resonators on the incident side but released to the waveguide.

Point (d) (3.2 kHz) locates at the resonant frequency of perfect HR. In **Figure 4(d)**, almost all the acoustic energy is localized in the first HR, which further demonstrates that pressure is hold up by the first resonant HR in the LRG. In each case, a high pressure environment exists in the resonant HR, which can be helpful for acoustic energy concentrating and high-pressure experiments. However, there is a slight difference between the two resonant modes showed in **Figure 4(b)** and **Figure 4(d)**. Due to more cells resonating, the depth and width of the second LRG are larger than the first one.

Point (e) (4.08 kHz) corresponds to a defect mode, which is a narrow transmission band is the forbidden band. It is obvious that, in **Figure 4(e)**, the acoustic energy is localized around the defect HR and its neighbors. The intensity reaches the largest value at the defect resonator, and then attenuates sharply to both sides. This is a typical property of the defect mode [12]. Since the defect mode is created by the coupling of the defect HR and perfect HRs, the defect mode frequency is not the same with both resonant frequencies. The defect mode is useful for realizing new filter, energy harvester and acoustic cloaking.

Point (f) (5.1 kHz) is in the pass band outside the LRG. As shown in **Figure 4(f)**, with the increment of the pressure in the waveguide, the pressure in the HRs decreases. Now, the energy is not localized in HR, but released to the waveguide. In this case, the HRs are like obstacles to short-wavelength sound. With this conclusion, it is imaginable that the harmonicity would be more obvious and the intensity would be higher in the waveguide for **Figure 4(g)** (7.5 kHz) and (h) (8.8 kHz). Point (h) just locates in the BG. In **Figure 4(h)**, due to multi-scattering, the intensity in the waveguide attenuates gradually, which tends to zero at the terminal end. On this condition, the BG appears.

To summarize, as shown in **Figure 4**, there are plenty resonant modes in the metamaterial containing HRs with point defect. When frequency is lower than the resonant frequency, the acoustic energy distributes in the waveguide and resonators symmetrically. As frequency turns to the resonant frequency, local resonant mode can localize the energy between the first resonant HR and the incident port. In the defect mode, a high pressure zone exists around the defect resonator. Finally, the energy in the resonant HR is released to the waveguide and transmits in the waveguide only when frequency is higher than the resonant frequency.

Figure 5 shows the corresponding phase distributions of **Figure 4**. In **Figure 5(a)**, the phase in the waveguide is the same as that in the shunted HR, which indicates that the resonator oscillates in-phase with the wave in the waveguide. In this case, the dynamic mass density must be positive [5] [18]. As frequency

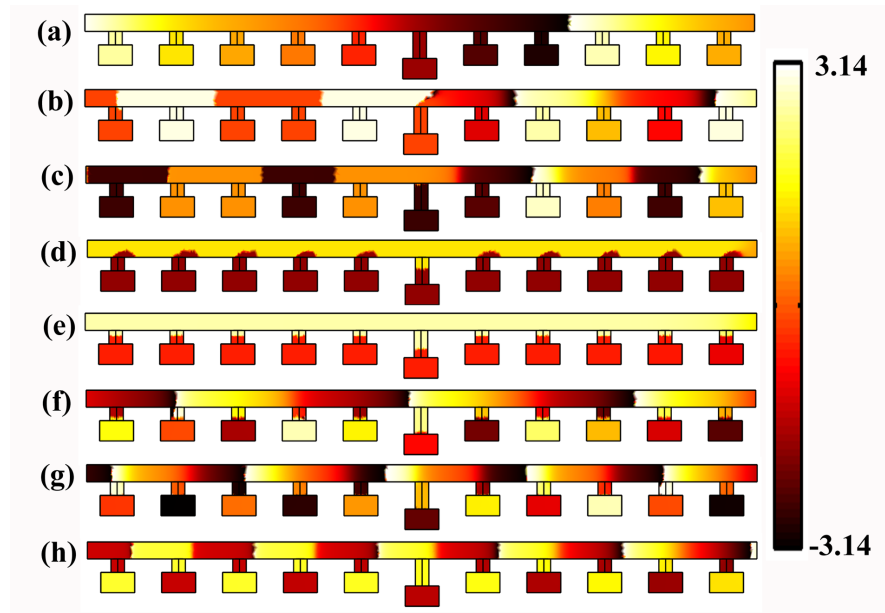


Figure 5. Phase distribution for the metamaterial containing HRs with point defect. Figures (a) to (h) correspond to the cases showed in **Figure 4**.

reaches the resonant frequency of the defect resonator (**Figure 5(b)**), though the in-phase property remains, the wave front around the defect HR is not parallel to the others due to strong oscillation of the resonant resonator. When frequency pass across the first resonant frequency (**Figure 5(c)**), a special effect must be noted that the phases between the defect HR and the waveguide are opposite, which accounts for that the local dynamic mass density becomes negative [5]. In this case, negative and positive parameters exist simultaneously in this structure.

If frequency is higher than the resonant frequency of the perfect HR (**Figure 5(d)**), the phase difference inside and outside the resonator is π . Since the HRs oscillate out of phase with the wave in the waveguide, the dynamic mass density turns negative in the whole structure. The negative parameter still exists in **Figure 5(e)**, which indicates that the negative dynamic mass density not only exists in the forbidden band, but also can be found in the pass band created by defect mode. In **Figures 5(f)-(h)**, the phase distribution in the waveguide corresponds with the property of harmonic wave.

Local resonant modes, such as energy and phase distributions, in the built-in units are typical characteristics of the local resonant phononic crystals [11]. In HR metamaterials, one unit contains only a neck and a cavity, the local resonant modes distribution in the neck and cavity indicates the basic characteristic of the structure. Therefore, we should pay attention to the intensity and phase differences between the neck and the cavity of the HR, which will be discussed below.

As shown in **Figure 6**, acoustic intensity ((a) and (b)) and phase ((c) and (d)) distributions for perfect HR in different gaps are given, in which **Figure 6(a)** and **Figure 6(c)** are at 3.2 kHz in the LRG, and (b) and (d) are at 8.8 kHz in the BG.

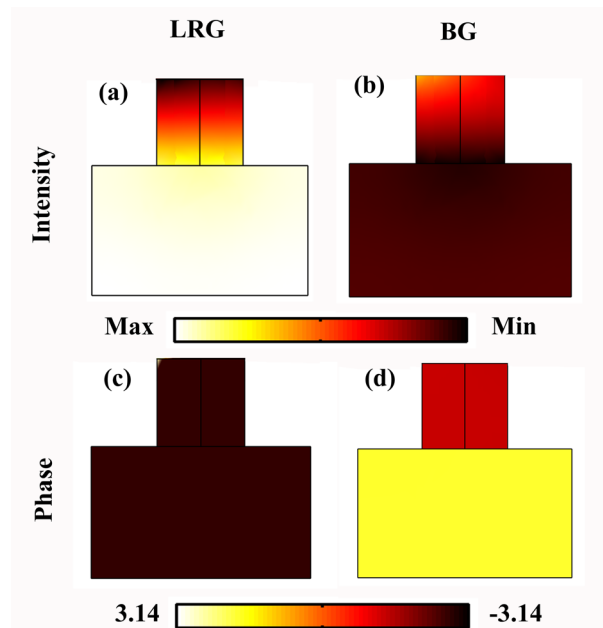


Figure 6. Acoustic intensity ((a) and (b)) and phase ((c) and (d)) distributions for Helmholtz resonator in different forbidden bands. The frequency of (a) and (c) is 3.2 kHz corresponding to the LRG; and (b) and (d) is 8.8 kHz corresponding to the BG.

In **Figure 6(a)**, the intensity at the opening of the neck is almost zero, while that in the cavity reaches the maximum. This indicates that local resonant mode appears in the cavity, where the energy is localized. It is opposite in **Figure 6(b)**, in which the intensity in the neck is bigger than that in the cavity. However, in view of **Figure 4(h)**, we can see that the intensity in the neck is continuous with that in its connecting waveguide. Besides, in **Figure 5(h)**, the phase in the short neck is totally the same with that in the waveguide. These all indicate that there is no local resonant mode in **Figure 6(b)**. Only one kind of local resonant mode exists in the metamaterial based on Helmholtz resonators, which is different from the three-component local resonant phononics, in which two local resonant modes are discovered [19].

As shown in **Figure 6(c)**, the neck and cavity oscillate in phase. Considering with **Figure 5(d)**, it should be insisted that the negative parameter is created by both the neck and the cavity oscillating out of phase with the wave in the waveguide. If the HR oscillates strongly enough, the dynamic mass in the metamaterial can be negative. However, it is opposite in **Figure 6(d)**, where the neck oscillates out of phase with the cavity, but in phase with the wave in the waveguide (**Figure 5(h)**). In this case, only the cavity oscillates out of phase with the wave in the neck and waveguide. Therefore, the negative dynamic mass density may exist as a local parameter. Due to the energy limitation, it may not be large enough to affect the parameter of the whole structure.

4. Conclusions

To study the resonant modes in the metamaterial constructed by Helmholtz re-

sonators with point defect is useful for understanding the mechanisms of acoustic band gaps and negative parameters. The distributions of acoustic intensity and phase for 1D HR structure with point defect were analyzed basing on 3D FEM. The results show that there are different oscillation modes for different frequencies. When frequency tends to the resonant frequency of any HR, the acoustic energy is gradually localized in the resonant resonator, which results in a local-resonant-type gap. At the point of defect mode, the energy locates around the defect cell. When the wavelength is twice of the lattice, the first Bragg type gap appears, when the acoustic energy almost entirely distributes in the waveguide with harmonic attenuation. The phase distribution demonstrates that when frequency is higher than the resonant frequency, the resonant HR can oscillate out of phase with the wave in the waveguide, which is the mechanism of the negative dynamic mass density. Furthermore, the negative parameter not only exists in the forbidden band, but also can be observed in the pass band created by defect mode. Different from the typical three-component local resonant phononics, there is only one local resonant mode in one-dimensional HR metamaterial, which exists in the local resonant forbidden band. This work will be helpful for designing new functional acoustic devices.

In this paper, only two-dimensional linear problems are investigated. More complicated models are not included here. For example, we also observe that there are non-parallel interfaces of the phase distribution in **Figure 5**, which indicates that there maybe nonlinear phenomena exist. Furthermore, we will pay more attention on these problems in our next program.

Funds

The work is supported by National Natural Science Foundation of China (Grant Nos. 11504425 and 41374005).

References

- [1] Sugimoto, N. and Horioka, T. (1995) *Journal of the Acoustical Society of America*, **97**, 1446. <https://doi.org/10.1121/1.412085>
- [2] Masuda, M. and Sugimoto, N. (2005) *Journal of the Acoustical Society of America*, **118**, 113. <https://doi.org/10.1121/1.1929237>
- [3] Hu, X.H. and Chan, C.T. (2005) *Physical Review E*, **71**, 055601(R). <https://doi.org/10.1103/PhysRevE.71.055601>
- [4] Fang, N., Xi, D.J., Xu, J.Y., Ambat, M., Srituravanich, W., Sun, C. and Zhang, X. (2006) *Nature Materials*, **5**, 452. <https://doi.org/10.1038/nmat1644>
- [5] Cheng, Y., Xu, J.Y. and Liu, X.J. (2008) *Physical Review B*, **77**, 045134. <https://doi.org/10.1103/PhysRevB.77.045134>
- [6] Hu, X.H., Ho, K.M., Chan, C.T. and Zi, J. (2008) *Physical Review B*, **77**, 172301. <https://doi.org/10.1103/PhysRevB.77.172301>
- [7] Wang, Z.G., Lee, S.H., Kim, C.K., Park, C.M., Nahm, K. and Nikitov, S.A. (2008) *Journal of Applied Physics*, **103**, 064907. <https://doi.org/10.1063/1.2894914>
- [8] Fey, J. and Robertson, W.M. (2011) *Journal of Applied Physics*, **109**, 114903.

<https://doi.org/10.1063/1.3595677>

- [9] Chen, H.Y. and Chan, C.T. (2010) *Journal of Physics D: Applied Physics*, **43**, 113001. <https://doi.org/10.1088/0022-3727/43/11/113001>
- [10] Zhang, X., Liu, Z.Y., Mei, J. and Liu, Y.Y. (2003) *Journal of Physics: Condensed Matter*, **15**, 8207. <https://doi.org/10.1088/0953-8984/15/49/001>
- [11] Liu, Z.Y., Zhang, X.X., Mao, Y.W., Zhu, Y.Y., Yang, Z.Y., Chan, C.T. and Sheng, P. (2000) *Science*, **289**, 1734. <https://doi.org/10.1126/science.289.5485.1734>
- [12] Sigalas, M.M. (1997) *Journal of the Acoustical Society of America*, **101**, 1256. <https://doi.org/10.1121/1.418156>
- [13] Munday, J.N., Bennett, C.B. and Robertson, W.M. (2002) *Journal of the Acoustical Society of America*, **112**, 1353. <https://doi.org/10.1121/1.1497625>
- [14] Oudich, M. and Assouar, M.B. (2012) *Journal of Applied Physics*, **111**, Article ID: 014504. <https://doi.org/10.1063/1.3673874>
- [15] Qiu, C.Y., Liu, Z.Y., Shi, J. and Chan, C.T. (2005) *Applied Physics Letters*, **86**, Article ID: 224105. <https://doi.org/10.1063/1.1942642>
- [16] Kinsler, L.E., Frey, A.R., Coppens, A.B. and Sanders, J.V. (1982) *Fundamentals of Acoustics*. Wiley, New York.
- [17] Zienkiewicz, O.Z. and Taylor, R.L. (2006) *The Finite Element Method*. 6th Edition, Elsevier.
- [18] Mei, J., Liu, Z.Y., Wen, W.J. and Sheng, P. (2006) *Physical Review Letters*, **96**, Article ID: 024301. <https://doi.org/10.1103/PhysRevLett.96.024301>
- [19] Wang, G., Wen, X.S., Wen, J.H., Shao, L.H. and Liu, Y.Z. (2004) *Physical Review Letters*, **93**, Article ID: 154302. <https://doi.org/10.1103/PhysRevLett.93.154302>



Submit or recommend next manuscript to SCIRP and we will provide best service for you:

Accepting pre-submission inquiries through Email, Facebook, LinkedIn, Twitter, etc.

A wide selection of journals (inclusive of 9 subjects, more than 200 journals)

Providing 24-hour high-quality service

User-friendly online submission system

Fair and swift peer-review system

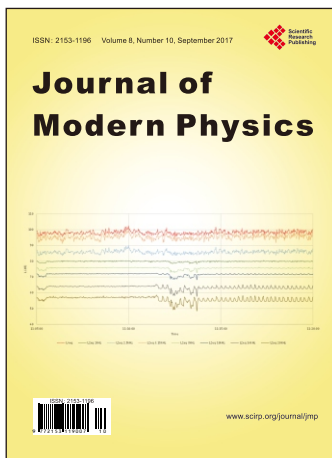
Efficient typesetting and proofreading procedure

Display of the result of downloads and visits, as well as the number of cited articles

Maximum dissemination of your research work

Submit your manuscript at: <http://papersubmission.scirp.org/>

Or contact jmp@scirp.org



Call for Papers

Journal of Modern Physics

ISSN: 2153-1196 (Print) ISSN: 2153-120X (Online)
<http://www.scirp.org/journal/jmp>

Journal of Modern Physics (JMP) is an international journal dedicated to the latest advancement of modern physics. The goal of this journal is to provide a platform for scientists and academicians all over the world to promote, share, and discuss various new issues and developments in different areas of modern physics.

Editor-in-Chief

Prof. Yang-Hui He

City University, UK

Executive Editor-in-Chief

Prof. Marko Markov

Research International, Buffalo Office, USA

Subject Coverage

Journal of Modern Physics publishes original papers including but not limited to the following fields:

Biophysics and Medical Physics
Complex Systems Physics
Computational Physics
Condensed Matter Physics
Cosmology and Early Universe
Earth and Planetary Sciences
General Relativity
High Energy Astrophysics
High Energy/Accelerator Physics
Instrumentation and Measurement
Interdisciplinary Physics
Materials Sciences and Technology
Mathematical Physics
Mechanical Response of Solids and Structures

New Materials: Micro and Nano-Mechanics and Homogeneization
Non-Equilibrium Thermodynamics and Statistical Mechanics
Nuclear Science and Engineering
Optics
Physics of Nanostructures
Plasma Physics
Quantum Mechanical Developments
Quantum Theory
Relativistic Astrophysics
String Theory
Superconducting Physics
Theoretical High Energy Physics
Thermology

We are also interested in: 1) Short Reports—2-5 page papers where an author can either present an idea with theoretical background but has not yet completed the research needed for a complete paper or preliminary data; 2) Book Reviews—Comments and critiques.

Notes for Intending Authors

Submitted papers should not have been previously published nor be currently under consideration for publication elsewhere. Paper submission will be handled electronically through the website. All papers are refereed through a peer review process. For more details about the submissions, please access the website.

Website and E-Mail

<http://www.scirp.org/journal/jmp>

E-mail: jmp@scirp.org

What is SCIRP?

Scientific Research Publishing (SCIRP) is one of the largest Open Access journal publishers. It is currently publishing more than 200 open access, online, peer-reviewed journals covering a wide range of academic disciplines. SCIRP serves the worldwide academic communities and contributes to the progress and application of science with its publication.

What is Open Access?

All original research papers published by SCIRP are made freely and permanently accessible online immediately upon publication. To be able to provide open access journals, SCIRP defrays operation costs from authors and subscription charges only for its printed version. Open access publishing allows an immediate, worldwide, barrier-free, open access to the full text of research papers, which is in the best interests of the scientific community.

- High visibility for maximum global exposure with open access publishing model
- Rigorous peer review of research papers
- Prompt faster publication with less cost
- Guaranteed targeted, multidisciplinary audience



**Scientific
Research
Publishing**

Website: <http://www.scirp.org>

Subscription: sub@scirp.org

Advertisement: service@scirp.org